Imagination is more important than knowledge.

Knowledge is limited. Imagination encircles the world.

- Albert Einstein

University of Alberta

ENERGY DISSIPATER FOR CONCENTRICALLY BRACED FRAMES:
BRACE MEMBER WITH COMBINED PROPERTIES OF METALLIC
STRUCTURAL FUSE AND FRICTION DAMPER

by

Alexander Melnik

A thesis submitted to the Faculty of Graduate Studies and Research
in partial fulfillment of the requirements for the degree of

Master of Science

in

Structural Engineering

Department of Civil and Environmental Engineering

Spring 2014
Edmonton, Alberta

Dedication

This thesis is dedicated to my parents for their love and support that made this work possible. It is my parents from whom I have learned to work hard, to strive for excellence and to dream.

Abstract

The main focus of this research is to develop and evaluate a high performance seismic energy dissipater for a concentrically braced frame that can be easily fabricated using common steel grades by a typical steel fabricator.

Developmental stage of the research has concluded that brace member with combined properties of metallic structural fuse and friction damper can achieve superior performance while being a cost-effective solution. An experimental program was conducted to evaluate hysteretic response of six configurations of prototype brace member. Physical tests demonstrate that proposed energy dissipater can sustain axial deformation of up to 140.0 mm under incrementally increasing cyclic load. Parametric study was performed using FEA to evaluate and postpone out-of-plane buckling within metallic structural fuse that was observed during the experiment.

Experimental program results demonstrate that developed seismic energy dissipater is capable of achieving high ductility and superior, in certain aspects, performance when compared to existing alternatives.

Acknowledgments

It gives me great pleasure to acknowledge the help of my supervisor Dr. J.J. Roger Cheng, who provided his guidance and support at each stage of this project. I am grateful for his decision to let me use my own idea as a foundation of a M.Sc. program – if it was not for Dr. Roger Cheng this research might have never became a reality.

The technical assistance and knowledge provided by Greg Miller and Cameron West was instrumental to the success of this project and is most appreciated.

I cannot find words to express my gratitude to my parents, Larisa and Oleg, and my sister, Kate, for the immense support and encouragement throughout the entire duration of this study. I would also like to thank the love of my life, Amanda, for her care, patience and understanding during very long nights I have spent doing research and writing this manuscript. These four people have spent countless hours reviewing my work, patiently listening to my presentations and providing very helpful and sometimes unexpected input. Their love and support is endless and it was them who motivated me, encouraged me and believed in me.

I would also like to thank my close friend, Aaron Manuel, for the invaluable feedback he provided on the quality, logic and writing style of this thesis.

The financial support provided by the NSERC Industrial Post Graduate Scholarship Program in partnership with Buckland & Taylor Ltd. is gratefully acknowledged and appreciated.

Table of Contents

List of Tables

List of Figures

List of Symbols

E	Young's modulus
F_u	Ultimate stress
F_y	Yield stress
h	Width of the Shear Link
h_0	Force applied to the Shear Link is defined through variable h_0 and is equal to yield resistance of rectangular steel section of thickness t and width h_0
h_s	Building story height
M	Applied moment
M_p	Plastic moment of section
R_d	Seismic demand reduction factor due to SFRS ductility
R_y	Factor applied to F_y to estimate probable yield stress
t	Thickness of the Shear Link
V	Applied shear force
V_{ALL}	Allowable shear force based on von Mises yield criterion
u_m	Peak deformation capacity of the prototype energy dissipater
u_y	At yield deformation capacity of the prototype energy dissipater
x	Axis direction parallel to centerline of (assumed) Prototype Brace
y	Axis direction parallel to centerline of un-deformed steel Shear Link and perpendicular to centerline of (assumed) Prototype Brace
z	Axis direction perpendicular to “x” and “y”
ε	Strain
ε_u	Ultimate strain
ε_y	Yield strain
μ	Ductility Factor

List of Abbreviations

AISC	American Institute for Steel Construction
ANSI	American National Standards Institute
ASTM	American Society for Testing and Materials
BRB	Buckling Restrained Brace
CBF	Concentrically Braced Frame
CSA	Canadian Standards Association
EDAQ	Electronic Data Acquisition (system)
EHL	Extended Hinge Links (Mullin, 2005)
FEA	Finite Element Analysis
LD	Limited Ductility
MD	Moderately Ductile
MTS	Material Test System
NBCC	National Building Code of Canada
SFDB	Self-Centering Friction Damping Brace (Zhu and Zhang, 2007)
SFRS	Seismic Force Resisting System
SMA	Shape Memory Alloy
YBS	(Cast Steel) Yielding Brace System (Gray et al., 2011)

1 Introduction

1.1 Problem Statement

Structural demands imposed on a structure under an earthquake are unique when compared to any other load cases given that they are applied as a ground motion and not an actual force. The ground motion serves as an excitation that results in a dynamic response of the entire structure, nature of which depends on the period of the structure and its damping capacity. For purely elastic structure, no damping takes place and lateral oscillations due to initial excitation will continue for an extended period of time and can potentially be amplified by subsequent ground motion input creating significant capacity demands within lateral force resisting system.

It was recognized that by allowing for controlled permanent deformation within lateral force resisting system under extreme earthquake event one will introduce energy dissipating properties / damping that will drastically reduce structural demands imposed by the ground motion. At the time of a significant earthquake permanent deformations of a seismic force resisting system (SFRS) are localized in a certain element, so-called energy dissipater. Given that traditionally braced frame is a very common and cost effective lateral force resisting system implemented in wide variety of structures, significant effort has been made to improve on its energy dissipating capabilities.

Two conceptually different approaches are typically used in laterally braced frames. One approach focusses on brace frame configurations that intentionally create eccentricity between centroids of brace members by connecting them to a linking overhead beam at an offset. Such configuration creates significant shear force within a beam link region during the seismic event. Beam link eventually yields in shear allowing for relative vertical displacement of connected brace ends which introduces ductile storey drift within a structure. National Building Code of Canada recognizes significant level of ductility achieved by such brace frame configuration and assigns a corresponding seismic demand reduction factor R_d of 4.0 (National Research Council Canada, 2010). There is a significant drawback to this approach of energy dissipation within a braced frame. Energy mechanism is such to introduce permanent “kinks” within the floor beam due to induced shear deformation in the linking region. Complete or partial replacement of the floor beam within and eccentrically braced frame can be fairly challenging (Gardiner, S. et al., 2013). Due to economic considerations this sort of repair is likely to be done only if structural integrity of the braced frame is compromised. In other cases a permanent localized deformation of the floor system above structurally sound but “activated” eccentrically braced frame is likely to be present. Another approach is to dissipate energy within a diagonal element of a concentrically braced frame (CBF). Traditionally in a CBF, buckling of the brace itself acts as an energy dissipating

mechanism of SFRS. Past research indicates that buckling mechanism of energy dissipation possesses a limited ductility when subjected to seismic force and can potentially fracture after several cycles of ground motion (Tang and Goel, 1989). Alternatively energy dissipation can be confined to axial deformations in a brace/gusset plate assembly that do not exhibit any out-of-plane behaviour. Gusset plate itself can act as an effective energy dissipater (Mullin, 2005). A prototype gusset plate has been successfully tested and evaluated; however relatively large dimensions of a physical specimen when compared to a traditional gusset plate can potentially limit its use in certain scenarios.

Alternatively introduction of deformation capacity within a brace member could result in a SFRS that is very effective in dissipating energy of the earthquake, visually pleasing and easy to maintain / replace after a major earthquake. Several proprietary solutions exist on the market today that allow for large axial deformation of the brace member in a concentrically braced frame. Some of those are Buckling Restrained Brace and cast steel Yielding Brace System. Energy dissipaters mentioned above require specialised manufacturing procedure and/or equipment and, as a general rule, cannot be easily fabricated by a typical steel fabricator.

A brace member that is easy and inexpensive to manufacture and which, at the same time, performs equally good or better to existing energy dissipating solutions for a CBF will allow for high-performing SFRS being incorporated into more designs in future.

1.2 Objectives and Scope

The objective of this research project is to design and evaluate an alternative seismic energy dissipater for a CBF that can be easily manufactured by a typical steel fabricator and that performs equal or better when compared to existing alternative energy dissipaters for an identical lateral load resisting system. Load versus displacement response of a proposed prototype brace should exhibit defined stiffening behaviour over the full range of ductility to encourage uniform residual story drift distribution over the full height of the structure. In addition, SFRS that incorporates the proposed prototype brace shall exhibit high stiffness at service load which is essential to eliminate damage to non-structural components, such as cladding and partitions, during low seismic conditions. During strong earthquakes, the prototype brace has to possess large deformation capacity to effectively dissipate energy of the ground motion. From the maintenance perspective sacrificial components of the prototype brace shall be easily replaceable after major earthquake in order to reduce repair costs associated with bringing building back in service after a major seismic event.

Scope of the research includes extensive evaluation of existing energy dissipating mechanisms of the CBF. When analyzing and evaluating existing energy dissipating mechanisms a particular attention is paid to their overall performance, ease of fabrication and drawbacks if any. Based on

the detailed evaluation of existing systems, an optimal energy dissipater is arrived at, and is followed by an experimental program that incorporates physical tests of the prototype. Discussion and evaluation of the test results is a concluding part of this research.

Development of the prototype brace will evaluate several proposed energy dissipaters with the help of finite element analysis models and practical considerations. An energy dissipater that best aligns with derived design criteria is to be designed, detailed and fabricated.

The experimental program will focus on physical testing of a prototype brace member. Loading history will be derived to reflect cyclic nature of the seismic force. Several loading histories will be considered; one of the loading histories suggested by North American design codes for testing of components of seismic force resisting systems will be adopted and if necessary modified to accommodate specific requirements of the experimental program. Test results obtained will be used to analyze performance characteristics of the developed prototype energy dissipaters.

1.3 Organization of Thesis

Organizational structure of the thesis is to be consistent with the chronologic timeline of the research project. Each chapter within the body of text corresponds to an associated research task.

Chapter 2, literature review is written as a concluding summary of the performance evaluation of existing energy dissipaters used within a CBF.

Chapter 3 outlines development stages of the prototype energy dissipaters that will correspond to certain design criteria.

Chapter 4 focusses on specimen fabrication, design of the experiment as well as all required auxiliary tests.

Chapter 5 presents test results obtained from the experimental program, along with necessary observations and low level analysis required for interpretation of the results.

Chapter 6 analyses, interprets and evaluates results obtained in Chapter 5. In addition, the performance of the prototype brace is evaluated under the scope and framework of relevant Canadian Design Standards and suggestions are made on further improvements to the design of the prototype energy dissipater. Finite element analysis required to evaluate, understand and improve the behaviour of sacrificial components of prototype brace is performed in Chapter 6 as well.

Lastly, summary, conclusions and recommendations are presented in Chapter 7.

2 Literature Review

2.1 Introduction

Traditionally, concentrically braced frames (CBF) dissipate the energy of an earthquake through buckling of brace members. Even though this energy dissipation mechanism proved to be efficient in cases that require SFRS to be of low or moderate ductility it has several drawbacks.

Inelastic response of such SFRS in tension and compression has significantly different corresponding force and deformation capacities. In addition to that, buckling of the brace places increased capacity requirements on a gusset plate connection as well as adjacent structural elements of the frame. Out-of-plane behaviour of the brace member can cause damage to non-structural wall partitions and/or cladding, which can create a potential safety hazard for the building occupants.

Several alternative mechanisms have been proposed to mitigate unwanted behaviour of a CBF that is subjected to a seismic load.

- Buckling restrained brace (BRB)
- Cast steel Yielding Brace System (YBS)
- Self-Centering Friction Damping Brace (SFDB)
- Friction damping devices
- Energy dissipation within gusset plate

Any of the given mechanisms does not rely on buckling of the brace member. Furthermore, it provides alternative methods of energy dissipation that result in a more symmetric hysteretic response.

In this chapter, the behaviour (and its shortcomings) of a traditional SFRS that utilizes buckling of the brace will be discussed in detail. In addition, a review of each of the above mentioned alternative methods of energy dissipation in a CBF is to be provided as well.

2.2 Concentrically Braced Frames from the Perspective of Canadian Design Standards

Concentrically braced frames that rely on buckling of the brace member as an energy dissipating mechanism can be classified either as a Limited Ductility (LD) braced frame or a Moderate Ductility (MD) braced frame (CAN/CSA S16-09, 2009). In terms of energy dissipation, a seismic demand reduction factor due to SFRS ductility R_d for LD CBF can be set to 2.0 and R_d of MD CBF is 3.0. In order to achieve R_d of 3.0, CBFs need to satisfy rigorous detailing and demand requirements as well as implementation limitations (CAN/CSA S16-09, 2009). These points above

indicate that a typical CBF that utilizes buckling of the brace member as an energy dissipating mechanism can achieve limited deformation capacity that in turn increases demand on the structure due to seismic force and drives overall construction costs up.

Improvement in behaviour of CBF due to addition of an energy dissipater is recognized by CAN/CSA S16-09 (2009). This design standard focuses on the use of BRB as an energy dissipating mechanism, recognizing that it can provide substantial deformation capacity that is stable and repeatable after many hysteretic cycles. The equivalent seismic demand reduction factor due to ductility of the SFRS that implements BRB is set to 4.0, which is second only to Ductile Moment Resisting Frame and Ductile Plate Wall that has $R_d = 5.0$.

CAN/CSA S16-09 (2009) does not acknowledge other existing energy dissipaters alternative to buckling restrained braces; however it does provide requirements for physical testing of BRB, which in turn can be potentially applied to other energy dissipating mechanisms.

2.3 Behaviour of a Concentrically Braced Frame under Seismic Load

The behaviour of a brace member (or braced frame) is well understood and is backed by extensive research in the past (Wakabayashi et al., 1977) and more recent years (Tremblay, 2002). A typical hysteretic response of a brace member (and frame) is shown below.

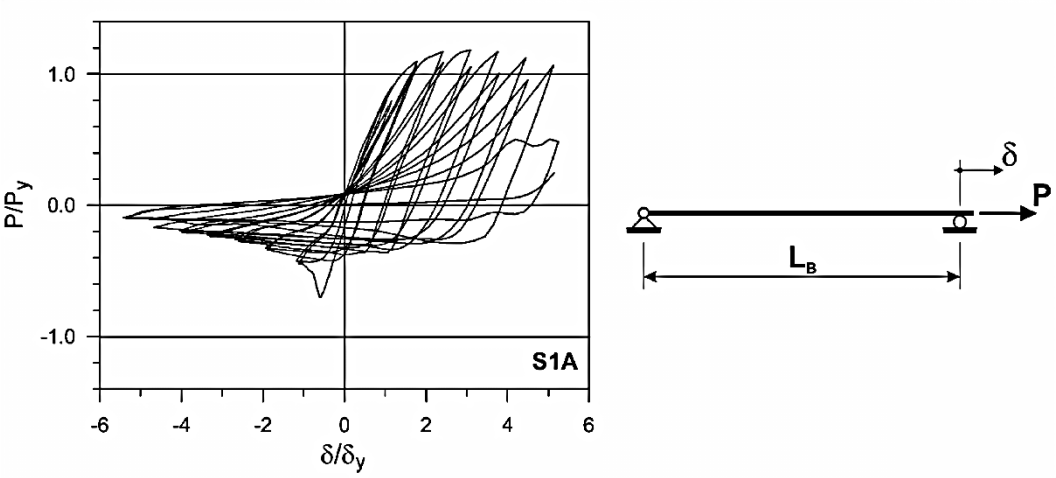

Figure 2-1: Force - Displacement Response of a Typical Brace Member (after Tremblay, 2002)

An important characteristic of this response is the fact that it is highly unsymmetrical due to extensive buckling of the brace (Wakabayashi et al., 1977), which creates certain design challenges. However, several successful models/design criteria have been developed to accurately predict behaviour and capacity of CBF under the seismic load (Perotti and Scarlassara, 1991).

Even though the mechanics of CBF are well understood, there are several reasons why one would want to improve on behaviour of CBF under seismic load.

Due to the common detailing practice, brace in a CBF is likely to buckle out-of-plane of the frame. Occasionally, it can cause damage/collapse of (sometimes) bulky non-structural partitions (Tremblay, 2002) which might endanger the lives of building occupants.

Lateral ductility of a typical CBF is low when compared to another SFRS such as moment resisting frame or BRB system (CAN/CSA S16-09, 2009). Higher stiffness of CBF decreases the natural period of a structure, which in turn increases the seismic forces that act on the entire building (Veletsos et al., 1965).

Overall CBF that utilizes brace buckling as an energy dissipating mechanism is a system that is well understood. However, it is susceptible to low cycle fatigue failure and can potentially increase the cost by driving up seismic demands imposed on other components of a building. Also care must be taken to ensure that out-of-plane buckling of the brace will not endanger the occupants of the structure.

2.4 Existing Energy Dissipaters within Concentrically Braced Frame

2.4.1 Energy Dissipation within Gusset Plate Connection

A gusset plate connection, designed using conventional guidelines, does not exhibit significant ductility at fracture of the connection in tension. In fact a typical 600 mm x 600 mm gusset plate subjected to cyclic loading could undergo only a limited deformation of maximum 13 mm before it would rupture in tension (Rabinovitch and Cheng, 1993). Such deformation is not sufficient to effectively dissipate and redistribute the energy of an earthquake. However in conventional construction, gusset plate ductility is not a critical factor since the majority of energy dissipation occurs through yielding and buckling of a brace member.

Several researchers attempted to change such trend and increase ductility of a gusset plate in order to make it an effective primary energy dissipater. Few approaches have been used, two of the more common ones are: use of low yield-ductile steel in a gusset plate and an engineered configuration of the gusset plate shape that would allow for more deformation.

Incorporation of a more ductile steel as a material for a gusset plate has resulted in increased ductile deformation. A conventionally designed stiffened 500 mm x 500 mm gusset plate manufactured using low yield point steel with F_y = 100 MPa and ε_u = 40% could accommodate a stable hysteretic deformation of up to 20 mm with maximum tensile load of 1150 kN (Chen and Chang, 2012). An identical gusset plate that employs a slot-type restrainer instead of a stiffener to eliminate buckling has an increased deformation capacity of up to 25 mm (Chen and Chang, 2012).

Evidentially, use of highly ductile steel does increase the deformation capacity of the gusset plate. However, such increase is insignificant when compared to deformation demands suggested by

allowable design drifts of buildings. For example even a high importance structure is expected to undergo up to 2% drift which would translate to ~60 mm of brace elongation for a typical 3700 mm x 6000 mm braced bay (National Research Council Canada, 2010).

An alternative approach to achieve higher deformation capacity is to modify gusset plate configuration. A very effective way to do so is by introducing strategically placed openings that will create so-called Extended Hinge Links (EHL) (Mullin, 2005). In such gusset plate configuration, out-of-plane behaviour of a gusset plate is to be restricted via use of cover plates which also act as friction dampers.

In this case, mode of failure of a gusset plate will transform from tensile rupture to bending yield. The ductility and strength of such gusset plate is governed by its size (the longer the links are, the more deformation is provided via bending), which makes it significantly larger than a conventional gusset plate of similar resistance. A 850 mm x 850 mm gusset plate that utilizes EHL provides maximum resistance of approximately1000 kN with maximum deformation of 120 mm in tension (Mullin, 2005). It is also worth noting that even after all EHL were fractured, the gusset plate assembly still resisted a significant load (around 600 kN) through friction and bearing while continuing to allow for significant deformation (Mullin, 2005).

Even though this particular energy dissipating system can accommodate large ductility demand, it has several drawbacks. The most obvious is the size – geometric configuration of EHLs results in a larger plate when compared to conventional gusset plates. Another area for improvement is poorly controlled boundary conditions of EHLs when more than one of them is present in a plate, which result in axial load within the link that leads to premature link rupture (Mullin, 2005).

2.4.2 Buckling Restrained Brace (BRB)

Buckling restrained brace (BRB) is a composite brace member that consists of a steel core. It dissipates energy through yielding in tension and compression, and a concrete filled steel tube that prevents buckling of the core (Watanabe et al., 1988). A schematic diagram as well as a typical hysteretic loop of a BRB is shown below (Tremblay et al., 2006).

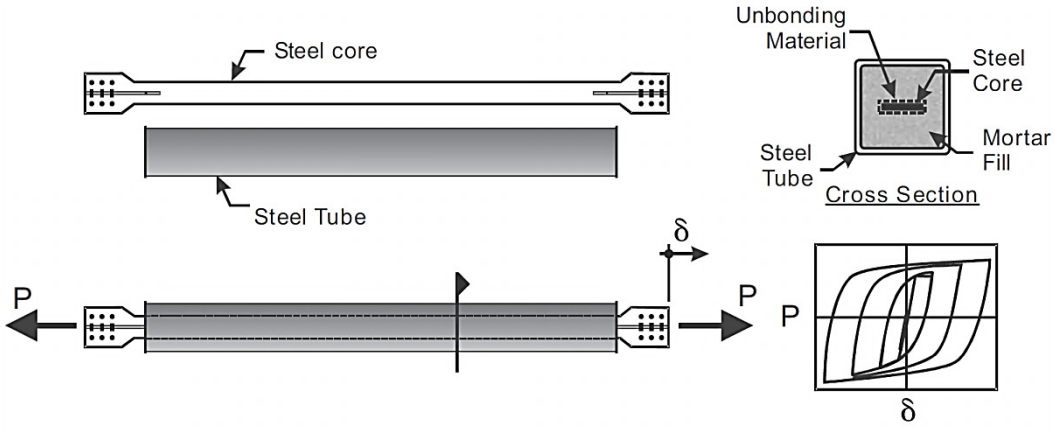

Figure 2-2: Schematic diagram of buckling-restrained brace (after Tremblay et al., 2006)

BRB has been in development since 1970's, when Kimura et al. (1976) tested a prototype brace member incased in steel tube and mortar. Even though the study reports few stable hysteretic loops, it has been noted that due to deterioration /deformation of the mortar, after a few cycles the restraining effect diminished, and the steel core buckled under compression loads that followed (Kimura et al., 1976).

It has been shown that if the buckling strength of a restraining steel tube is larger (approximately 1.5 times) than the yield strength of the steel core, then buckling of a BRB will not occur and the assembly will behave in a stable manner under tension and compression (Watanabe et al., 1988).

In 2003, Sabelli et al. conducted an extensive inelastic analysis of several configurations of braced bays that incorporate buckling restrained brace in comparison to similar traditional CBFs that rely on buckling of the brace member for energy dissipation. Five configurations of concentrically braced frames and two configurations of frames that utilize BRB for both three and six story structures have been analyzed. A nonlinear structural analysis software SNAP-2DX (Rai et al., 1996) has been utilized to evaluate the behaviour of traditional CBFs as well as braced frames that incorporate BRB (Sabelli et al., 2003). This particular study has shown that buckling restrained bracing system performs significantly better than traditional concentrically braced frames (Sabelli et al., 2003).

In the early 2000's Black et al. conducted a comprehensive study of five BRB specimens. The study focused on evaluating stability of the BRB, validating its energy-dissipating capability, and predicting the macroscopic hysteretic behaviour of the brace (Black et al., 2004). Test results have confirmed a ductile and stable hysteretic behaviour of the brace. Proposed Bouc–Wen model has proven to provide good prediction of overall behaviour of the brace. Overall, the study has confirmed that braced frame which incorporates BRB is a reliable, high performance alternative to traditional CBF and provides improved ductile performance during earthquake loading (Black et al., 2004).

Nevertheless, buckling restrained bracing system has a few potential drawbacks that can be attributed to its high post yield ductility. A fairly significant post-earthquake residual drift is one of them, as noted by some researchers (Uang and Kiggins, 2003). Also in case of BRB failure the braced frame loses its full capacity unlike, for example, EHL gusset plate or friction dampers SFRS.

2.4.3 Cast Steel Yielding Brace System (YBS)

Cast steel yielding fuse integrated into brace connection is a fairly new approach proposed by Gray et al. in 2010. In a proposed system, energy dissipation during cyclic load is concentrated in a socalled yielding finger (Gray et al., 2012) that undergoes plastic bending deformation. proposed connector incorporates a number of those "yielding fingers" that are , on one side, connected to a brace member and on another side to a splice plate that provides a "roller" boundary condition with displacement axis that is perpendicular to the brace axis (Gray et al., 2010). Such splice plate ensures that no tension occurs in the "yielding finger" during its bending. A schematic representation of such connector follows below.

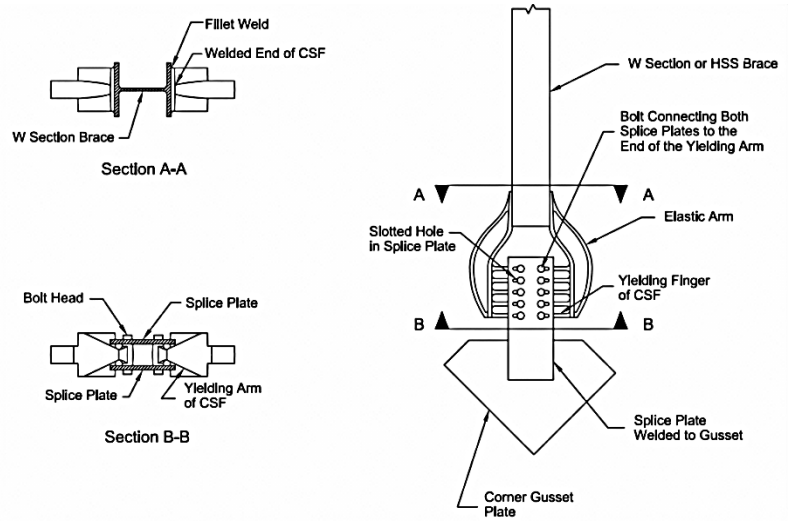

Figure 2-3: Cast steel yielding fuse schematic diagram (after Gray et al., 2010)

Full scale testing of cast steel yielding fuse has been carried out. Test protocol included four identical cast steel connection specimens. Two of the specimens were tested directly by application of tension/compression load, and two other specimens were tested within a full scale braced frame subjected to cyclic lateral load. Proposed cast steel connection was able to accommodate deformation of up to 120 mm, demonstrating stable and repeatable hysteretic behaviour (Gray et al., 2011).

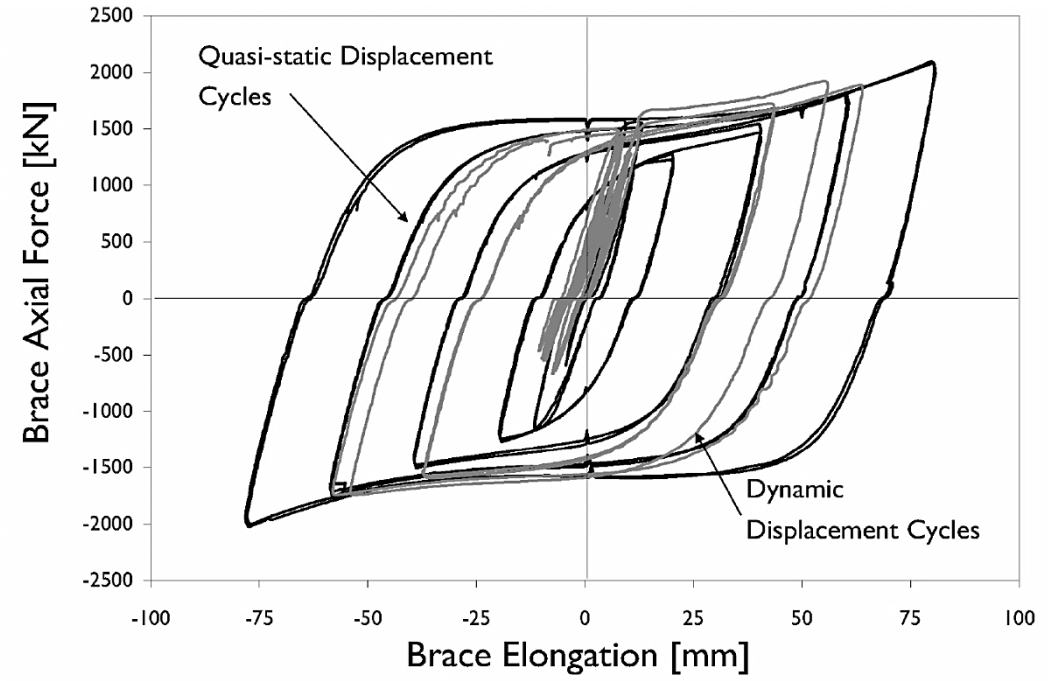

Figure 2-4: Hysteretic response of a cast steel yielding fuse prototype - full-scale frame test (after Gray et al., 2012)

Hysteretic response of such energy dissipater is very similar to BRB even though yielding mechanisms are different for those two SFRS (yielding in tension for BRB versus yielding in bending for YBS). It provides high ductility, is stable and repeatable (Gray et al., 2011).

Full scale testing of a braced frame that incorporates this particular cast steel energy dissipater has confirmed that such SFRS mechanism meets and exceeds performance requirements imposed on buckling-restrained braces by Appendix T of AISC 341-05 *Seismic Provisions for Structural Steel Buildings* (Gray et al., 2011).

2.4.4 Friction Damped Brace Frame

Friction damped brace frames provide a viable alternative to seismic force resisting systems that utilize inelastic deformation in either primary structural members (concentrically and eccentrically braced frames) or energy dissipaters as described above. Friction damping device dissipates energy of the earthquake through sliding preventing buckling of the braces in a CBF it is incorporated in.

A variety of friction-based energy dissipating devices have been proposed; one of the more common friction dampers used in North America has been developed by Avtar Pall (Pall and Pall, 1996). It is important to control surface properties of the friction dampener. It has been shown that untreated or metallized surfaces provide the highest initial slip load, however their overall behaviour is very unpredictable; on the other hand use of brake lining pads or sandblasted steel surfaces has shown much more consistent results (Pall, 1979). Use of polyethylene coating on a

steel surface has provided fairly consistent hysteretic response with low slippage load. However, the dynamic friction resistance deteriorated over time due to introduction of polyethylene dust between surfaces and loss of pretension due to deterioration of the polyethylene layer (Pall, 1979). It is possible that such deterioration can be significantly reduced by using composite materials similar to nickel polyethylene composite (Abdel Hamid and Ghayad, 2002).

Hysteretic behaviour of a friction damper that utilizes brake lining pads is symmetric, stable and follows a nearly perfect elastic-plastic load/displacement path (Pall and Marsh, 1982).

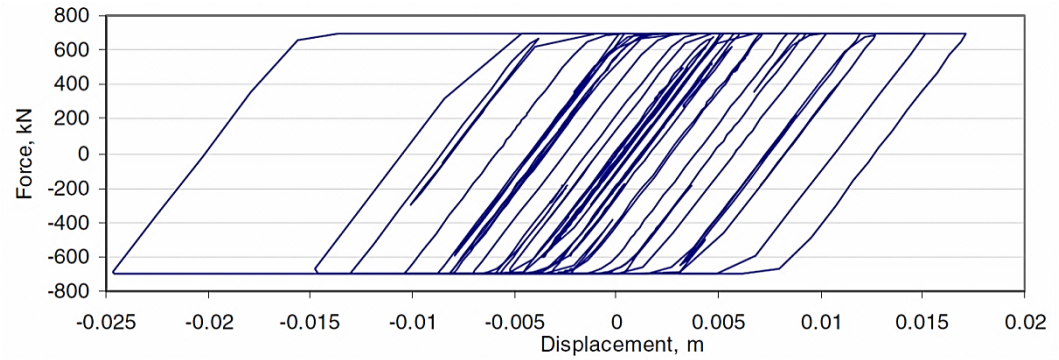

Figure 2-5: Hysteretic response of a friction damper in a diagonal brace (after Pasquin et al., 2002)

Up to date, seismic induced behaviour of lateral load resisting systems that incorporate friction dampers has been thoroughly evaluated. One of the large scale tests evaluates behaviour of a nine-story one quarter scale steel frame that was loaded with additional weight to simulate real-world loading conditions (Aiken et al., 1988). According to the testing protocol, the frame, which was placed on a shaking table, was subjected to ground motion signals of several earthquakes. Depending on the magnitude of the earthquake, friction dampers were capable of dissipating approximately 70% of the energy of ground motion (Aiken et al., 1988).

Given favorable test results and relatively low cost of friction dampers, they have been extensively used for retrofit of existing buildings with moment resisting frames as well as new construction (Pall and Pall, 1996).

It is important to note that even though friction dampers do demonstrate good hysteretic behaviour, commercially available friction dampers cannot accommodate deformations comparable to BRB or cast steel YBS mentioned in previous sub chapters. In addition, the friction damper that exhibits elastic-to-perfectly plastic hysteretic properties can cause story drift concentration at lower levels of the building (Sabelli et al., 2003) when subjected to seismic force (note that while Sabelli et al., 2003 evaluated behaviour of BRB, an elastic-perfectly plastic hysteretic model was used in his study) .

2.4.5 Self-Centering Friction Damping Brace (SFDB)

Use of superelastic shape memory alloys (SMA) as an element of a SFRS has been gaining traction within the structural engineering research community. A unique property of SMA is to recover the plastic deformation via temperature treatment; the hysteretic behaviour of a rod or wire made of SMA has a distinctive flag-shaped loop (DesRoches et al., 2003). Even though the properties of a shape memory alloy can be very beneficial (i.e. it can provide self-centering capabilities), its pseudoelastic properties (Tamai and Kitagawa, 2002) can have a negative effect on energy dissipating qualities. For relatively large deformations the alloy will remain elastic and thus no energy dissipation will occur through plastic deformation (Zhu and Zhang, 2007).

In order to improve on the energy dissipating capabilities of the seismic fuse that incorporates SMA, a unique energy dissipating mechanism was created that combines a friction damper and a SMA metallic fuse (Zhu and Zhang, 2008). Two solid blocks of steel are bolted to each other in a way that allows block A to slide on the surface of block B, given that block B has a long slot along its length (Zhu and Zhang, 2008). The SMA metallic fuse is introduced in a form of stranded super-elastic Ni-Ti alloy wires that are attached to both blocks via use of anchoring fixtures (Zhu and Zhang, 2008).

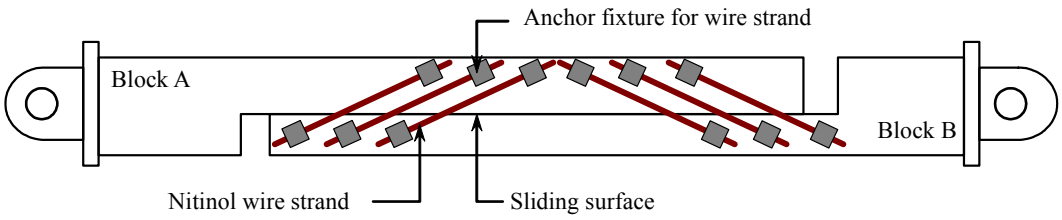

Figure 2-6: Self-centering Friction Damper; Schematic Diagram (after Zhu and Zhang, 2007)

The friction mechanism of the damper effectively dissipates seismic energy, while the SMA wire strands provide self-centering characteristics of the energy dissipater and account for a certain portion of energy dissipation within the fuse (Zhu and Zhang, 2008).

Cyclic tests of a scaled Self-Centering Friction Damping Brace confirmed nearly ideal self-centering behaviour of the prototype brace. Tests have shown that increased friction improves energy dissipation capacity of the SFDB significantly. There was no strength degradation or significant strain accumulation observed in Ni-Ti alloy wire strands even after 50 cycles of loading which correlates to the expected properties of the alloy and allows SFDB to potentially sustain several earthquakes before replacement of the damper (Zhu and Zhang, 2008).

Nonlinear time history and push over analysis of prototype buildings that incorporate SFDB have confirmed significant reduction of inter-story drift when compared to similar structure that utilizes

buckling restrained bracing as an energy dissipating mechanism. SFDB was capable of providing good energy dissipating properties that ensured that maximum story drifts and peak accelerations were comparable to BRB equipped buildings (Zhu and Zhang, 2008).

2.5 Literature Review Summary

Several alternative seismic energy dissipaters for CBF have been already developed and are used to varied extent.

Most commonly used buckling restrained brace proved to be very effective, however, it does require specialized manufacturing facilities for its fabrication, has practically unlimited post yield ductility and, if ruptured, loses its entire capacity. Cast steel YBS demonstrates very good hysteretic behaviour that is similar to one of BRB; unlike BRB a fracture of one of its links will not lead to complete failure of the brace. Unfortunately, geometric configuration of the energy dissipater does result relatively large overall assembly. In addition, cast steel YBS does require specialized manufacturing equipment. Gusset plate with enhanced deformation capacity (Mullin, 2005) does have a benefit of being a high performance, cost-effective solution that engages inelastic deformation of custom cut gusset plate in order to effectively dissipate energy of an earthquake. It can accommodate large deformation demand, can be easily manufactured by any steel fabricator and assembled using bolts either in shop or on site. Its geometric proportions might create certain challenges for a practical implementation and few design issues should be resolved to enhance life-to-rupture of the sacrificial component.

Overall the majority of energy dissipaters that exist on the market do have adequate level of performance, however, typically they either require highly specialized fabricator (BRB or cast steel YBS), have certain geometric constraints (cast steel YBS and modified gusset plate) or both (cast steel YBS). Friction based devices does not have shortcomings similar to those mentioned above; however its elastic to perfectly plastic hysteretic behaviour can potentially have an undesirable impact on the overall structure response.

This research will focus on developing an energy dissipater for a concentrically braced frame that will further develop strengths of existing systems while mitigating some of their shortcomings. Particular focus will be given to ease of fabrication, large deformation capacity, hysteretic behaviour that will encourage redistribution of residual story drift and resistance to complete brace member capacity loss. In addition, compactness of the prototype will be considered. It is of an interest to develop an energy dissipater that performs equal or better when compared to existing solutions and can be easily manufactured by a typical steel fabricator using common steel grades.

3 Developing Energy Dissipater Prototype

Given a lack of all-steel seismic energy dissipaters that can be easily fabricated from common steel grades and steel profiles, the development stage of this project did not have sufficient prior research to rely on and had to be executed from basic engineering principles with end goals in mind.

The seismic energy dissipater discussed herein is a product of a thorough development stage confined to certain parameters. At the very early stage of the research project the long standing goal was to come up with a seismic force energy dissipater for a CBF that can be easily manufactured by a general steel fabricator. Most of the commercially available energy dissipaters generally are highly specific and proprietary in their mechanisms. Such devices often demand customized manufacturing techniques and/or materials which would require a certain premium in a price and impose certain constrains on mass manufacturing (take for example cast steel yielding device or BRB). The purpose of this research is to develop a cost-effective and practical solution that satisfies certain design requirements. Those requirements are summarized in a section 3.1 of this chapter.

Concept development of the prototype started with a design philosophy that system providing rigidity and confining deformation of the brace in the direction of its axis should be separated from elasto-plastic energy dissipating mechanism. Such an approach would ensure in-plane and out-of-plane stability of the brace member without introducing complications to the individual elements of the energy dissipater. Additionally, it will provide a certain level of redundancy to the energy dissipating mechanism. For instance, if elasto-plastic component of the energy dissipater fails it would not necessarily cause failure of mechanism as a whole.

One way to constrain deformation to one direction only is via use of slotted bolted connection. A pair of steel plates of sufficient thickness that incorporate long slots can be used to connect two segments of a brace in such a way that would allow for sliding with respect to each other. Such an arrangement would provide a means of stability to the brace while allowing for significant axial deformation. One must note that use of slotted plates as a means of seismic energy dissipation has been explored before, however, as a general rule, it was limited to providing limited deformation capacity at the brace end connection (Pall and Pall, 1996).

Slotted bolting connection proposed above acts similarly to rigid sliding rails that would guide the deformation of a yielding energy dissipating mechanism of the system. Provided proper attachment points are present, one can use various metallic yielding mechanisms for energy dissipating purposes. A few options were explored in the scope of this research and their thorough evaluation is to follow.

The rest of this chapter will focus on the development of design criteria for the prototype, finalizing the overall concept, and evaluation of several alternatives for ductile metallic seismic fuse.

3.1 Design Criteria

Following section outlines design criteria selected for the prototype energy dissipaters.

3.1.1 Design Criteria Based On North American Design Standards

Desired behaviour of the brace prototype developed is to be somewhat similar to behaviour of a BRB. Corresponding design requirements and guidelines provided by North American design codes are used as a basis for the design criteria of a prototype energy dissipater developed herein.

3.1.1.1 National Building Code of Canada (2010)

The National Building Code of Canada (NBCC, 2010) has relatively limited information regarding the use of energy dissipaters. Nevertheless it does acknowledge the ductility capacity of the BRB SFRS. A minimum R_d factor of 4 can be used during the static procedure outlined in NBCC for a braced frame that incorporates BRB. With that in mind the prototype energy dissipater should have a ductility factor that is at least equal to or exceeds $R_d = 4.0$.

In addition NBCC provides guidelines on allowable story drifts during a design seismic event. Even though allowable story drift does not directly define energy dissipating properties of the SFRS it provides limits for the deformation that can be used for energy dissipation. In other words, prototype energy dissipaters should be able to achieve and if necessary exceed story drift limits outlined by NBCC. The maximum story drifts are as follows (National Research Council Canada, 2010):

- $0.01 \times h_s$ for buildings classified as Post-Disaster;
- $0.02 \times h_s$ for buildings classified as High Importance;
- $0.025 \times h_s$ for all other buildings.

3.1.1.2 CAN/CSA S16-09 (Design of Steel Structures)

Canadian steel design standard has a separate section dedicated to designing SFRS that incorporates BRB (CAN/CSA S16-09, 2009). Below is a brief summary of the performance based requirements from CAN/CSA S16-09.

"Buckling restrained bracing shall resist, without buckling and with positive strain hardening slope, force and deformation demands that correspond to building achieving twice the design story drift" (CAN/CSA S16-09, 2009 Section 27.8.6). With regards to the testing protocol, CAN/CSA

S16-09 references to Appendix T of AISC 341-05 *Seismic Provisions for Structural Steel Buildings* which will be discussed next.

3.1.1.3 ANSI/AISC 341-05 (Seismic Provisions for Structural Steel Buildings)

Handbook Seismic Provisions for Structural Steel Buildings (ANSI/AISC 341-05, 2005) has very similar guidelines for design of frames fitted with buckling restrained braces to CAN/CAS S16-09. AISC 341-05 also includes a very detailed guideline on requirements for testing procedure of BRB specimens. Exact test protocol outlined in the appendix will be discussed in detail in chapter 4. It is worthwhile to note that testing protocol specified by AISC 341-05 is consistent with requirements of CAN/CSA S16-09 and in slow increments increases deformation of the brace specimen until the specimen completes two cycles at deformation amplitude that corresponds to twice the design story drift. As per ANSI/AISC 341-05 Appendix T design story drift cannot be less than $0.01 \times h_s$ which is consistent with NBCC (2010).

3.1.2 Design Criteria Based on Literature Review

Careful evaluation of alternative energy dissipating mechanisms for CBFs has uncovered several key parameters that have to be incorporated into development of the prototype energy dissipater. Meeting these criteria will ensure that not only this particular prototype brace will match the performance level of the competing systems but will also circumvent several drawbacks discussed in the literature review.

1. **Proposed energy dissipater should be easily and cost-effectively manufactured by a general steel fabricator using common steel grades.** Ease and low cost of manufacturing is crucial for wider use of an engineered structural element. Optimal hysteretic behaviour of an energy dissipater is important. However, it is not a defining factor for acceptance of a new SFRS. Design philosophy behind developing this energy dissipater is to optimize damping and hysteretic properties of the structural element while ensuring that it can still be manufactured by a wide range of steel fabricators.
2. **Proposed energy dissipater must not be susceptible to catastrophic failure under any reasonable circumstances.** Engineered properties of energy dissipating mechanisms such as BRB or cast steel yielding device do prove to be excellent at dissipating energy of an earthquake. At the same time in an unlikely but nevertheless possible scenario of failure, such an element would see its capacity decrease to zero and the energy dissipater would no longer provide resistance to seismic force. As mentioned in the literature review, experimental tests of BRB, for example, have shown that specimen can sustain as many as 17 cycles of 2% strain prior to rupture (Black et al., 2004). The study, however, did not account for potential influence of fatigue that would take place in a core of the brace subjected to tension – compression loads under SLS condition. Hence, in a real life scenario buckling restrained

brace might not be able to withstand as many cycles of deformation as the tests suggests, and when it fractures a brace bay that incorporates it will not provide any resistance to lateral story drift induced by the earthquake.

3. **Load versus displacement curve of energy dissipater should exhibit defined strain hardening behaviour to encourage redistribution of the residual story drift over the full height of the building.** When evaluating an inelastic response and behaviour of a structure that uses braced bays with BRB, the following phenomenon was noted. A structure incorporating seismic damper that exhibited elastic-to- perfectly plastic hysteretic properties experienced story drift concentration at lower levels of the building (Sabelli et al., 2003) when subjected to a seismic force that would correspond to a major earthquake. Such behaviour is due to energy dissipater becoming unstable when its capacity is reached (i.e. deforms with no further input of force) providing natural location for damage concentration. Such damage concentration would become more defined as the input force increases and possibly exceeds the original design earthquake force (Sabelli et al., 2003). Carefully engineered stiffening that takes place after reaching the design capacity will assist in distributing seismic force demand through the entire height of the building. One could draw a parallel between this phenomenon and base isolation of a building in order to reduce design seismic demand. Once design capacity of a base isolator is reached it will become a location for deformation concentration and energy dissipation, passing a fraction of the seismic energy to higher levels of the structure (Kelly, 1986). If a base isolator becomes stiffer (or if in our case prototype energy dissipater exhibits stiffening after a yield point) a larger fraction of seismic energy will be passed to and dissipated by upper stories of the building, making sure that residual story drift is uniformly distributed along the full building height. That is why a controlled stiffening of the proposed energy dissipater is an important design criterion to be incorporated.
4. **High stiffness at service loads and significant ductile deformation capacity at ultimate limit states** is an essential criterion for an energy dissipater in a CBF. For serviceability considerations, one must limit lateral story drift to an acceptable level that will ensure that no damage is done to non-structural elements of the building at a typical load (i.e. moderate earthquake load). At the ultimate limit states (under strong earthquake load), controlled lateral story drift is essential to successfully dissipate seismic energy transferred to the structure through ground motion. Achieving both those parameters at the same time can be fairly challenging – for example a stiff structure will likely not provide sufficient deformation capacity and a more slender SFRS will cause excessive story drifts causing damage to non-structural components such as architectural cladding. An alternate approach is needed to ensure that relative stiffness of the energy dissipater will vary significantly under service and ultimate limit states.

5. **Proposed energy dissipater is to be re-usable even after a major earthquake.** A braced frame that incorporates the proposed energy dissipater should have a capability to be brought back in service without a need for replacing the brace itself. This would involve replacing disposable fuse elements of the energy dissipater and realigning the brace member to eliminate residual story drift. Care must be taken when designing the brace prototype to ensure that both conditions can be met – in other words to ensure that fuse element is to be attached to the energy dissipater with removable fasteners and that energy dissipater incorporates a rigid framework that will allow for further realignment of the brace specimen. While self-centering energy dissipaters do exist and were successfully tested (Zhu and Zhang, 2008), a typical hysteretic loop of such a device would imply very little inelastic deformations when compared to its alternatives and is not as effective at dissipating seismic energy.

Design criteria discussed above are to be considered and implemented in the energy dissipaters developed within the scope of this research project.

3.2 Basic Concept Development

At the initial stage of the concept development a decision was made for the dissipater to incorporate both friction and inelastic deformations as the mechanism of energy dissipation within the brace prototype. Primary reason for this approach is that inelastic deformations within a steel fuse do require attachment restraints with certain level of rigidity, given that inelastic deformation can be fairly unstable if an accidental eccentric axial load or bending moment exists. One of the ways to provide such rigidity is via use of slotted holes that can act as guiding rails to the inelastic fuse elements. A certain amount of friction would be present in a slotted connection even if it was not explicitly used to dissipate energy. It is a logical step to quantify the friction contribution and use it as a supplement for energy dissipation. The inelastic component of the energy dissipating mechanism would ensure a certain level of strain hardening within the system as well as provide for additional resistance. A simplified concept of the brace prototype is illustrated below.

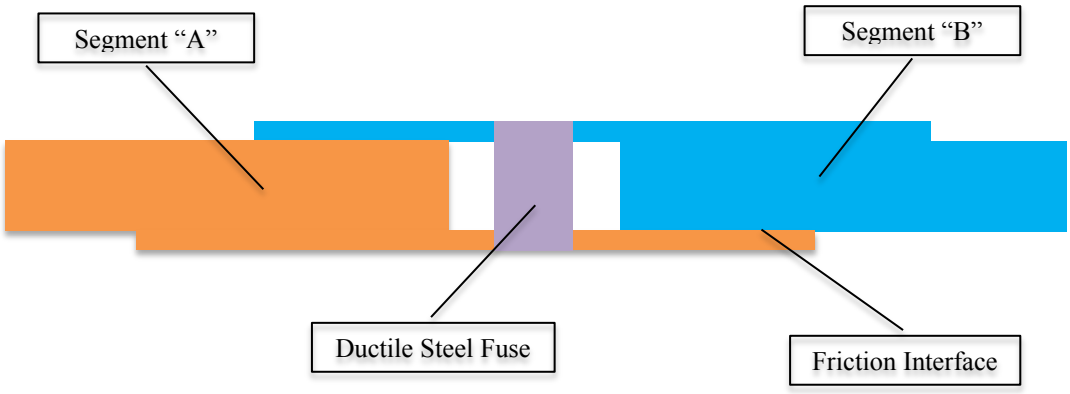

Figure 3-1: Energy Dissipater - Overall Concept

As one can see from the concept diagram in Figure 3-1, a brace prototype consists of two segments, segment “A” and segment “B”. Those two segments can slide with respect to each other as they are connected via use of a slotted connection (not shown). While sliding, said segments will apply a certain amount of shear deformation to the steel plate fuse that is connected to both segments. This conceptual diagram above describes starting point of the design development; arrangement of components changed at the end of the design process. In particular, the steel fuse was shifted from a position in between the segments to either side of the gap in order to better resist local moments that arise due to localized axial force eccentricities within the prototype brace.

From the conceptual stage, the brace prototype went through development of the two core mechanisms – friction and inelastic steel plate fuse. Each mechanism required a few iterations to arrive at a solution that satisfies design requirements.

3.3 Steel Plate Fuse Development

3.3.1 Finite Element Model – General Properties

The finite element analysis software ABAQUS was used extensively as a tool to assist verification of several fuse concepts. Unless noted otherwise, certain default values for the steel fuse plate model have been used.

- **A S4R Shell Element** has been used to model ductile deformations in the steel fuse plate. Detailed properties of the element are as follows (provided within ABAQUS): a 4-node doubly curved thin or thick shell, reduced integration, hourglass control, and finite membrane strains.
- **High performance low yield steel** properties have been used in the analysis for comparison purposes only. Initially steel with high ductility and low yield point of 100 MPa was planned to fabricate steel plate fuse. However, further FEA modeling concluded that widely available CSA G40.21 - 300W steel is capable of providing sufficient ductility to satisfy design criteria for a steel plate fuse. Prior to this decision being made, all preliminary modeling was carried out using properties of low yield – high ductility steel plate material; given models were used to compare different steel plate fuse concepts. The properties of the material used in the analysis are shown below.

Table 3.1: Material Properties - Low Yield – High Ductility Steel (Fy = 100 MPa)

Plastic Properties		Elastic Properties	
Stress [true]	Plastic Strain [true]	Young's Modulus	Poisson's Ratio
MPa	%	GPa	% / %
100.0	0%	200	0.3
101.8	4%		
190.0	11%		
235.0	16%		

250.0	22%
251.3	23%
252.5	25%
253.8	26%
255.0	28%
256.3	29%
257.5	31%
258.8	32%
260.0	34%
258.8	35%
257.5	37%
256.3	48%

- **Fuse plate dimensions** vary and depend on the steel plate fuse concept evaluated. At preliminary stage, thickness and/or dimensions of the fuse steel plate were varied independently trying to achieve optimal deformation capacity. At a later stage, the most successful concept was refined to a certain shape and thickness. However, all initial preceding concepts were left as is since they serve no other purpose but to demonstrate steel fuse plate design process.
- **Load applied** was specified in a Static Riks analysis step which is an arc-length analysis method that is incrementally changing applied load with increments small enough to find a determinate solution (Memon and Su, 2004). Load was applied along the (imaginary) axis of a brace prototype. Initial load value was 1.0 kN (arc length of 1.0) with an arc length increment that varied from 1xE-5 to 1xE+36 in subsequent steps.
- **Boundary conditions** ensured in-plane only deformations at the attachment points of the steel plate fuse; attachment points were placed in the expected bolt locations with restraints that imitate behaviour of the bolt (the only rotation allowed is about the axis of the "bolt"). Out-of-plane displacement of the steel plate at any other location but attachment points was allowed and expected.

3.3.2 Steel Fuse Plate Concept – Primarily Shear Deformation – Unstiffened

When considering possible options for steel plate fuse, initially shear deformation was considered as a primary way to accommodate ductility and provide required energy dissipation. This philosophy arose from knowledge that shear deformation generally is very stable, predictable and possesses a fair amount of ductility. In fact shear deformation is already successfully used in a eccentrically braced frame as a primary method of energy dissipation (Popov and Engelhardt, 1988). However, a few core differences in the nature of deformation can possibly limit the ductility of shear deformations of steel within proposed energy dissipater when compared to an eccentrically braced frame. One of them is the boundary condition of the fuse plate at the attachment points. Boundary conditions at the top and bottom of the fuse plate subjected to shear are rigid given that connecting bolts provide rotational fixity to the plate.

Properties of the model are as described in section 3.3.1; in addition to the thickness of 12 mm, the x – dimension of steel shear "link" is 300 mm, and the y – dimension of the steel shear "link" is 200 mm. Dimensions have been chosen to accommodate the size of an expected brace prototype segment beam (W200 x 59) and to minimize stress concentration at the inside corners, while keeping x – dimension of the shear "link" reasonably small.

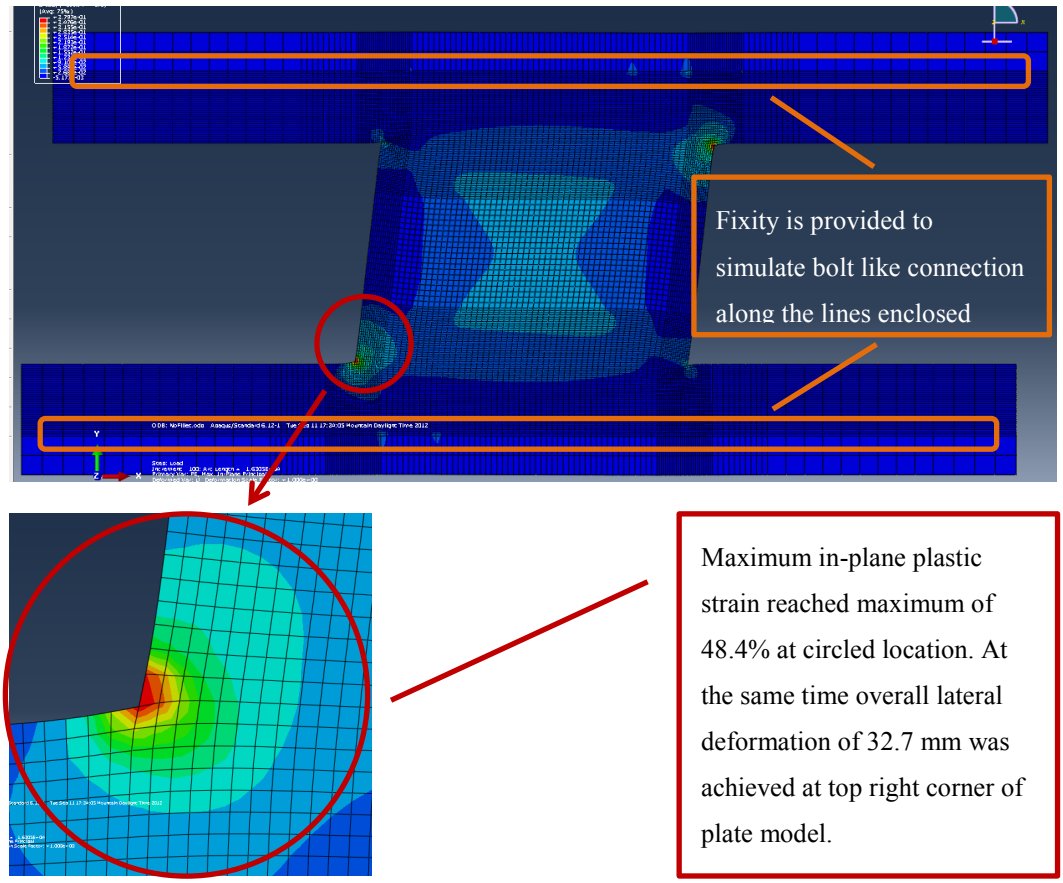

Figure 3-2: Steel Fuse Plate Concept – Primarily Shear Deformation – Unstiffened with 90° corner

As visible from the FEA model in Figure 3-2, there is significant strain concentration at the inside corners of the steel plate fuse. The primary cause for the stress concentration is the fact that while shear deformation is primarily relied on x – axis deformation of the steel fuse plate, a significant local moment about z – axis exists within the shear "link". In order to restrain rotation introduced by local moment a plastic strain concentration is developed within a steel plate fuse, as shown in Figure 3-3.

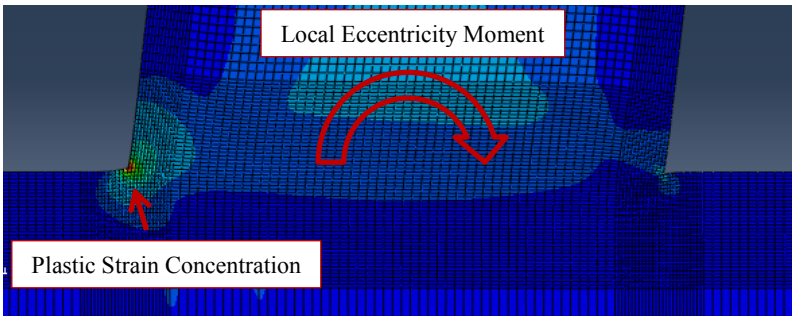

Figure 3-3: Steel Fuse Plate Concept – Source of Stress Concentration

Additionally, sharp 90 degree angle of the inside corned imposes certain geometric restrictions to stress flow which would contribute to the existing plastic strain concentration due to local moment alone.

In order to improve on lateral deformation of the steel plate fuse as a function of maximum strain, it was decided to incorporate fillets in the inside corners of the shear "link". Several fillet sizes were evaluated using FEA model. Properties of the model were the same as in case of steel plate fuse (shear only) that did not incorporate any fillet as shown in Figure 3-2. Evaluation has shown that the larger is fillet size the less strain concentration is present at the inside corner of a steel fuse plate, as shown in Figure 3-4.

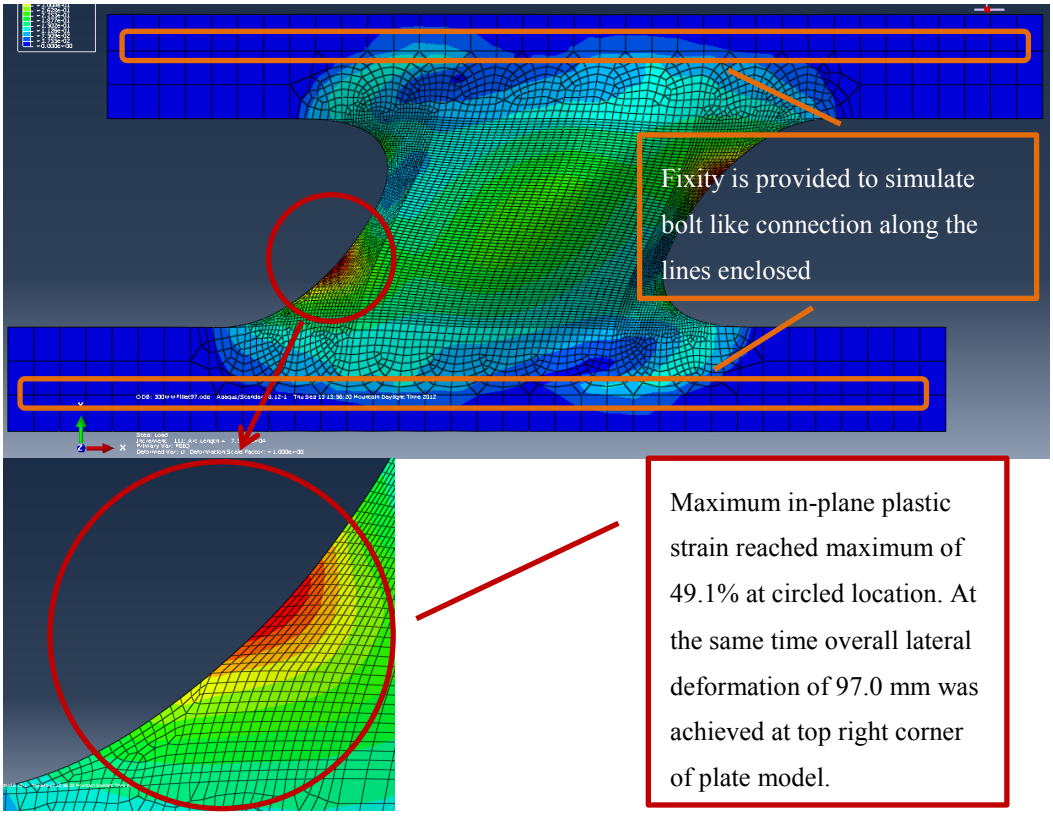

Figure 3-4: Steel Fuse Plate Concept – Primarily Shear Deformation – Unstiffened with 100 mm Fillet

As seen in Figure 3-4, in which a maximum fillet of a 100 mm was used, at the limiting strain value of 49.1% (for low yield high ductility steel), deformation of the steel fuse plate is 92.9 mm, which is significantly higher than in a steel plate with no fillet in the inside corners. Even though according to section 3.1.1, this deformation is sufficient to satisfy test protocol requirements for BRB from Appendix T of *Seismic Provisions for Structural Steel Buildings* ANSI/AISC 341-05, low cycle fatigue is likely to cause premature rupture at the high stress concentration location shown in Figure 3-4.

An alternative approach is required to redistribute the strain along the full height (y – axis) of the steel plate fuse.

3.3.3 Steel Fuse Plate Concept – Primarily Shear Deformation – Stiffened

In order to redistribute shear along the full height (y – axis) of the steel plate fuse shear link (shear only) a pair of stiffeners on each side of the plate were used. Model properties are as per section 3.3.1; in addition the thickness of both plate and stiffeners is 15 mm. Vertical (y) and horizontal (x) dimensions of shear link are 200 x 200 mm, height of the stiffener is 55 mm.

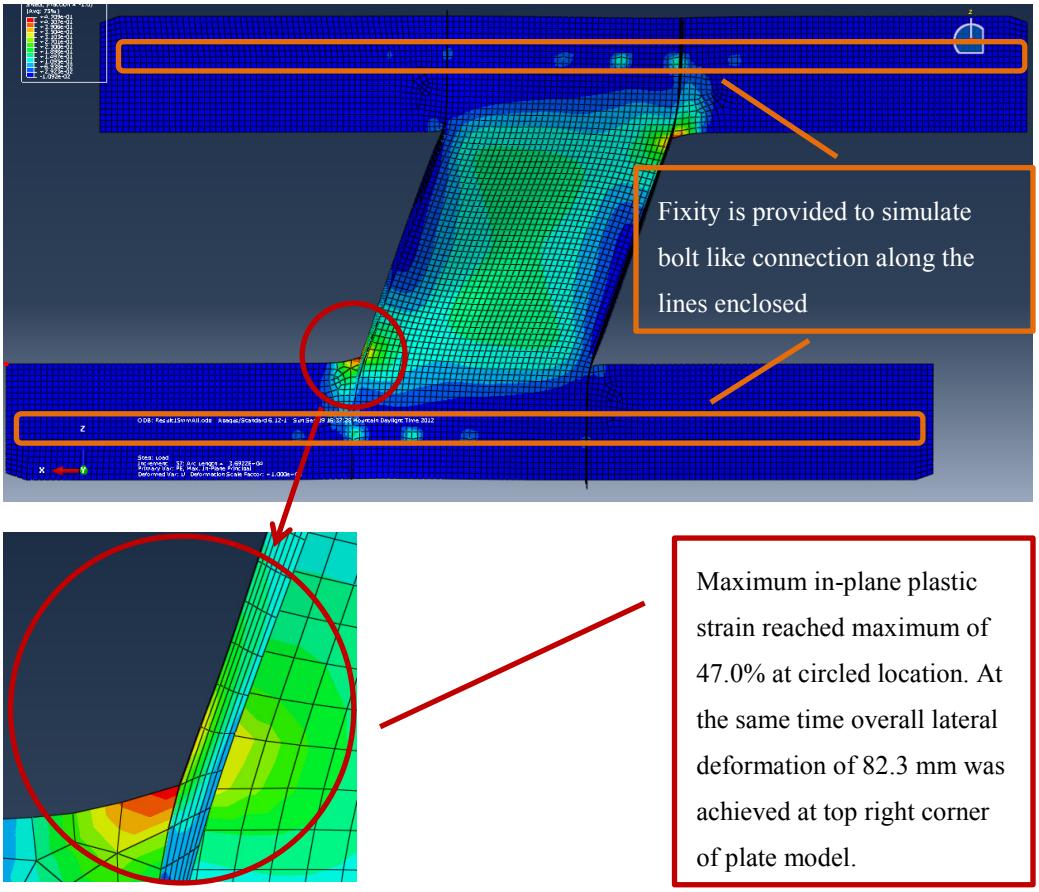

Figure 3-5: Steel Fuse Plate Concept – Primarily Shear Deformation – Stiffened

Addition of the stiffener did increase deformation of the fuse plate along the x – axis when compared to an unstiffened steel plate with no fillet at the inside corners. However the increase in deformation capacity was not as large as in a case of an unstiffened plate with 100 mm fillets at the inside corners of the steel fuse plate. By carefully varying height and thickness of the stiffened plate, one can arrive to values that will possibly allow for x – axis deformation to exceed deformation achieved by an unstiffened plate with 100 mm fillet. However, even if a stiffened fuse plate is capable of achieving larger deformation capacity, it will not exceed the deformation capacity of an unstiffened plate by a significant margin. At the same time, fabrication costs related to attaching stiffeners to a plate is significantly higher than fabrication costs due to the use and operation of a CNC plasma cutter to ensure proper fillet at the inside corners of the steel plate fuse (shear only).

3.3.4 Steel Fuse Plate Concept – Moment and/or Shear Deformation

From the analysis described in sections 3.3.2 and 3.3.3 it becomes apparent that a flaring shape of the shear link within the steel fuse plate is a preferred option to achieve both significant deformation in the x direction and ensure that the steel fuse is cost effective to fabricate. Also it was demonstrated that a major stress concentration in a steel plate fuse that is designed to deform in shear only is due to local moment introduced by shear force couple. A logical approach is to design for this moment and to ensure that a shear link has a proper shape that will allow for yielding to be constant throughout the full height (y – axis) of the shear link and will account for both moment and shear effects.

Such shape has been already analytically developed and verified by an experiment in a research project that focuses on the energy dissipation within a gusset plate (Mullin, 2005). Detailed guidance can be found from Mullin's work on how to derive width (x – axis) of the shear link as a function of height (y – axis) from the base of the shear link. Derivation is based on the formula:

(3.1) $$\frac{V}{V_{ALL}} + \frac{M}{M_P} = 1$$

In this equation V_{ALL} is shear force that corresponds to von Mises yield criterion of the cross-section of the shear link at any point along y – axis and M_P is plastic moment resistance of a rectangular section of height "h" and width "t", that correspond to width and thickness of the shear fuse link correspondingly. The resulting relationship between width of the link h(y) (where h_0 is width of the shear link at its neck) and distance from the neck of the shear link "y" is shown in Equation 3.2. The full derivation of equation (3.2) can be found from Mullin, 2005.

(3.2) $$h(y) = h_0 \cdot [\, 0.5 + 0.5 \cdot \sqrt{1 + 16 \cdot 0.577 \cdot {}^{y}/_{h_0}}\,]$$

The shape defined by this relationship has been used as a starting point of a concept of a steel fuse plate that uses both moment and shear induced deformations to provide ductility to the energy

dissipater. A necessary improvement has been made to the original concept in order to obtain required deformation capacity. In the original design by Mullin (2005), the y – coordinate originated from a midpoint of the shear link and the width of the link was gradually increasing towards both y – axis extremes. The research indicated that because more than one shear link is forming the fuse, necking and rupture at the midpoint of the shear link is possible due to introduced axial force (Mullin, 2005). This was demonstrated by FEA analysis when implementing this design into the energy dissipater. Given that 16 mm thick steel fuse plate is rigidly restrained at either y – axis extremes, necking due to introduced axial force was significantly amplified and was a primary factor limiting deformation capacity along the x – axis of the steel fuse plate.

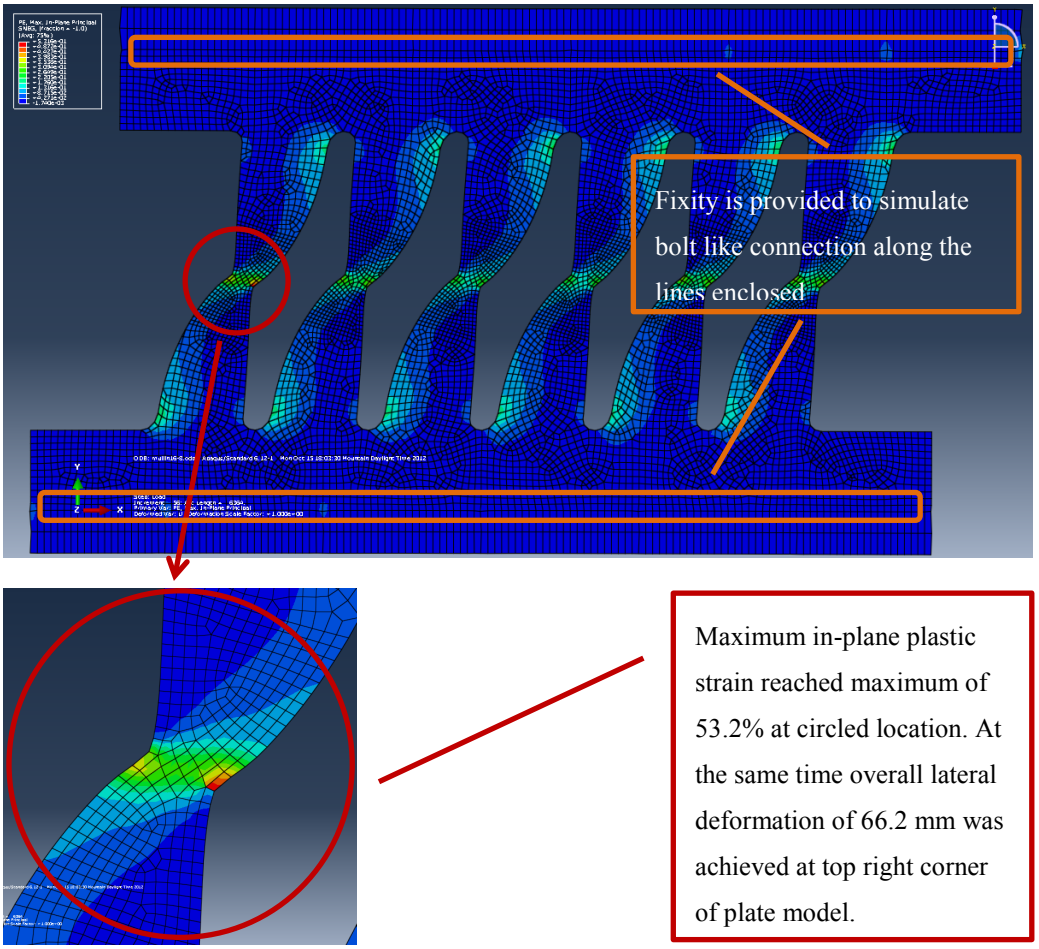

Figure 3-6: Steel Fuse Plate Concept – Shear and Moment Deformation - Similar to Mullin (2005)

Main cause of necking in this particular model is the presence of rigid boundary conditions at the top and bottom of the steel fuse plate. Whereas Mullin indicated that in case of multiple shear links, the rotation and displacement at the boundary condition was only partially restrained (Mullin, 2005), in the proposed shear link the boundary condition provided by bolts is rigid and does not allow for any rotation and/or deformation along the axis of the shear link. It is important

to note that even though bolts might allow for some slippage within the bolt hole, this slippage is very limited and was ignored in modeling steel fuse plate.

A steel fuse plate with shear link shape that ensures constant strain along the full length of the link does have a benefit of accommodating large deformation along the brace axis while being less susceptible to low cycle fatigue when compared to alternatives whose geometry introduces stress concentration. However, in this particular implementation rigid boundary conditions of the steel fuse plate introduced axial force within shear link that cause stress concentration or necking. Revision to boundary conditions is necessary to mitigate this effect.

3.3.5 Steel Fuse Plate Concept – Moment and/or Shear Deformation (Revised Boundary Conditions)

3.3.5.1 Evaluating / Designing Proper Boundary Condition

As concluded in section 3.3.4 in order to engage full deformation capacity of the steel fuse plate that incorporates discussed shear links, one must ensure boundary conditions that do not restrain deformation of the steel fuse plate along the axis of the shear links.

One of the possible options is to change the type of the connection at one end of the steel fuse plate. Instead of using a steel fuse plate that is rigidly connected to its guiding rails, one can introduce a slip connection that will provide a reaction force in the direction of axial loading within assumed prototype brace, but will be free to slip in the direction of the shear link once it is subjected to an axial force.

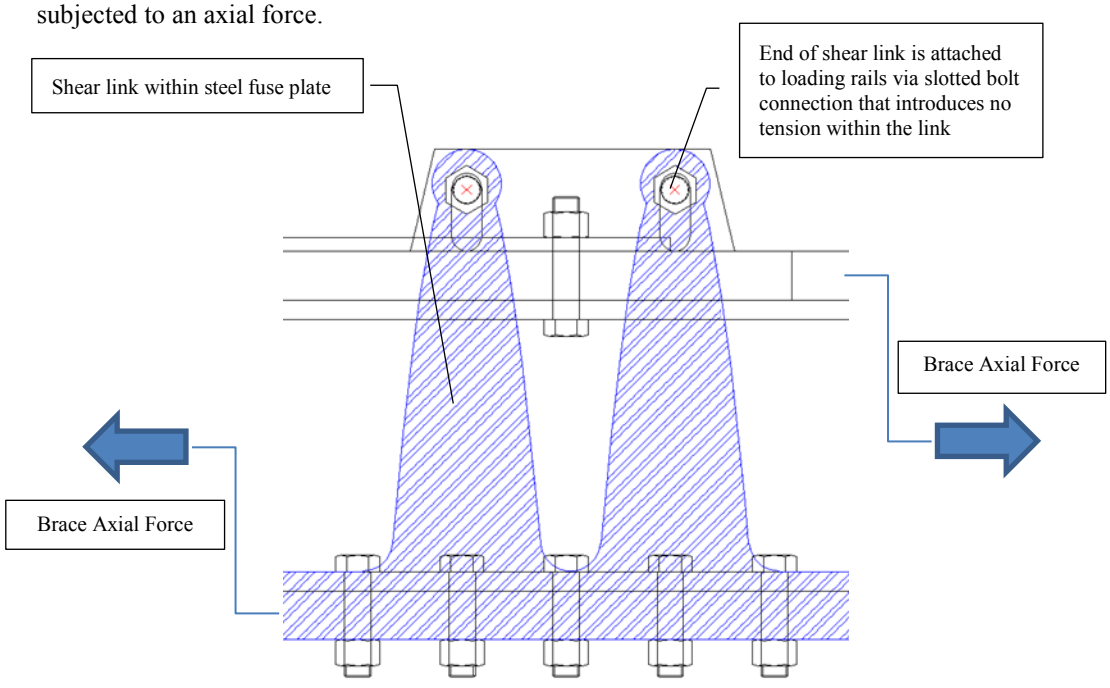

Figure 3-7: Shear Link - No Axial Force Boundary Condition

When shear link deforms due to axial brace force applied eccentrically to the steel fuse plate through loading rails, it will not be subjected to axial tension and necking will not occur.

3.3.5.2 Evaluating / Designing Optimal Shape of a Shear Link

Altering the boundary condition of the shear link within the steel fuse plate eliminates necking as a source of a stress concentration and eventual failure. However, for optimal performance of the energy dissipating element, one must optimize geometry in such a way to minimize the possibility of stress concentration within the fuse due to its shape.

Geometry of the steel fuse plate defined by equation (3.2) in section 3.3.4 with h_0 = 15 mm is developed based on the equations that intend to maximize yielded volume of the shear link by accounting for both induced moment and shear within the link (Mullin, 2005), and is defined as geometry C1.

Property h_0 in this case defines the amount of shear force applied at the top of the fuse; in fact it is the allowable shear capacity for any given section with thickness "t" and width "h_0" derived using von Mises yield criterion. Equations (3.2) and (3.4) use property h_0 to define the shape of the shear link that is aimed to achieve an optimal plastic strain distribution at large displacement applied to the top of the shear link.

Once the shear link is fully yielded, plastic strain is indeed uniformly distributed along the length of the shear link as one can note from the FEA model.

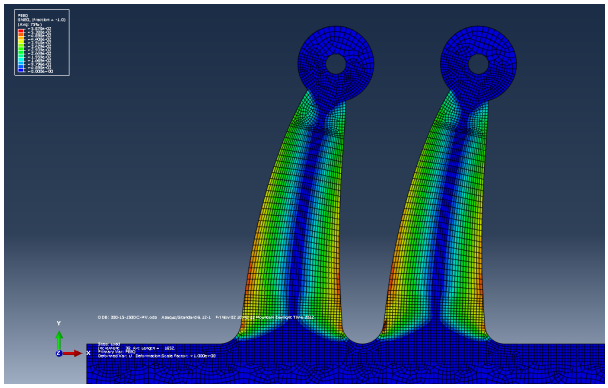

Figure 3-8: Plastic Strain Distribution within Fully Yielded Shear Link Type C1

However, if one was to track the propagation of the plastic strain within the shear link, there seems to be a significant strain concentration at its bottom at the onset of yielding (10 mm deformation), as shown in Figure 3-9, which will not be present once the specimen is fully yielded (Figure 3-8) but will eventually re-appear at a larger deformation in a direction of assumed brace axis (Figure 3-11).

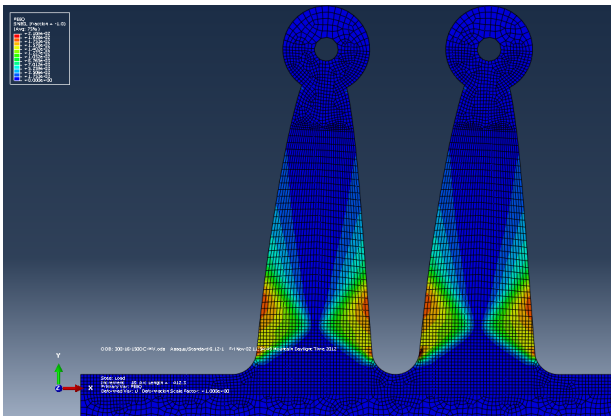

Figure 3-9: Plastic Strain Distribution within Shear Link C1 at the Onset of Yielding

A possible explanation for the observed plastic strain concentration is the fact that equation 3.1 was used for design of the steel plate geometry (Mullin, 2005), however past research (Drucker and Providence, 1956) suggests that

(3.3) $$(\frac{V}{V_0})^4 + \frac{M}{M_0} = 1$$

Given that effect of shear on overall section demand is very limited when compared to moment, and that shear strain hardening might have positive effect on moment capacity of the section, the decision was made to ignore shear demand altogether when designing geometry of the shear link. Exclusion of the shear component from the equation results in a shape formula that should have uniformly distributed moment induced strain parallel to the shear link edge through entire height of the link. In this case the equation that relates the width of the link *h* to the distance from the neck of the link *y* is as follows.

(3.4) $$h(y) = 2 \cdot \sqrt{h_0 \cdot 0.577 \cdot y}$$

The origin of coordinate "y" (y = 0) is defined as the point where load is applied to the shear link, i.e. centroid of the bolt hole at the top of the shear link.

Geometry defined using this equation is classified as geometry C3. Similarly to geometry C1, the value of h_0 was set to 15 mm. Geometry C3 demonstrates more uniform plastic strain distribution at the onset of yielding (10 mm deformation) as shown by FEA model.

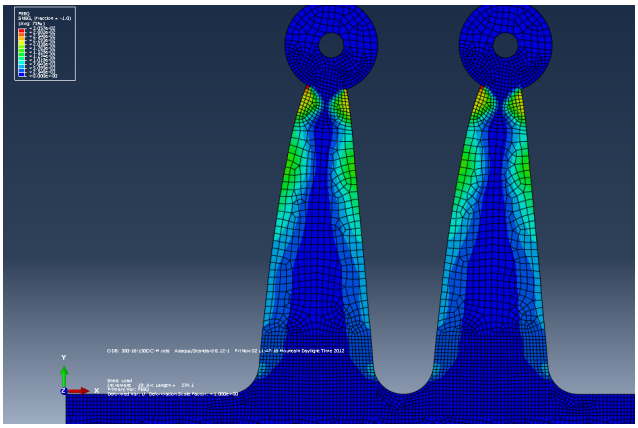

Figure 3-10: Plastic Strain Distribution within Shear Link C3 at the Onset of Yielding

At larger deformations in the direction of the assumed brace axis (e.g. 130 mm) the difference in the plastic strain distribution becomes more apparent – shear link type C1 exhibits noticeable stress concentration at the base of the link, while shear link type C3 has a uniform plastic strain along the edge of the steel plate, as shown in Figure 3-11.

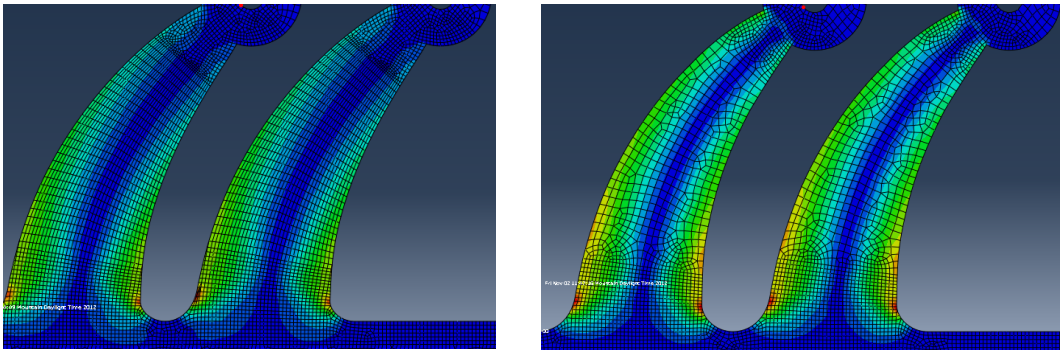

Figure 3-11: Plastic Strain Distribution within Shear Link C1 (Left) and C3 (Right) at Deformation of 130 mm in a Direction of Assumed Brace Elongation

Even though distribution of plastic strain is more uniform in case of shear link type C3 than shear link type C1, at the base of either link, one can observe a significant localized stress concentration, the magnitude of which is not present elsewhere within the shear link. Geometrically induced change from the plastic shear link to a much stiffer un-yielded steel plate below the link is a source of this localized stress concentration that can eventually cause a low cycle fatigue failure.

It is very challenging to eliminate stress concentration described above. However one can introduce an intended stress concentration in a location that does not have abrupt geometry change. In case of either shear link type C1 or shear link type C3, a uniform stress distribution along the edge of the link is achieved by a steel plate geometry that happens to have a curved outline. If one was to eliminate the curve by connecting the base and the neck of the shear link geometry with a straight line, a mathematically justified stress concentration will be introduced in

the middle of the shear link length. This geometry, defined as geometry C4, can serve a dual purpose. On the one hand it will simplify fabrication of the link, since only two points along its length will need to be defined by the design equation. On the other hand it will place small stress concentration at the onset of yielding (10 mm deformation) within the shear link to a location that does not have any changes in geometry away from either neck or base of the link.

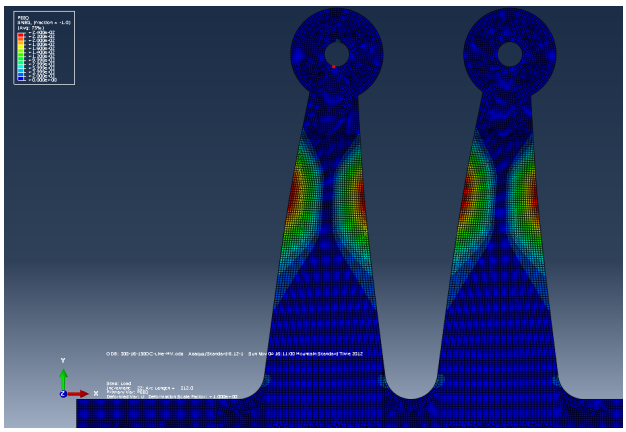

Figure 3-12: Plastic Strain Distribution within Shear Link C4 at the Onset of Yielding

The stress concentration is expected to disappear due to eventual strain hardening that will further redistribute stress along larger section of link length and eventually will result in a uniform plastic strain along the edge of the shear link. Such assumption was subsequently confirmed by an FEA model.

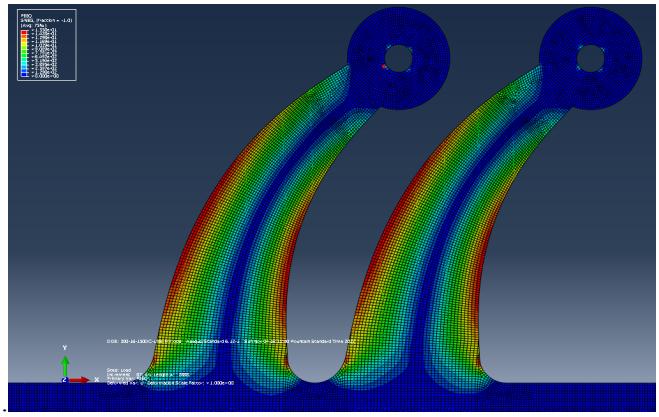

Figure 3-13: Plastic Strain Distribution within Shear Link C4 at Deformation of 130 mm in a Direction of Assumed Brace

The stress concentration is still present in shear link type C4, as shown in Figure 3-12; however at large shear link deformation due to force applied in a direction of the assumed brace it results in a more uniform distribution of plastic strain along the edge of the link when compared to either shear link type C1 or type C3. Considering the above, FEA model indicates that shear link type C4 is less susceptible to low cycle fatigue failure.

The decision was made to perform a physical test on all three types of steel shear links to confirm that actual specimen behaviour is similar to the FEA analysis results. Corresponding steel fuse plate types C1, C3, and C4 were incorporated into experimental program.

Steel fuse plate type C2 is not discussed at the present time and will be defined in chapter 4 as a derivative of shear link geometry type C4.

3.4 Friction Interface

One of the primary design criteria defined at the onset of the research project is to ensure that proposed energy dissipater is cost-effective and can be easily manufactured by a common steel fabricator. With this goal in mind use of virgin steel surface in a sliding mechanism can prove to be a viable solution.

Extensive research has been carried out to evaluate and predict static friction properties of bolted joints connecting structural steel plates with surface mill scale (Grondin et al., 2007). An evaluation of test datasets consisting of 397 experimental tests carried out to determine the coefficient of slip of structural steel plates with clean mill scale surface indicates that the mean value for slip coefficient of 0.31 with coefficient of variation is equal to 0.253 (Grondin et al., 2007). This particular statistical evaluation accounts for variation of slip coefficient both between and within the heats of steel.

Research that evaluates hysteretic behaviour of friction surfaces within a bolted connection is limited. Nevertheless a comprehensive research program has been carried out to evaluate dynamic (hysteretic) behaviour of bolted joints with several types of friction surface (Pall, 1979). Surfaces treated with zinc-rich paint, polyethylene, PVC, as well as metallized, sand-blasted and clean mill scale surfaces were evaluated and compared on the basis of dynamic friction behaviour (Pall, 1979). In addition, a bolted joint that incorporates a brake lining pad has been evaluated and compared to the above (Pall, 1979). The results are summarized and presented herein. Polyethylene and PVC coated surfaces exhibited significant surface deterioration under cyclic load as well as the lowest friction coefficient of the surfaces tested. Zinc rich paint surface showed significant (~50%) degradation of the friction coefficient under hysteretic loading before its behaviour stabilized after 17 cycles of loading. On the other hand, metallized surface exhibited a continuous increase in friction coefficient during testing cycles with a total increase of 50% after 24 cycles. Sand-blasted and clean mill scale surfaces showed a rise and fall in the friction coefficient value that did not stabilize until after 20 cycles of load; such behaviour is attributed to surface galling within the friction interface. Bolted joint that incorporates brake pad exhibited the most favorable behaviour. Initial slip loads showed to be very stable after many cycles of loading with virtually no degradation (Pall, 1979).

Overall after 20 cycles of loading, the bolted joint with brake pad lining showed nearly perfect hysteretic behaviour with no force degradation. Among other surface conditions both clean mill scale and sandblasted surface demonstrated behaviour that was just as stable, or better than every other surface type excluding brake pad lining (Pall, 1979).

The decision was made to use clean mill scale surface for the friction interface in the development of the prototype energy dissipater given that except for brake pad lining its behaviour was very comparable to other surface types under cyclic loading and it also requires virtually no additional treatment. An option with a brake pad lining as a friction interface was reserved in case clean mill scale surface will not behave as expected or if its friction properties will not stabilize.

3.5 Proposed Energy Dissipater

Seismic energy dissipater for a CBF developed within the scope of this research project combines a friction damper and ductile steel yielding elements.

Bolted connections that incorporate long slots are to act as a mechanism for friction damper. Besides providing for energy dissipation, the frictional mechanism acts as rigid sliding rails that allow for ductile deformation of yielding steel fuse to be constrained in the direction of brace axis. The surface condition within the bolted connection is to be clean mill scale.

Within prototype energy dissipater developed, several options for steel fuse plate have been considered in section 3.3. Energy dissipating mechanisms through bending, shear and axial deformations have been considered and evaluated using FE analysis. Based on the modeled performance of the fuse, an energy dissipating mechanism through combined bending and shear was selected to be used in the brace prototype. Fuse plate types C1, C3 and C4 are to be used as discussed in section 3.3.5. Detailed description of the prototype brace specimen will be covered in chapter 4.

4 Experimental Program

4.1 Introduction

Cyclic tests on prototype braces have been conducted in order to evaluate behaviour of the proposed energy dissipaters as well as to see how well behaviour of the steel fuse plate correlates to the finite element analysis model developed in chapter 3.

4.1.1 Structure of This Chapter

This chapter will expand on the methodology of the experimental program, its purpose, a detailed description of the test specimens, and test protocol. A brief overview, as well as results from auxiliary tests (such as tension coupon tests and bolt pretension tests), are provided. Detailed overview of the experiment will include description of test specimens, test protocol, and instrumentation used to capture and record data at each stage of the experiment. The chapter will go over the nature of the results collected by the experimental setup. Actual test results and their evaluation will be covered in chapter 5.

4.1.2 Purpose of Experimental Program

The purpose of the experimental program is to validate the concept of the prototype brace developed from chapter 3. There are several key factors that have to be considered and incorporated into the experimental program; those factors or "sub-purposes" are discussed below.

Experiment conducted in a scope of this research does not seek to replicate or approach the behaviour of the prototype brace developed under true seismic loading. Purpose of the experiment is to observe and evaluate the behaviour of the prototype, and relate observations to the hysteretic response of the brace prototype. The latter is essential for a "product development" stage which will not be covered in the scope of this research. Detailed visual observations of the behaviour of the steel plate specimen were performed and documented to provide additional input on boundary conditions of the finite element analysis model for the steel fuse plate.

The experimental program evaluates behaviour of the brace prototype that incorporates two mechanisms of the energy dissipation – inelastic deformations of the steel fuse plate and friction mechanism developed between surfaces of the slotted connection. The experimental program was developed to be able to separate those two mechanisms. Individual tests that focus on the behaviour of the friction component of the energy dissipater will evaluate friction resisting force during both tension and compression stage of the loading and will be performed at a rate similar to the rate of primary tests that focus on the overall behaviour of the brace prototype.

Even though the experiment was not conducted to simulate neither true earthquake loading nor behaviour of the specimen under such, it is important to ensure that the test protocol of the experiment is similar to the standards used by other researchers. So, one can make relatively definite conclusion / judgment on the feasibility of the prototype brace and prospects for its potential application. Hence the experiment is conducted and recorded based on the existing design standards.

4.1.3 Methodology

Methodology of the experimental program incorporates a number of key elements discussed herein.

4.1.3.1 Data Collected Throughout the Experiment

Seismic energy dissipation is generally quantified as an amount of work done by a dissipating element through deformation. In order to be able to evaluate such work, one must know the amount of deformation as well as the magnitude of the force that accompanied such deformation.

Axial force within the prototype brace was measured and recorded using several input sources to confirm the validity of the calculated values. Force values recorded via built-in sensors within MTS 6000 have been compared to the values obtained by installed strain gages. In addition to axial force obtained from the instrumentation, accompanying moments have been calculated from the strain gage output as well.

Similarly, relative axial deformation of the test specimens has been recorded using both built in sensors of the test system as well as additional instrumentation attached to the experimental setup. Given that proposed energy dissipater incorporates two slip surfaces that can potentially have different instantaneous slip rate, relative slip displacement at both surfaces has been recorded.

4.1.3.2 Raw Data Initial Calibration

Except for data obtained directly from the test system (MTS 6000), force within the test setup was calculated based on the data obtained from strain gages installed onto the test specimen. As to be discussed in section 4.2.3, the experimental program was carried out using a single brace prototype, with interchangeable steel fuse plates of a different shape being a variable of the experiment. Since the single brace prototype was used for all tests, one can expect a certain degree of strain to be introduced at the fixed ends of the brace prior to the start of the experiment in case an end moment was present at the end of a previous test. This strain has to be accounted for to make sure it does not distort data obtained from strain gages. In addition initial strains can be introduced within slotted plates due to elastic deformations during assembly and/or differential slip accumulated at the end of the previous test.

To account for an initial state of the brace prototype, output recorded from strain gages has been calibrated to result in zero values for initial axial force as well as moment due to deformations accumulated prior to the start of the test.

4.1.3.3 Stability Evaluation of the Brace Prototype

The energy dissipater developed within the scope of this research is a new concept that has not been experimentally evaluated before. Redundancy of the load path within the brace introduces a possibility of unequal axial force being transferred to two slotted connections. Such a condition can cause a formation of a hinge due to potentially unsymmetrical slip of two friction planes. Once the moment due to axial force eccentricity exceeds combined moment capacity of two slotted plates, a rotational hinge will be formed and the brace will deform in-plane unless it is restrained at the ends.

Due to potential uncertainties in the behaviour of the prototype, its potential modes of failure have been deliberately limited to exclude failure due to in-plane or out-of-plane instability of the brace member. This has been achieved by introducing fixed boundary conditions at both ends of the brace. It is known that in a real world scenario, the true boundary conditions of the brace member can vary from fixed (fixity is provided by gusset plates) to pinned if a custom end connection is used. In order to evaluate possible stability issues within the brace specimen at the same time ensuring that failure due to stability deficiency of the brace is not allowed, an analytical approach has been used. To evaluate moment demand at the midpoint of the brace prototype, end moments have been calculated from strain gage data and corresponding midpoint moment has been interpolated using beam theory. Calculated moment provides implications of stability of the brace prototype at any point of time, while actual physical stability is provided by boundary conditions of the brace.

4.1.3.4 Evaluating the Behaviour of Steel Fuse Plate

During the development stage of the research project, finite element analysis model of the steel fuse plate exhibited very stable deformation with no out-of-plane behaviour. Different geometrical shapes of the steel fuse plate demonstrated a strain pattern that could define the degree of susceptibility to rupture due to low cycle fatigue.

It is crucial to be able to capture behaviour of the steel fuse plate in sufficient detail that can verify validity of the initial FEA model and capture any deviations from an expected deformation pattern. One would need to know an accurate true strain distribution should the rupture occur in order to make predictions regarding life to failure of the specimen due to low cycle fatigue.

A stereoscopic correlated camera setup has been used to capture instantaneous deformation pattern within steel fuse plate at any point of time during the experiment. Data obtained from the setup is

to be used to validate the FEA model as well as provide corrective input to the model should actual behaviour of steel fuse plate differ from expected behaviour.

4.1.3.5 Independent Evaluation of Friction and Inelastic Steel Fuse

Given that the brace prototype developed utilizes a combined approach to energy dissipation (incorporates both friction and inelastic mechanisms) one of the main principles of the experiment is to be able to separate two mechanisms and evaluate them independently. In order to achieve this, every test evaluating combined behaviour of the two mechanisms was supplemented with a friction-only test performed at a rate identical to the primary test. A friction-only test was performed both before and after the experiment at the loading rate used in the main test to accommodate possible change of friction force during the hysteretic test of the brace prototype. Friction force during the prototype brace test can be obtained by interpolating its value from before and after the experiment while accounting for the change in the displacement rate at different stages of the test. If friction behaviour of the prototype is to be proven to be stable and predictable this approach will allow to evaluate friction only behaviour of the specimen during the test and separate it from the combined data output.

4.2 Auxiliary Tests and Material Properties

4.2.1 Tension Coupon Test – Steel Fuse Plate Material Properties

In addition to primary cyclic test of the prototype brace, two auxiliary tests had to be carried out. Even though material properties of the steel specimens have been obtained from the fabricator, it was decided to conduct a tension coupon test to obtain a stress versus strain curve for the steel fuse plates. It is essential for the numerical analysis of the steel fuse plate to have accurate input data so it can replicate response of the steel fuse plate during the cyclic test. Typical dimensions of the test coupon used are shown below.

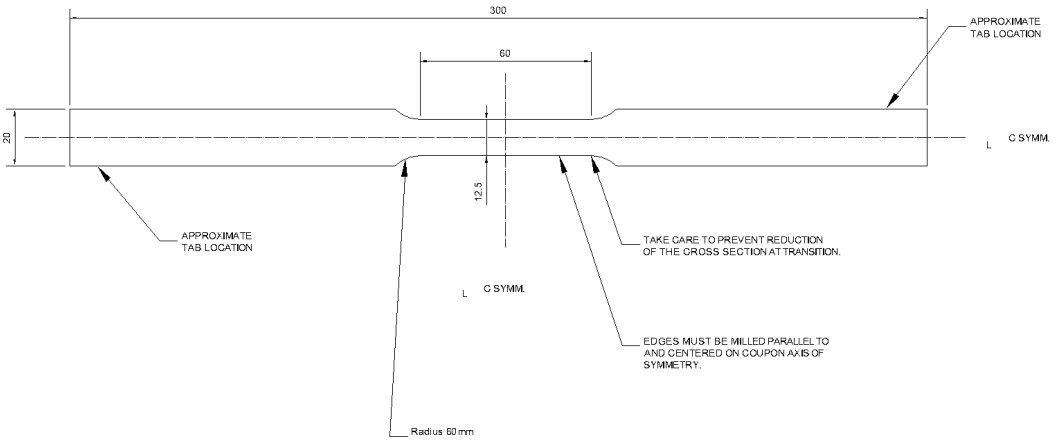

Figure 4-1: Tension Coupon Dimensions (15.8 mm thick)

Five coupons have been cut and four of them were subsequently tested – two in transverse and two in longitudinal direction of the steel plate, as shown in Figure 4-2.

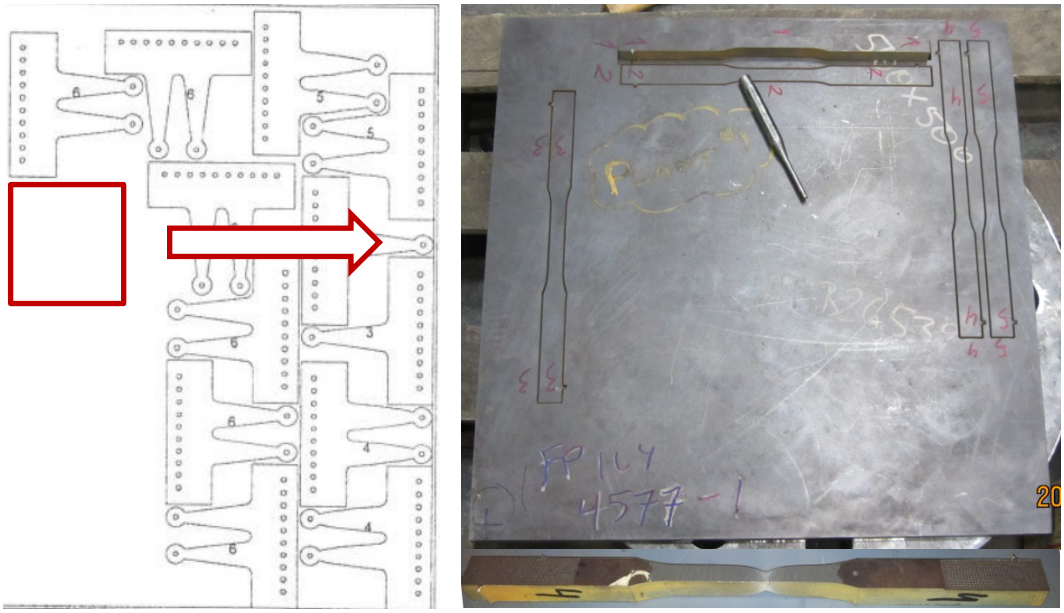

Figure 4-2: Tension Coupons - Nesting Diagram and Specimen Photo

Tension coupons were tested in accordance with ASTM E8/E8M−11 (2011) test protocol. Strain rate of 0.01 [mm/mm]/[min] was used up to a deformation value where strain hardening became apparent. Once strain hardening was noted, the strain rate was increased to 0.04 [mm/mm]/[min] in accordance with ASTM E8/E8M−11. An extensometer was used to accurately measure elongation of the test coupon up to approximately 200,000 microstrain. Afterwards, crosshead displacement output was used to approximate strain value within the coupon.

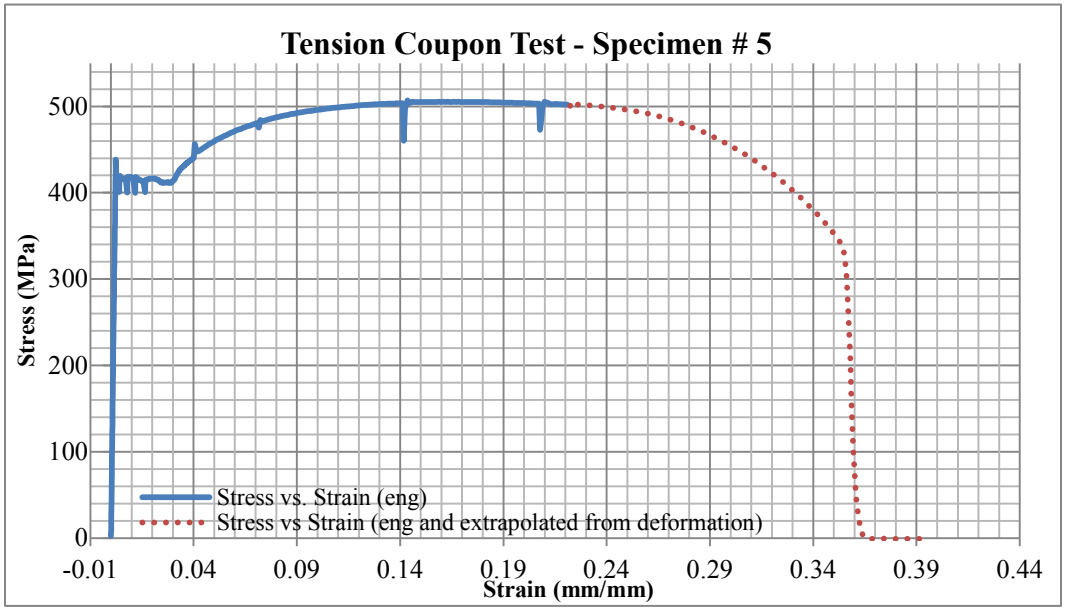

Figure 4-3: Tension Coupon Test - Sample Stress vs. Strain Curve - Specimen # 5

Dynamic values for yield stress F_y and ultimate stress F_{ult} proved to be very similar for two orthogonal directions within the sample steel plate.

Table 4.1: Tension Coupon Tests - Numerical Results

		Engineering Strain				Static		Dynamic	
	Coupon	ε @ hard.	ε @ ult.	ε @ rupt.	E	F_y	F_{ult}	F_y	F_{ult}
	ID	mm/mm	mm/mm	mm/mm	GPa	MPa	MPa	MPa	MPa
Direction 1	1	0.031	0.2	0.36	200	380	465	410	499
	2	0.031	0.22	0.345	200	386	475	413	506
Direction 2	4	0.031	0.21	0.334	190	397	475	420	507
	5	0.031	0.23	0.354	190	399	462	417	506

It is acknowledged that dynamic properties of steel obtained during uniaxial tension test cannot be directly correlated to dynamic properties of steel within shear link subjected to bending. It is also acknowledged that uniaxial strain rate cannot be directly related to strain rate within the shear link during the experiment. However loading history of the experiment does introduce strain rate dynamic effect. This shall not be neglected in FEA model when attempting to understand experimental behaviour given that difference between dynamic and static F_{ult} can be as high as 9.5%. Rate of increase of maximum strain value in a shear link due to brace deformation within MTS 6000 is on average 0.02 strain / min (strain vs. displacement function is measured using FEA model of steel fuse plate). Even though this strain rate cannot be directly related to strain rate of tension coupon test, its magnitude suggests that use of dynamic steel properties in post experimental FEA model will closer represent as tested behaviour than use of static steel properties.

Table 4.2: Tension Coupon Tests – Tests Results Averaged for Both Orthogonal Directions

Engineering Strain				Static		Dynamic	
ε @ hard.	ε @ ult.	ε @ rupt.	E	F_y	F_{ult}	F_y	F_{ult}
mm/mm	mm/mm	mm/mm	GPa	MPa	MPa	MPa	MPa
0.031	0.22	0.35	195	391	469	415	505

Based on the values in Table 4.2 and averages of coupon test stress versus strain curve profiles following input data for the FEA model have been developed.

Table 4.3: Tension Coupon Tests - Input for Numerical Analysis

Strain [eng]	Stress [eng]	Strain [true]	Stress [true]	Plastic Strain [true]
mm/mm	MPa	mm/mm	MPa	mm/mm
0	0	0	0	0
0.002128	415	0.002126	415.8832	0
0.0022	415	0.002198	415.913	0
0.031	416	0.030529	428.896	0.0283
0.032	422	0.031499	435.504	0.0293
0.035	432	0.034401	447.12	0.0321
0.04	444	0.039221	461.76	0.0369
0.045	452	0.044017	472.34	0.0416
0.05	459	0.04879	481.95	0.0463
0.06	470	0.058269	498.2	0.0557
0.07	478	0.067659	511.46	0.065
0.08	485	0.076961	523.8	0.0743

0.09	490	0.086178	534.1	0.0834
0.1	494	0.09531	543.4	0.0925
0.12	500	0.113329	560	0.1105
0.14	503	0.131028	573.42	0.1281
0.16	505	0.14842	585.8	0.1454
0.18	505	0.165514	595.9	0.1625
0.2	504.5	0.182322	605.4	0.1792
0.22	504	0.198851	614.88	0.1957

4.2.2 ASTM A325 7/8" Diameter Bolt Pretension Test (Torque Wrench Calibration)

In order to accurately predict friction resisting force at slip, one must know amount of pretension within the bolts. Calibrated torque wrench was used to impose accurate pretension within the bolt in a slotted connection. Skidmore-Wilhelm Bolt Tension Calibrator Model "M" load cell was used to correlated torque (in ft-lb) applied by the calibrated torque wrench to pretension force in a 7/8" diameter ASTM A325 bolt (in kN).

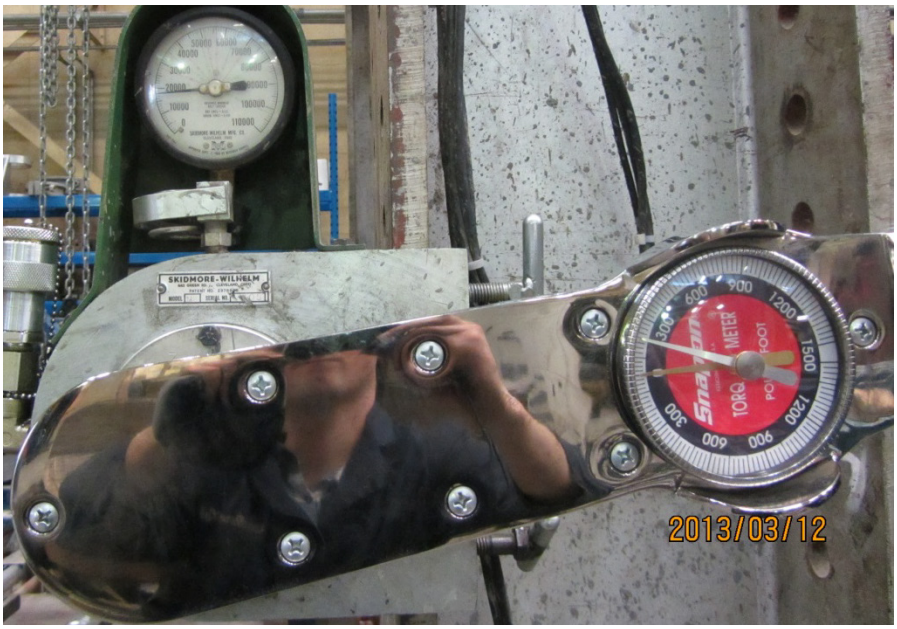

Figure 4-4: Bolt Pretension Test (Torque Wrench Calibration)

Four bolts in total were tested. Average values for relationship between pretension force to torque values with standard deviation of approximately 7.5 ft-lb is shown below.

Table 4.4: Bolt Pretension - Averaged Test Results

Load		Torque
$x10^3$ (lb)	kN	ft-lb
10	44.5	112.5
15	66.8	183.5
20	89.0	249.6
25	111.3	320.0
30	133.5	387.0
35	155.8	451.4
40	178.1	509.5

4.2.3 Material Properties – Friction

Known friction properties of the surface in a slotted connection are essential to accurately estimate slip load of the friction interface. Two types of friction interface have been used in the experiment. In one case clean mill scale was used as a friction surface; its mean value for slip coefficient is 0.31 and coefficient of variation is equal to 0.253 as per Grondin et al. (2007). If the use of clean mill scale as a friction interface proves to be unstable, a readily available non-asbestos non-metallic glass fiber reinforced friction sheet material is to be used instead. Datasheets supplied by the manufacturer of this particular material indicate low rate of wear and stable friction properties with a friction coefficient of 0.52.

4.3 Description of Test Specimen

The prototype brace consists of two segments that slide with respect to each other as shown in Figure 4-5.

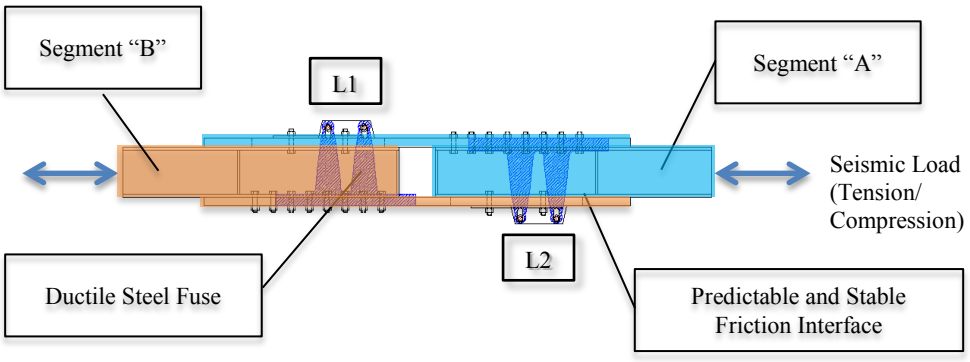

Figure 4-5: Prototype Diagonal Brace Specimen - Schematic Diagram

In each segment a primary load carrying member is a W200 x 59 steel beam that transfers its axial load to a slotted plate which in turn transfers axial force to both the friction interface and to steel fuse plates.

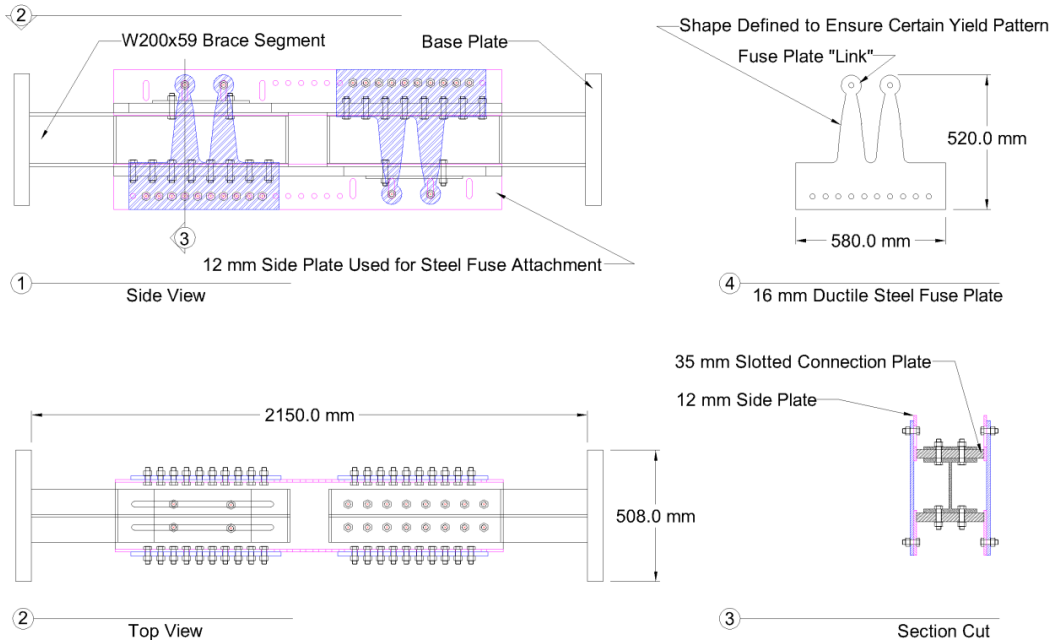

Figure 4-6: Prototype Diagonal Brace Specimen - Design Blueprint

The final design for the prototype brace can be separated into 3 main parts: primary load carrying brace components, steel fuse plate, and friction interface.

Primary load carrying brace components do not get replaced throughout experimental program. Friction interface, which is a property of primary load carrying components, does not get replaced either, however pretension force is varied during the test to better meet the needs of the experiment. Given that eventually frictional resistance and resistance due to inelastic deformation of the steel plate has to be separated, their corresponding values should be comparable so one resistance component does not "overshadow" another. With that in mind, friction resistance is to be set to be approximately equal to steel fuse plate resistance.

Steel fuse plates are a variable element of the experimental program, different configurations of which are expected to have different yield / strain concentration patterns and different levels of susceptibility to out-of-plane behaviour.

4.3.1 Primary Load Carrying Components of the Prototype Brace

The prototype brace is designed to ensure fixity at its ends. As seen from Figure 4-7, either end of the prototype brace is welded to a thick baseplate (approximately 90 mm) that is designed to behave elastically under imposed loading and is to be attached to the testing apparatus MTS 6000. Attached to the baseplates are W200 x 59 steel beams fabricated from 350W grade steel with a minimum F_y of 350 MPa. On either side of the W200 x 59 beam, a slotted plate is attached to facilitate relative displacement of the two brace segments with respect to each other, as schematically presented in Figure 4-5.

In order to easily swap steel fuse plates, a side attachment plate was welded to the slotted plate. Bolt holes within the side attachment plate are used to connect interchangeable fuse plates. It is important to note that ends of the shear link are connected to a short slotted plate within the connecting side plate; this ensures a "roller" boundary condition at the end of a shear link that imposes no (or little) axial demand on the link.

An exploded view of the prototype brace is presented in Figure 4-7 to give a better understanding how its components where connected between each other.

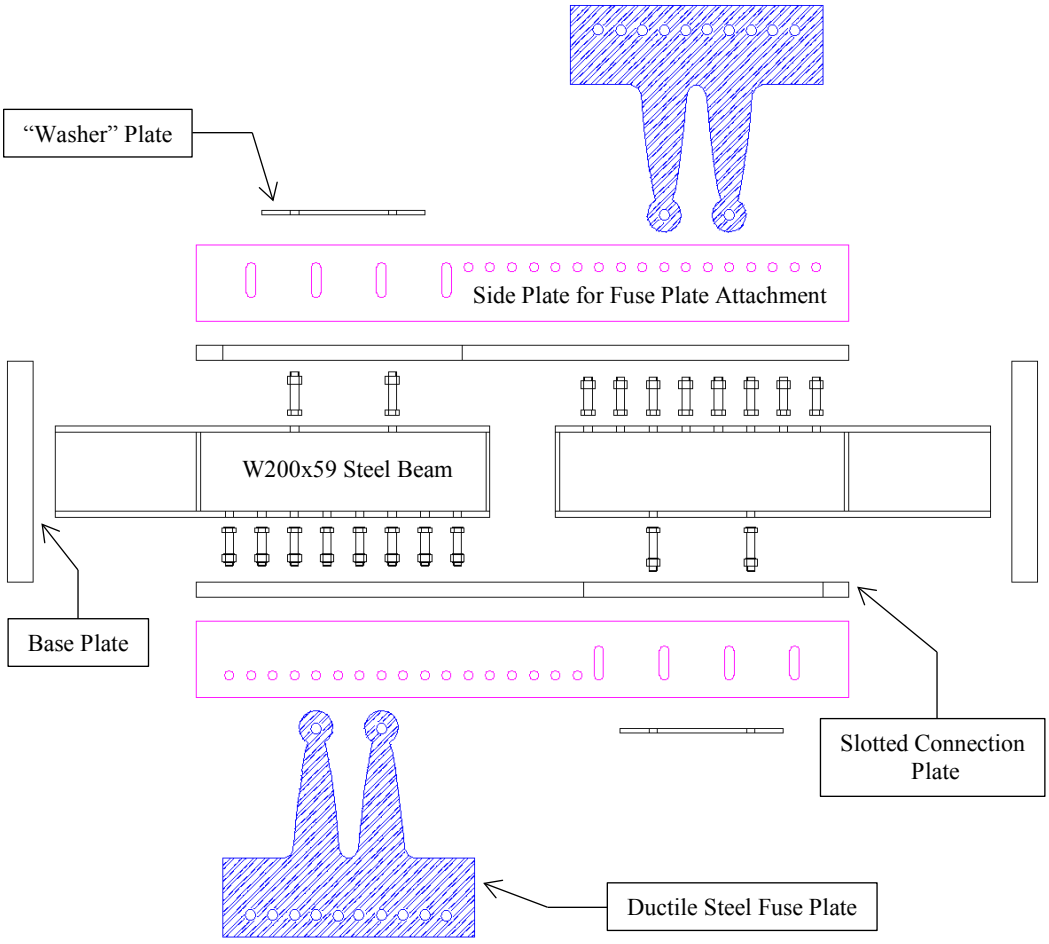

Figure 4-7: Primary Load Carrying Components of the Prototype Brace

Prototype brace components that required welding were attached to each other by fabricator. Final assembly of the prototype brace was performed in the structural lab using ASTM – A325 and A490 7/8" bolts. Except for friction-critical slotted connections assembly was performed using turn-of-nut method (compressor driven impact wrench).

Figure 4-8: Primary Components - Assembly

4.3.2 Friction Interface

Initially it was planned to use clean mill scale as a friction interface. Use of proprietary friction material was reserved in case use of clean mill scale proves to be impossible from the performance or durability perspective.

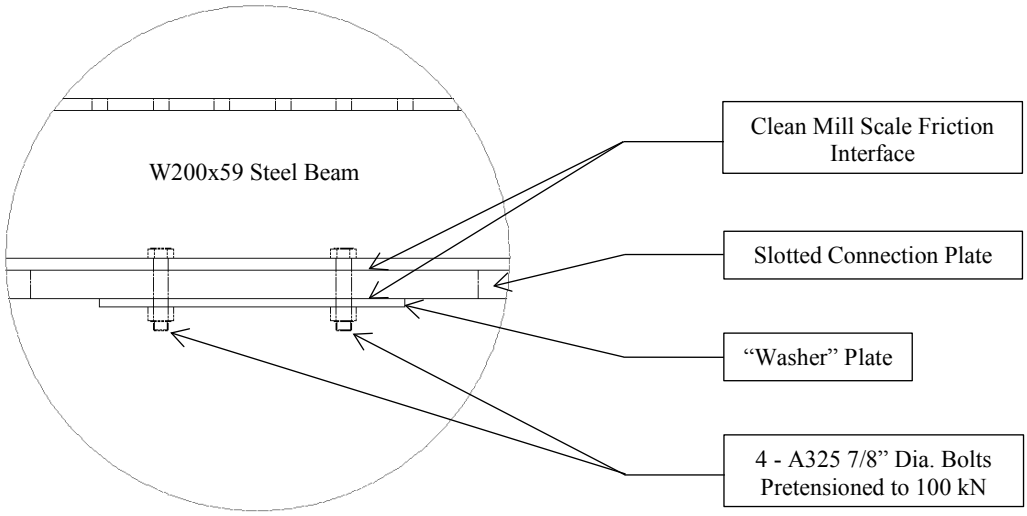

Figure 4-9: Friction Interface - Clean Mill Scale

As shown in Figure 4-9, a clean mill scale friction surface specimen was assembled without any additional modifications, and bolts in a slotted hole connection were pre-tensioned to 113 kN each. Coefficient of friction was estimated to be 0.253 as per section 4.2.3 for either friction interface surface.

Use of proprietary material required somewhat different approach than simply bolting components together. Given that its coefficient of friction is much higher (0.52) it was decided to induce friction only between W200 x 59 beam and slotted plate. This was done to make sure there is no significant bending load imposed on bolts.

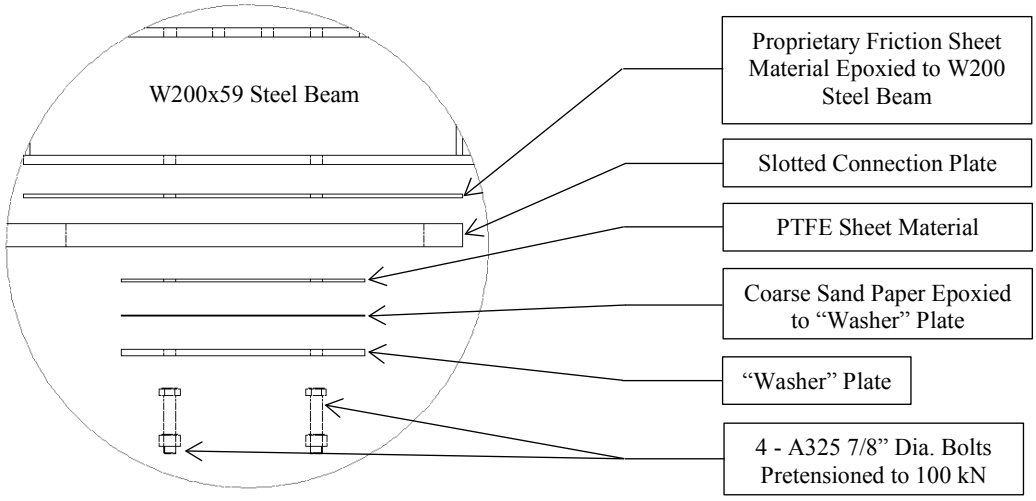

Figure 4-10: Friction Interface - Proprietary Friction Interface

Friction sheet material described in section 4.2.3 was epoxied to the surface of W200 x 59 beam (mill scale removed). The interface between slotted plate and "washer" plate is designed to have a lower friction coefficient of approximately 0.05 via the use of sheet PTFE material (Stranton and Taylor, 2010). In order to secure sheet of PTFE so it does not slip out under cyclic loading a layer

of sand paper was glued to the "washer" plate – once bolts were pre-tensioned it proved to be a reliable way to mechanically fasten a PTFE sheet to the plate.

Bolts were initially pre-tensioned to 100 kN per bolt in each case. A calibrated torque wrench with axial force versus torque relationship developed in section 4.2.2 was used. It is important to note that initial pretension force in bolts was a rough estimate to obtain a 50/50 ratio for friction resistance versus steel fuse plate resistance. This ratio was selected arbitrarily to make sure that post-experimental separation of friction and steel fuse plate response can be easily done. In real-life design situation, pretension force can be specified such that friction resistance of the brace member can carry in-service demands without engaging steel shear links of the fuse plates.

4.3.3 Ductile Steel fuse plate

Four types of ductile steel fuse plates were used. While being geometrically different, their basic dimensions and bolt patterns were identical and are as pictured below.

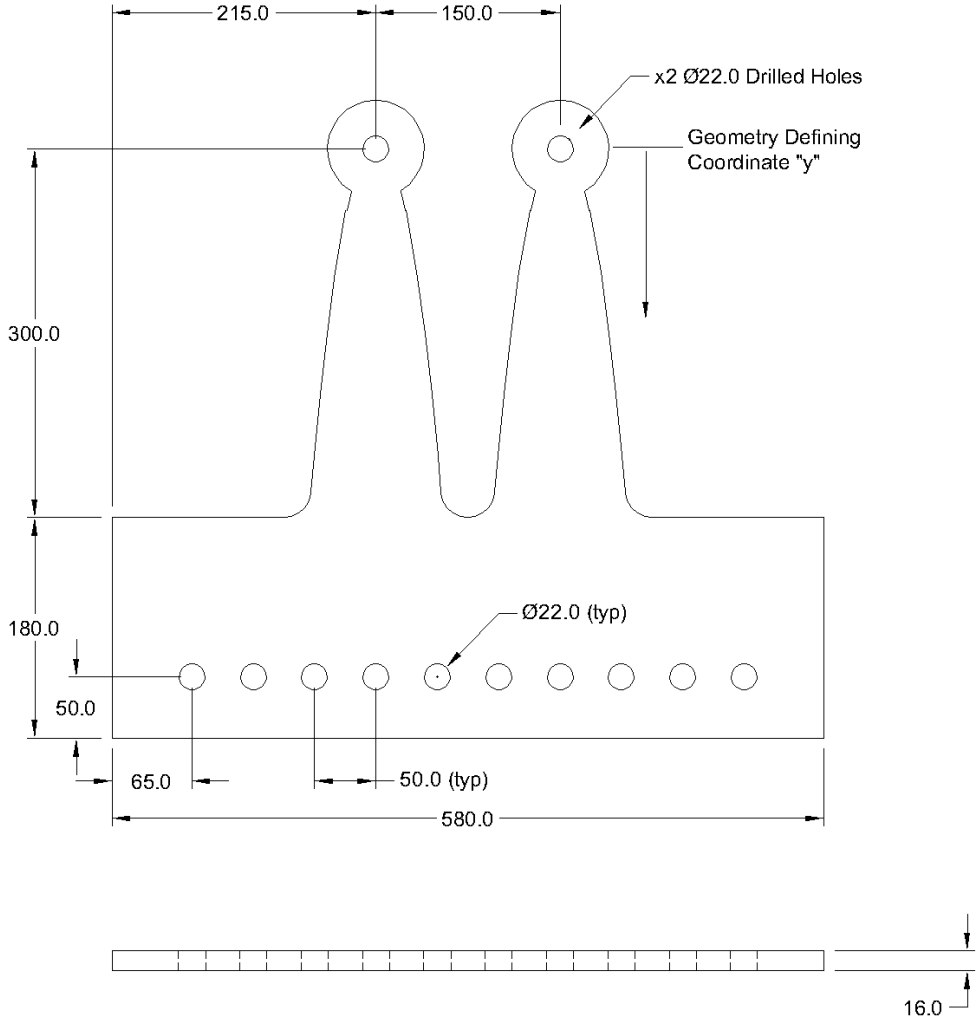

Figure 4-11: Ductile Steel fuse plate - General Geometry

Ductile steel fuse plates tested had four different geometries of the link, C1 to C4. In particular, the width of the link as a function of geometry defining coordinate "y" (see Figure 4-11) differs for different steel fuse plates as discussed in section 3.3.5.2.

Figure 4-12: Ductile Steel Fuse Plates - Schematic Diagram

Initial purpose of different types of steel fuse plates was to evaluate the shear link shape that results in most favorable stress distribution at large deformations, and to evaluate the effect (if any) of ratio of steel fuse plate resistance to friction resistance.

- Fuse plate C1 ensures uniform yield along the edge of the plate during bending by taking into account both bending and shear resistance of the plate.
- Fuse plate C2 is similar to C1; however it is designed to create a minor stress concentration in the middle of the steel plate link in order to remove potential stress concentration from geometric locations that are more susceptible to fracture. In particular width at y = 0 mm and y = 300 mm was calculated as per equation used to maximize yielded volume of the shear link (section 3.3.5.2), geometry in between those two points was defined by a straight line. In addition, fuse plate C2 has only one link.

- Fuse plate C3 ensures uniform yield along the edge of the plate during bending by taking into account bending resistance of the plate only.
- Fuse plate C4 is identical to C2; however it incorporates two steel links instead of one.

When calculating geometry of fuses C1 to C4, a force demand defining property h_0 = 15 mm has been used. Property h_0 in this case defines the amount of shear force applied at the top of the fuse; in fact it is the at-yield shear capacity for any given section with thickness "t" and width "h_0" derived using von Mises yield criterion as discussed in section 3.3.5. Once this shear capacity is reached the section will start deforming plastically in shear, limiting amount of shear force applied to the rest of the shear link (Mullin, 2005).

4.3.4 Boundary Condition at the Top of the Shear Link

As per initial design boundary conditions at the top of the shear link within the steel fuse plate shall be such to restrain movement of the shear link in the "Z" direction .

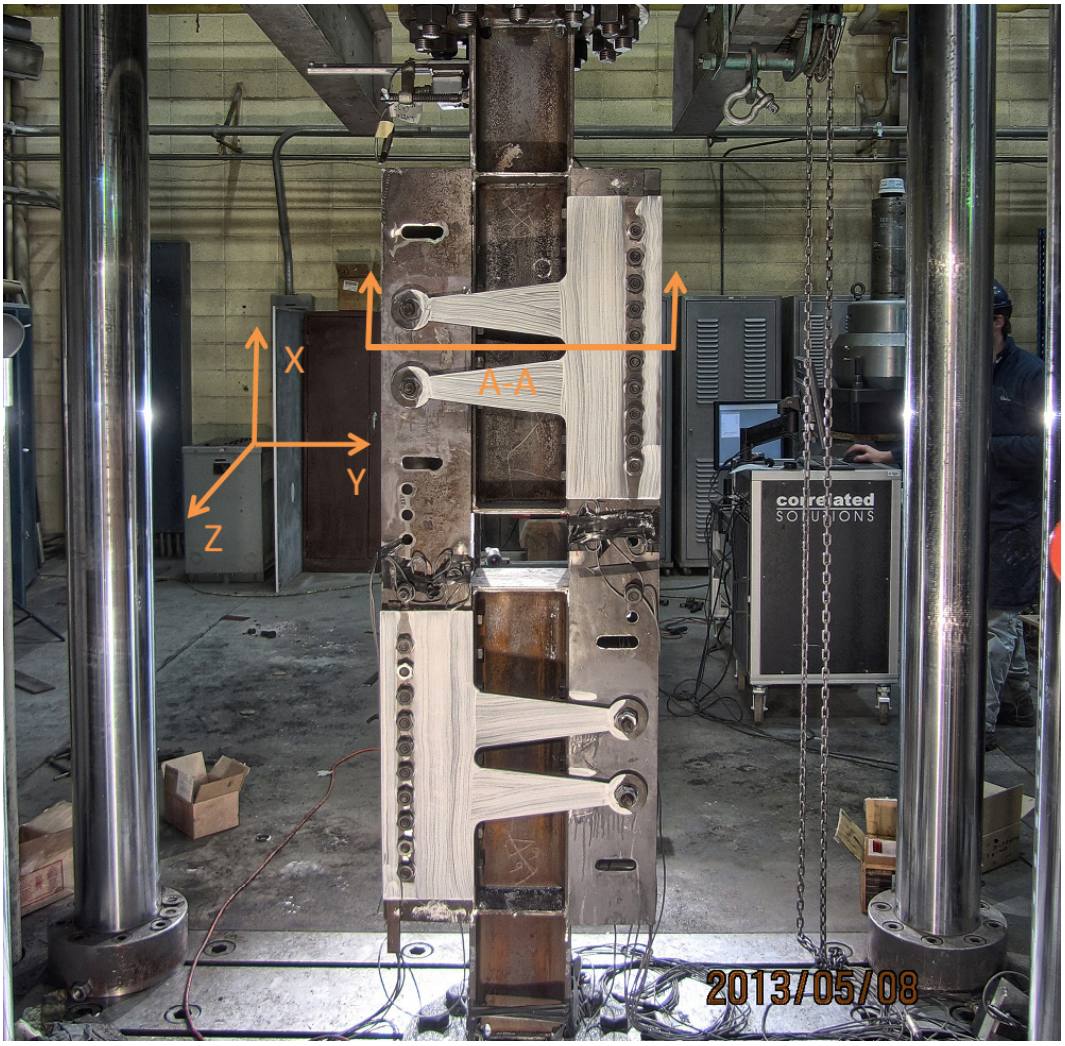

Figure 4-13: Prototype Brace - Typical Configuration

In addition, the bolted connection at the top of the shear link was meant to restrain rotation about the “X” and “Y” axis.

However, significant distortion of the cross-section of slotted plate assembly due to welds has occurred as indicated on the section cut A-A.

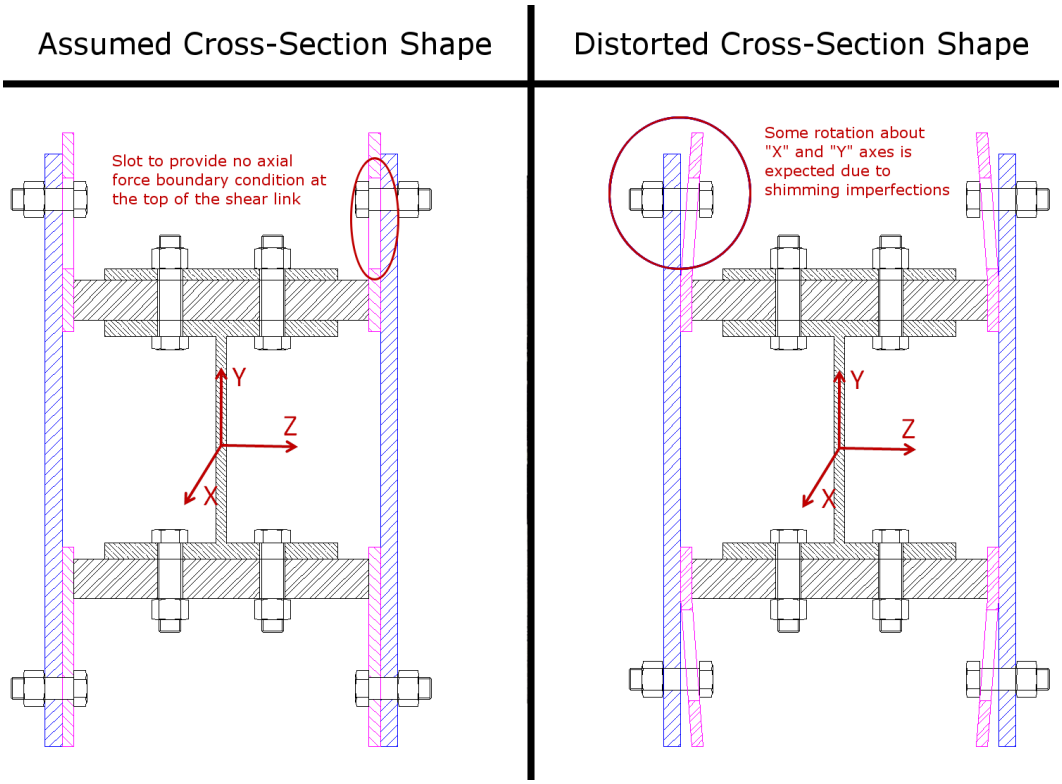

Figure 4-14: Prototype Beam - Section Cut A-A - Distortion Due to Welding

Due to distortion, top of the shear link did not come into direct bearing contact with the fuse attachment plate as per Figure 4-14. In fact a steel plate shim had to be introduced to minimize the gap between top of the shear link (steel fuse plate) and fuse attachment plate. Given the significant range of motion of the top of the shear link within the slot of the fuse attachment plate, a shim (no matter how accurate it is) could not provide firm contact between the two without introducing a possibility of jamming. Relatively loose contact between the top of the shear link and steel fuse attachment plate changed the boundary condition at the top of shear link from fixed against rotation about “X” and “Y” axes and displacement along “Z” axis to pinned (rotation about “X”, “Y” and “Z” axes) and fixed against displacement along “Z” axis. Implications of the free-to-rotate boundary condition at the top of the shear link are to be evaluated in the post-experiment FEA model in chapter 6.

4.3.5 Test Specimen Configuration

Test specimen configuration at the beginning of experimental program was proposed as follows:

4.3.5.1 Test Specimen # 1

Prototype brace consisting of primary load carrying components with clean mill scale friction interface and two ductile steel fuse plates C4 placed on both sides of the W200 x 59 section at location L1, as shown in Figure 4-5.

4.3.5.2 Test Specimen # 2

Prototype brace consisting of primary load carrying components with clean mill scale friction interface and two ductile steel fuse plates C1 placed on both sides of the W200 x 59 section at location L1, as shown in Figure 4-5.

4.3.5.3 Test Specimen # 3

Prototype brace consisting of primary load carrying components with clean mill scale friction interface and two ductile steel fuse plates C3 placed on both sides of the W200 x 59 section at location L2, as shown in Figure 4-5.

4.3.5.4 Test Specimen # 4

Prototype brace consisting of primary load carrying components with clean mill scale friction interface and four ductile steel fuse plates C4 placed on both sides of the W200 x 59 section at locations L1 and L2, as shown in Figure 4-5.

4.3.5.5 Test Specimen # 5

Prototype brace consisting of primary load carrying components with clean mill scale friction interface and two ductile steel fuse plates C2 placed on both sides of the W200 x 59 section at location L2, as shown in Figure 4-5.

4.4 Instrumentation and Test Setup

4.4.1 Test Setup

Test setup of the experimental program was designed to apply cyclic axial force of gradually increasing amplitude at a constant but variable rate to the prototype brace. A hydraulically actuated MTS 6000 test system was used to achieve desired loading condition.

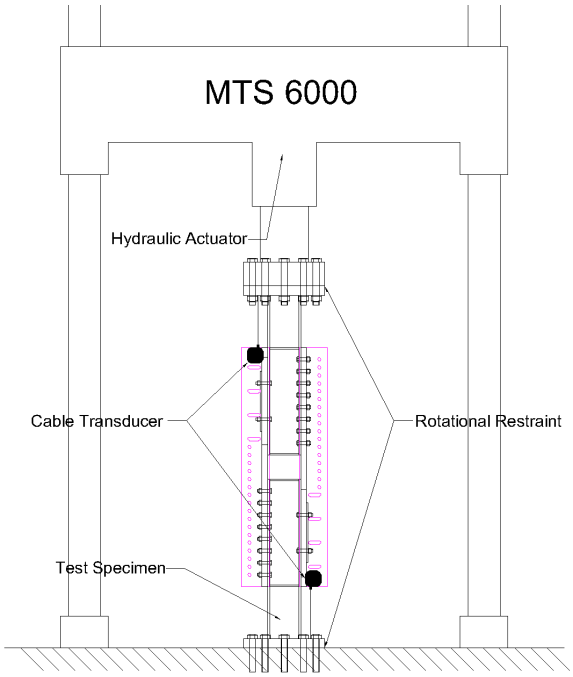

Figure 4-15: Test Setup

At either end of the test specimen, a bolted connection with 12 - A325 38.1 mm diameter bolts provides a fixed boundary condition to the brace. In a conventional braced frame, an actual brace (W-section) at its end is believed to have no moment restraint about its weak axis and full or partial moment restraint about its strong axis provided by gusset plate. However, given that the prototype brace is not susceptible to buckling about its weak axis, a fixed – fixed boundary condition provides a reasonable representation of a steel brace rigidly connected to the gusset plates at its ends. Stability implications of different end conditions are to be evaluated analytically.

Cyclic axial load was applied to the top of the specimen acting at the centroid of the brace. An electronic data acquisition system was used to capture and record output from the MTS' load cell, displacement transducer, cable transducers and strain gages as a function of time. Data output from the stereoscopic correlated camera setup was linked to the time variable of the electronic data acquisition (EDAQ) system output. Detailed description of the instrumentation used is to follow in section 4.4.2.

4.4.2 Instrumentation

Instrumentation setup for the experimental program consisted of a load cell and displacement transducer within the MTS 6000 test machine, two cable transducers and 18 strain gages placed at four locations of interest along the length of the prototype brace. Each strain gage was oriented along the axis of the prototype brace.

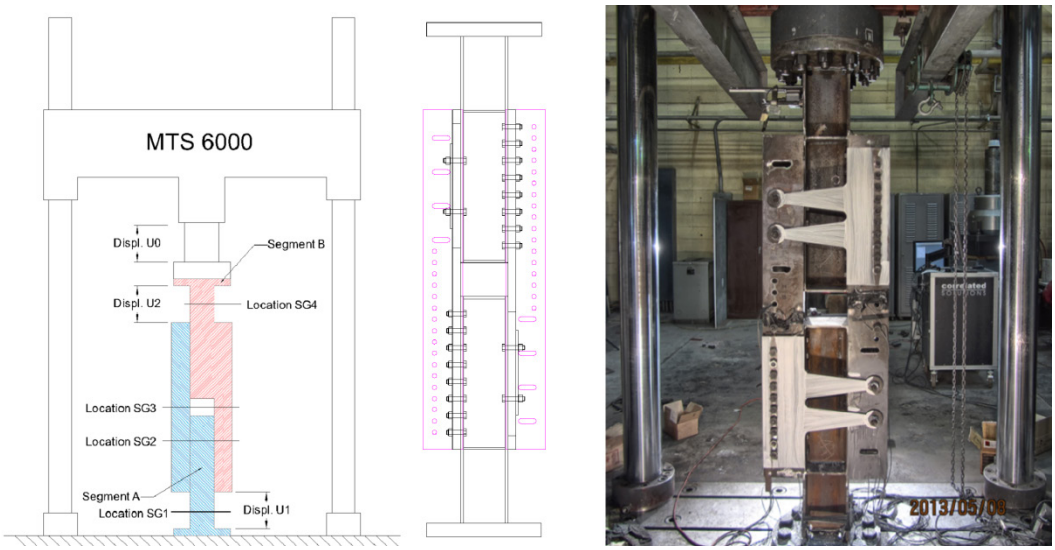

Figure 4-16: Instrumentation - Overall Layout

4.4.2.1 MTS 6000 Force and Displacement Output

The MTS 6000 test system does have a built-in load cell and displacement transducer (Displacement U0 as per Figure 4-16) data output from which was recorded during the experiment. Given that nominal capacity of the MTS 6000 system is 6000 kN, and that as the tested resistance of prototype brace on average did not exceed 800 kN it is a possibility that the built-in load cell of the MTS 6000 is not sensitive enough to measure smaller loads and should be checked against alternative methods.

4.4.2.2 Cable Transducers

Relative displacement of segment "A" versus segment "B" (as per Figure 4-16) was measured by two cable transducers (displacement U1 and displacement U2). It is important to note that if these two segments behaved as rigid bodies fixed at the ends, displacements U1 and U2 will be the same. However, rotational hinge at midpoint of the brace is introduced due to differential slip at two slotted connections displacements U1 and U2 will differ from each other.

4.4.2.3 Strain Gage Layout

Strain gage setup at location SG1 is used to capture the strong and weak axis moment as well as the axial force within the W200x59 beam. Four 5 mm strain gages were installed in accordance with the manufacturer's requirements. Both strain gages are oriented with their respective longitudinal axis parallel to the centerline of the brace prototype. Based on the sectional properties of the beam strong axis moment, weak axis moment and axial force demand can be calculated from data output obtained from strain gages. These values can be related to the brace end moment and axial reactions.

Strain gage setup at location SG2 is similar to SG1 and is used to capture axial force and strong axis moment. Strain gages are placed at the midpoint of the longitudinal line of bolts providing a fixed connection between the slotted plate and W200 x 59 beam. Strain gages at location SG2 are used to track ratio of axial to moment demand in a W200 x 59 beam at the midpoint of the slotted plate attachment.

At location SG3, strain gages are used to capture axial force and moment demands within slotted / side plates.

Strain gage setup at location SG4 is used to capture strong axis moment and axial force within W200 x 59 beam. Two 5 mm strain gages were installed in accordance with manufacturer's specifications. Both strain gages are oriented with their respective longitudinal axis parallel to the centerline of the brace prototype. Based on the sectional properties of the beam, the strong axis moment and axial force can be calculated from data output obtained from strain gages. These values can be related to the brace end moment and axial reactions.

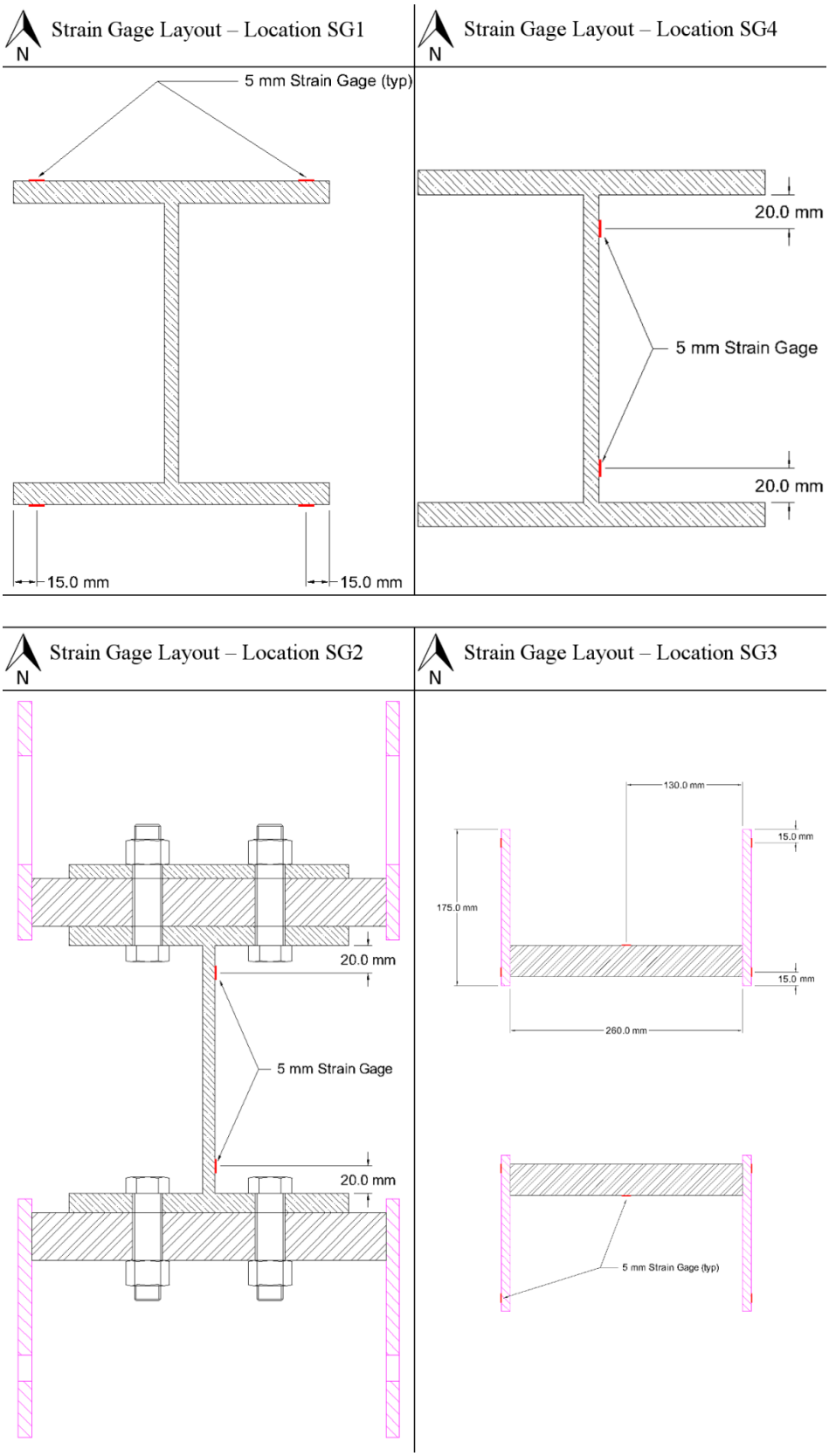

Figure 4-17: Strain Gage Layout - Each Location

4.4.2.4 Stereoscopic Correlated Camera Setup

To precisely capture deformation of the steel fuse plate for further analysis, a stereoscopic correlated camera setup was used. Cameras were calibrated as per manufacturer's specification for every experiment. Focal depth of the camera setup was adjusted to capture any possible out -of - plane deformation of the steel plate. Relative angle between cameras was set to be 25 degrees. Distance from the camera setup to the specimen was set to be 2.3 meters. Deformation sensitivity of less than 0.075 mm was achieved for any given experiment according to instrument calibration procedure.

4.5 Test Protocol

In order to select the most appropriate test protocol for the prototype brace being evaluated, a review of hysteretic tests performed on similar seismic energy dissipating elements has been performed. In particular, test procedures for buckling restrained brace used by (Black et al., 2004), cast steel yielding fuse evaluated by (Gray et al., 2010), and geometrically modified gusset plate energy dissipater (Mullin, 2005) were considered when deciding on the test protocol used for the prototype brace in this study. Test procedures for those particular energy dissipating systems were considered due to similarity of their hysteretic response to the expected behaviour of the prototype brace. In addition, energy dissipaters developed by (Mullin, 2005) and (Gray et al., 2010) are similar in basic engineering principle to the prototype brace evaluated within the scope of this research. It is important to note that while loading history of earlier tests of (Mullin, 2005) and (Black et al., 2004) relied on an older SAC Background Document SAC/BD-97/02 developed specifically for cyclic tests of moment resisting frames, a more recent evaluation of cast steel yielding fuse (Gray et al., 2010) used a test procedure specifically developed for BRB described in Appendix T of ANSI/AISC 341-05. While being similar, there are several differences between two protocols that were evaluated to come up with a loading history that will be suitable for this particular experimental program.

4.5.1 Loading History - SAC Background Document SAC/BD-97/02

Loading history presented in SAC/BD-97/02 was specifically developed for evaluation of seismic performance of beam to column connections of the moment frame. Given the brittle nature of beam to column connection failure if weld fracture occurs, the loading history had to closely evaluate susceptibility of a particular moment frame to low cycle fatigue. In addition since the strength deterioration of a fractured moment connection is rapid, SAC background document recommends testing at least three identical specimens as per ATC-24 (Clark et al., 1997).

Basic loading history within the SAC Background Document is defined as a function of story drift angle θ and is as follows.

Table 4.5: SAC Background Document 97/02 - Basic Loading History (Clark et al., 1997)

Load Step #	peak deformation θ (rad)	number of cycles, n
1	0.00375	6
2	0.005	6
3	0.0075	6
4	0.01	4
5	0.015	2
6	0.02	2
7	0.03	2
Continue with increments of 0.01, and perform two cycles at each step until severe deterioration occurs. Severe deterioration is defined as condition when resistance at peak deformation is less than 40% of overall peak load observed (Clark et al., 1997).		

An important note to consider is that above protocol was derived with inelastic deformations in mind, based on the idea that the lower bound of story drift angle for yield deformation to occur is $\theta = 0.005$ radians and upper bound is $\theta = 0.01$ radians (Clark et al., 1997).

In a study of seismic performance of BRB (Black et al., 2004), a full basic history was used initially with the addition of three steps that represent 25%, 50% and 75% of at-yield deformation of BRB. Recognizing that the relationship between story drift and level of inelastic deformation is different between the moment resisting frame and buckling restrained brace (BRB reaches yield sooner) a later stage of experiment used a loading history that limited number of cycles of SAC basic loading history to two while introducing two cycles each at drift corresponding to 25%, 50%, 75% and 100% of at yield story drift(Black et al., 2004).

The study *Gusset Plates as Energy Dissipaters in Seismically Loaded Structures* by Dean Thomas Mullin uses loading history similar to the SAC Background Document, gradually increasing the amplitude at a set step (Mullin, 2005 Section 4.8). A single load cycle for any given deformation amplitude was used.

4.5.2 Loading History - Appendix T of ANSI/AISC 341-05 - Qualifying Cyclic Tests of Buckling Restrained Braces

Loading history discussed herein was developed specifically for testing buckling restrained braces to satisfy potential seismic demands. Loading protocol is derived based both on at yield deformation of the specimen as well as the design story drift. Two cycles were performed per each deformation amplitude corresponding to at yield elongation (Δ_{by}), half of the design story drift (Δ_{bm}), $1.0 \times \Delta_{bm}$, $1.5 \times \Delta_{bm}$ and lastly $2.0 \times \Delta_{bm}$. In addition, if cumulative inelastic deformation of $200 \times \Delta_{by}$ is not achieved, cycles at $1.5 \times \Delta_{bm}$ shall be performed until this requirement is satisfied (ANSI Appendix T).

In addition, the test specimen has to replicate (within practical limits) an actual brace within a real building (including detailing, material, and connections).

As described, this loading history is proven to be adequate to test the deformation capacity of a buckling restrained brace. Given that the prototype brace developed in this research does rely on inelastic deformation of steel to accommodate large axial deformations and serves purpose very similar to BRB, this test protocol shall be applicable.

4.5.3 Loading History Used in the Experimental Program

Appendix T of ANSI/AISC 341-05 is, in theory, a more representative testing protocol since it was developed for a BRB (that is expected to have a similar response to the brace prototype developed herein) rather than a recommended beam to column connection loading history of SAC Background Document. A the same time, if one were to use a design story drift of 1.5% (0.5% less than High Importance building (National Research Council Canada, 2010) Basic loading history as per SAC Background Document will cover all the cycles of Appendix T ANSI/AISC 341-05 and include few additional.

Given the above, it was decided to use basic loading history as per the SAC Background Document while adding additional cycles (two of each) at $0.5 \times \Delta_{by}$, $0.75 \times \Delta_{by}$, and $1.0 \times \Delta_{by}$ amplitudes to obtain a more gradual increase in deformation amplitude when compared to the loading history of Appendix T of ANSI/AISC 341-05. Cumulative inelastic deformation of the brace prototype was calculated to confirm that it is satisfies AISC 341-05 (i.e. is larger than 200 x Δ_{by}); Δ_{by} of the assumed brace member of 7050 mm was taken as 90% of at yield elongation of said member (12.69 mm) given that in a capacity based design, primary non-sacrificial load carrying components are not designed to carry 100% of their capacity.

Table 4.6: Loading History - Experimental Program

Load Step #	peak deformation, θ	number of cycles, n	brace elongation, ΔL	rate	Cumulative Inelastic Deformation
	rad		mm	mm/min	x Δ_{by}
1	N/A	2	3.875	4	0.0
2	N/A	2	4.4375	4	0.0
3	N/A	2	5	4	0.0
4	0.00375	2	11.8	10	3.4
5	0.005	2	15.73	15	9.4
6	0.0075	2	23.58	15	20.2
7	0.01	2	31.42	15	36.0
8	0.015	2	47.08	15	61.7
9	0.02	2	62.71	15	97.2
10	0.03	2	93.86	15	152.4
11	0.04	2	124.9	15	227.2
12	N/A	2	140	15	311.4

The rate of deformation imposed on the specimen shall ideally be equal to the rate imposed by a seismic event. However, given that this is not achievable, the rate of the test will be limited so that the test is representative of a quasistatic loading condition. Given that possible behaviour of the

specimen is currently unknown, a quasistatic load case will allow for more accurate observation of the test. Also, if actual dynamic response is required it can be numerically estimated from a given quasistatic response. With this in mind, and to accommodate reasonable test duration of 5-6 hours, the crosshead displacement rate was set to 15 mm/min. If related to the strain rate induced within steel fuse plate due to bending of the shear links, this rate is within the range of recommended rates for determining of at yield properties of a tension coupon as per ASTM E8/E8M which is deemed adequate for quasistatic loading rate.

5 Experimental Results

5.1 Introduction

Seven tests have been carried out. Two of the tests evaluated friction properties of the slotted connection – one friction only test for a clean mill scale surface and one friction only test for a surface with friction sheet material. Five different arrangements of steel fuse plates within prototype brace were evaluated as a part of the experimental program.

During the test an electronic data acquisition (EDAQ) system recorded output from MTS 6000MTS 6000, cable transducers and strain gages located on a specimen.

Data output from the strain gages was "zeroed" manually in an excel spreadsheet. Strain gage recorded data is not presented in its unprocessed state; instead strains recorded on a surface of the specimen are converted to axial forces and moments. Axial force demand as well as in-plane and out-of-plane moment demand in the W200 x 59 beam has been calculated using elastic properties of the section.

In addition to numerical data, a stereoscopic correlated camera setup was adjusted to take a pair of images every four seconds. Time of the image taken was related to the displacement and force readings of MTS 6000 in order to know the time stamps of the particular photo.

In this chapter, test results as well as visual observations will be presented for each test. Response of the prototype brace will be presented in a form of a hysteretic loop of axial force versus displacement for every value of deformation amplitude of the experiment. Additional numerical information, such as end moments of the brace and axial force carried by either pair of a side plate / slotted plate assembly, will be introduced on an as-required basis.

Axial force data in tests that incorporate steel fuse plates combines response due to friction mechanism and inelastic deformations of the fuse plates. In order to separate the two responses, a friction only test has been conducted before and after each experiment. Following procedure has been used to separate data output due to two different mechanisms. A typical friction hysteretic loop has been analyzed and a representative sixth order polynomial equation has been developed to match the profile of friction only curve for both tension and compression. A tension force value at zero displacement from before and after the experiment has been recorded. Friction resisting force at zero displacement for any time point of the experiment is to be calculated by gradually change from the before-test-value to after-test-value based on the ratio of cumulative friction path length at any point of time to total friction path length of the entire test. In addition, a tension force value at zero displacement has been recorded for a typical friction hysteretic loop. For any time point of the experiment, a friction force can be evaluated by multiplying a corresponding friction

force from a typical hysteretic loop by a ratio of a current friction resisting force at zero displacement to friction resisting force at zero displacement of a typical hysteretic loop. Once friction resisting force has been evaluated, a corresponding fuse resisting force can be obtained by subtracting a friction only resisting force from the overall hysteretic response of the prototype brace. It is important to note that this method of analytical response separation is not sensitive enough to effectively separate friction and inelastic response during loading stage with large combined stiffness (i.e. initial loading or direction change). During this stage both mechanisms can potentially contribute to overall force versus displacement curve, however, analytically it was assumed that steel fuse plate contribution is zero. Accuracy of response separation during steady continuous slippage is unaffected by such approximation.

Strain and deformation output from the stereoscopic correlated camera setup is to be used for evaluation of the strain distribution within different types of ductile steel fuse plates. In addition, a deformation gradient of the steel fuse plate can be used to evaluate initiation of out-of-plane behaviour of the shear link. Above data is essential for calibrating a numerical model should the need arise.

In addition to quantitative results, comments on overall behaviour of the tests specimen as well as wear of its individual components will be noted on as-needed basis.

5.2 Test Results

This section will focus on evaluation of the load versus displacement hysteretic response of the prototype brace. Given that discrepancy between axial load values obtained from strain gauge data and directly read out of MTS machine is typically under 6% (after initial zero calibration) it was decided to use MTS output for the load versus displacement response evaluation.

5.2.1 Friction Only Test 1 – Load versus Displacement

First two tests of the experimental program were carried out on the prototype with no steel fuse plate attached. In the first friction test the interface between sliding surfaces was clean mill scale. Based on the calculated bolt pretension level of 113 kN per bolt, four bolts per slotted connection with two planes of slippage the predicted friction force of the prototype brace is 460 kN. Given the uncertainty of frictional behaviour of the connection at slip, initial rate of loading was set to 0.56 mm/min and subsequently increased to 15 mm/min at 16 mm of displacement. During initial loading in tension (cycle 1) several loud bangs were heard from the test setup. Initially the sound was attributed to bolt aligning themselves in the long slots.

Load carrying capacity of the prototype brace was somewhat unstable but progressively increasing up to 839 kN in tension at displacement of 140 mm (elongation) – well in excess of predicted 460 kN. Initial guess was a conservative assumption of either pretension force or friction properties of

the clean mill scale. Furthermore, Axial deformation of the prototype brace was continuously accompanied by loud noise originating from the test setup.

At elongation of 140 mm, deformation applied by MTS 6000MTS 6000 has reversed direction and the prototype brace was subjected in compression. Almost immediately compression load picked up to previously achieved tension load of 839 kN and started to steadily increase. During the compression part of the cycle, banging sound originating from setup got louder and more frequent. Compression capacity of the brace progressively increased to 1295 kN at displacement of 30 mm at which point it was decided to stop the test. The axial load versus displacement curve of Test 1 is shown in .

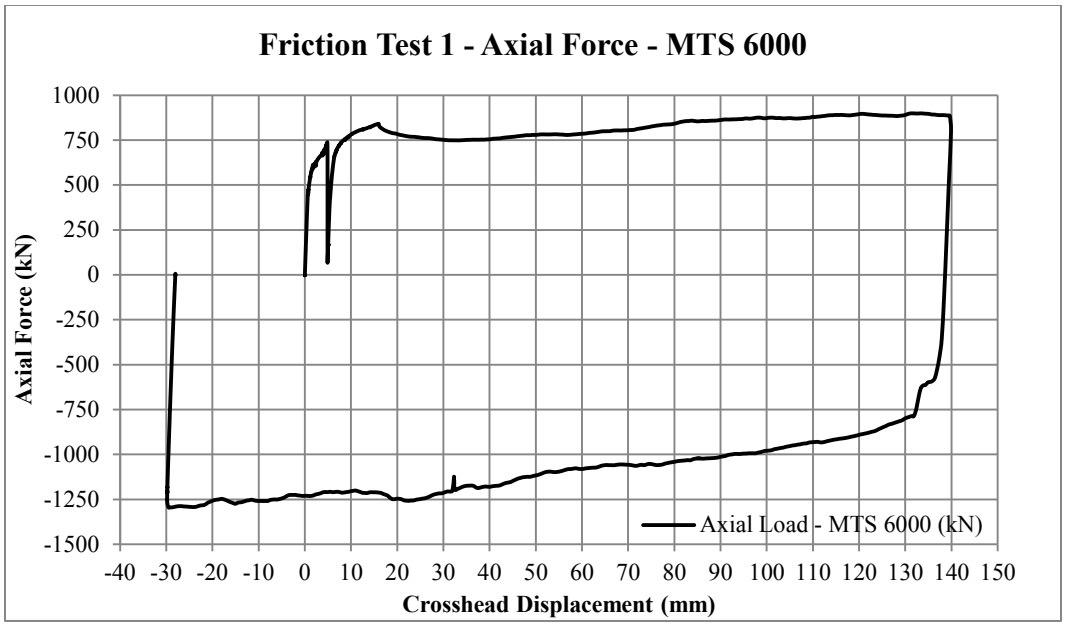

Figure 5-1: Axial Force versus Displacement - Friction Test # 1

Upon disassembly, severe galling at the friction interface has been observed; grooves of up to 5 mm depth and 20 mm width formed on the steel surface while mill scale was gone at the contact points, as shown in Figure 5-2.

Figure 5-2: Galling at Friction Interface

Additional literature review with regards to galling of steel surfaces has been performed. Even though it is known that at certain degree of pretension, effect of galling is quite small, i.e. mild wear (Archard and Hirst, 1956), it is difficult to be certain if the rate of wear can become sufficiently small to sustain 6 tests with cumulative wear path of approximately 26,000 mm.

Due to this fact it was decided to abandon the idea of using clean mill scale as friction interface and to apply a readily available nonmetallic glass reinforced sheet friction material for the rest of the test program.

5.2.2 Friction Only Tests 2 and 3

Friction tests #2 and #3 were attempted but are not presented due to technical difficulties mentioned below. After sliding surfaces has been repaired, specimen was reassembled, however layer of sandpaper to secure PTFE sheet (as per Figure 4-10) has not been provided – it was assumed that bolts themselves would provide enough resistance to PTFE to initiate sliding on one

surface only. During the initial loading, a low crackling noise could be heard – bolts had torn the PTFE sheet and it was slipping out of the connection sliding interface, as shown in .

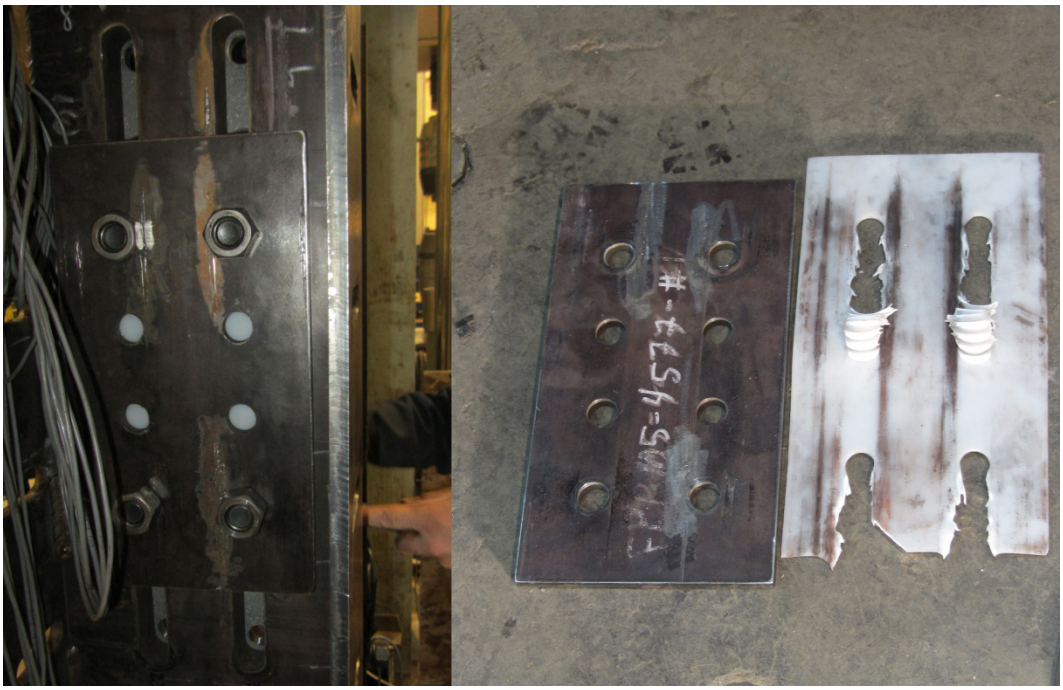

Figure 5-3: Friction Test 2 - PTFE Sheet Slip Out

5.2.3 Friction Only Test 4 - Load versus Displacement

In order to force slippage of the PTFE sheet on the slotted surfaces and effectively fix the sheet to the "washer" plate, a layer of coarse sand paper was glued to the washer plate as per Figure 4-10. specimen was re-assembled using eight bolts per connection instead of four and the test continued. Bolts were pre-tensioned to 72.5 kN each. Expected friction resistance based on eight bolts per sliding surface, two sliding surfaces and friction coefficient of 0.52 for friction material and 0.05 for PTFE is 661 kN.

Loading rate was set to approximately 1.1 mm/min. Initial slip load peaked at 420 kN at displacement of 2 mm. After reaching the peak value friction resistance has dropped to and stabilized at 315 kN.

At crosshead displacement of 17 mm, loading rate was increased to 15 mm/min and axial resistance of the brace increased to 350 kN in tension (a 11% increase in force for 1264% increase in loading rate). The complete axial force versus displacement curves of friction only Test 4 are shown in .

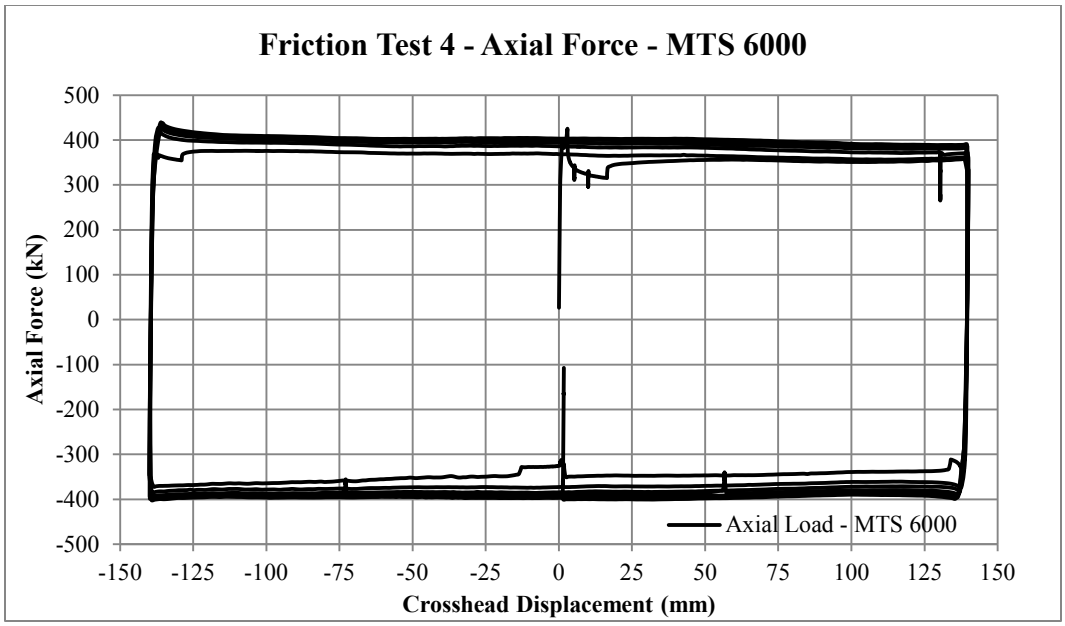

Figure 5-4: Axial Force versus Displacement - Friction Test # 4

Each cycle friction resistance of the slotted connection continued to increase. The increase is attributed to wearing out of dry lubricant placed between Teflon sheet and steel surfaces of the slotted plate.

After six cycles, friction resisting force stabilized at 402 kN at 0 mm crosshead displacement. As-tested friction resistance in first successful friction only test that incorporates friction sheet material was 39% less than predicted value. It is suspected that initial setting of compressible friction sheet material is the source of this discrepancy as suggested by research done on structural slotted connections that incorporate braking pads (Pall, 1979). Friction only tests # 5 and # 6 are expected to demonstrate significantly smaller discrepancy between predicted and actual friction force given that friction sheet material was already compressed during current test (# 4). Friction properties of the sheet material proved to be very stable with at slip friction coefficient being the same as dynamic friction coefficient as displayed by several pauses introduced in a loading history.

5.2.4 Friction Only Test 5 & 6 – Load versus Displacement

Two more friction only cyclic tests have been carried out using same slip surface in order to confirm stability within friction properties. Both tests were done at loading rate of 15 mm/min.

Test 5 has been carried out without changing pretension achieved during friction only Test 4. During first cycle, resisting force changed from 400 kN at 0 mm displacement to 428 kN at 0 mm (end of cycle one). During cycle two to four, change of the friction force was relatively small and at the end of cycle four at 0 mm displacement it was equal to 422 kN.

Pretension was changed for friction only Test 6 to 55.8 kN per bolt. Based on the friction coefficient of 0.57, expected resistance of the brace is 509 kN. Three cycles of loading has been performed. Friction resisting force varied from 450 kN to 457 kN at 0 mm crosshead displacement, which would correspond to overall friction coefficient of 0.51. Discrepancy between actual and predicted friction force is equal to 10% and is significantly smaller when compared to friction only test # 4. The decrease is likely due to setting of the material after initial pre-tensioning of the friction interface during friction Test 4. During friction Tests # 5 and # 6 additional setting of the material was insignificant given that it have already been previously compressed.

Overall, after initial "setting" of the material, friction resistance provided by the glass fiber reinforced friction sheet material is very stable within a single cycle – variation is in a range of 2%. However, it is somewhat challenging to accurately predict the value of resisting friction force based on calculated pre-tension force. In order to measure friction-only resistance for tests that incorporate both steel fuse plate and friction interface, a friction only pre-test and after-test shall be done.

5.2.5 Test Specimen # 1 - Load versus Displacement

Loading history has been applied to Test Specimen # 1 (with fuse type C4) as per section 4.5.3, however, given it is the first test in series, a number of cycles per each deformation amplitude has been reduced to one. Friction pretest has been performed prior to full test. The Test Specimen #1 prior to test, in the setup, is shown below.

Figure 5-5: Test Specimen # 1 - Prior to Test

Hysteretic loops of the friction pretest were very stable and friction resistance in tension at zero displacement was equal to 400 kN. Due to the time restraints, removal of the fuse plates and following after test took place on the following day (as a pretest to Test Specimen # 2). Friction resistance in tension at 0.00 mm displacement after Test Specimen #1 was completed equaled to 327 kN. Relaxation of the friction force is attributed to wear and setting of friction material that occurred due to significant compressive force applied to the friction interface by a "bottomed out" shear links as it will be discussed further.

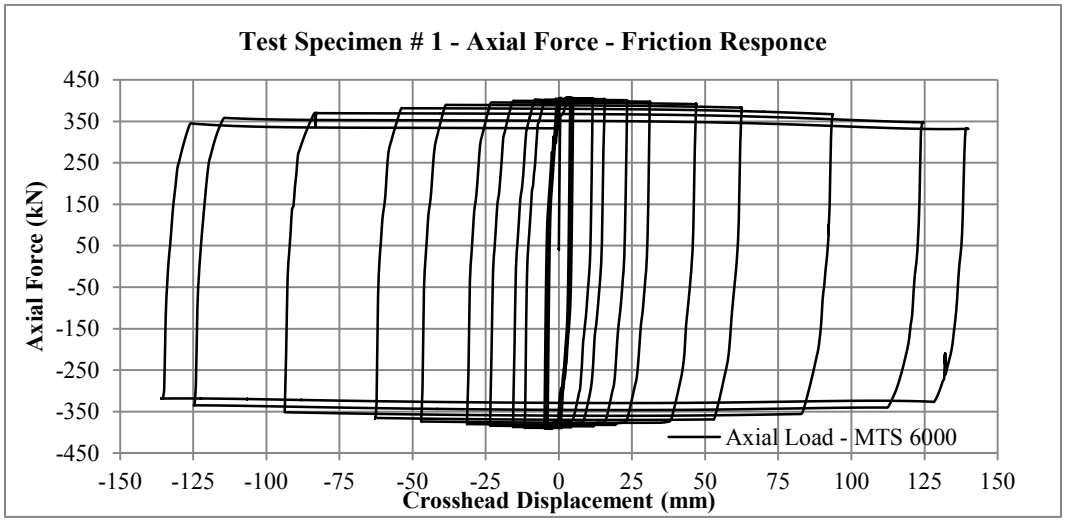

Figure 5-6: Axial Force versus Displacement - Test Specimen # 1 - Friction Response

Combined response of the prototype brace proved to be stable with a positive slope except for last few cycles of large deformation amplitude. Maximum deformation achieved by the prototype brace was recorded at +140 and -135 mm. Steady state pre-fuse-buckling load carrying capacity was recorded to be 618 kN in tension after 47 mm cycle at 0 mm displacement, as shown in Figure 5-7.

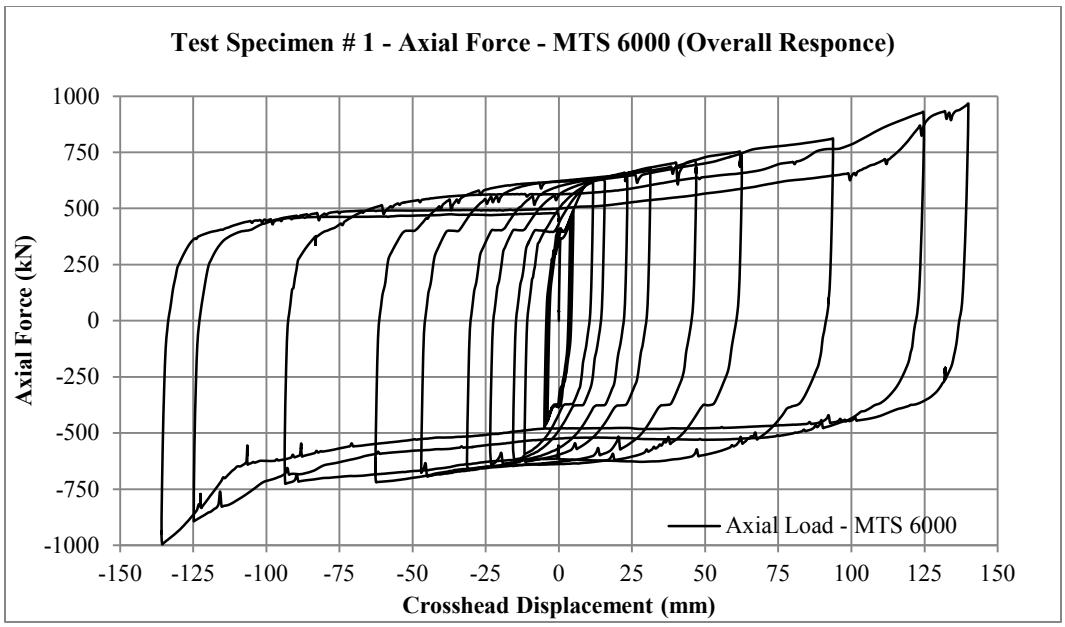

Figure 5-7: Axial Force versus Displacement - Test Specimen # 1 - Combined Response

Loading of the brace specimen was accompanied by load noise originating from the slots within side attachment plate connecting the top of the shear link within ductile steel fuse plate to primary load carrying components of the brace. After each noise instance, a small drop and a following rapid recovery in a resisting load has been observed. After disassembly it became apparent that slots were deforming plastically during the test, forming peaks and valleys that were restraining motion of the shear link and causing loud abrupt noise.

In order to track displacement pattern of the top of a shear link an additional cable transducer has been installed.

Resistance of the steel fuse plates degraded over time due to buckling that started to become apparent at crosshead displacement equal to and larger than 60 mm. At zero displacement maximum overall resistance degradation of the prototype brace was ~20%, however this would include a very stable response due to friction force that can be quantified analytically as a function of friction resistance values from before and after the main test.

Hysteretic response of the steel fuse plate can be separated in four stages.

Stage one is characterized by elastic response of the steel fuse plate during hysteretic loops one to three as depicted in Figure 5-8. During elastic stage fuse contribution is very limited given that friction only slip due to oversized slots in fuse attachment plates is large when compared to overall deformation amplitude. Loading rate for stage one was set to 4 mm/min primarily to obtain more data points for short amplitude cycles.

Figure 5-8: Axial Force versus Displacement - Test Specimen # 1 - Hysteretic Loops 1 to 3

During stage two that encompasses hysteretic loops four to eight response of the steel fuse plate is no longer elastic however it continues to behave primarily in plane with no strength degradation due to buckling, as shown in Figure 5-9.

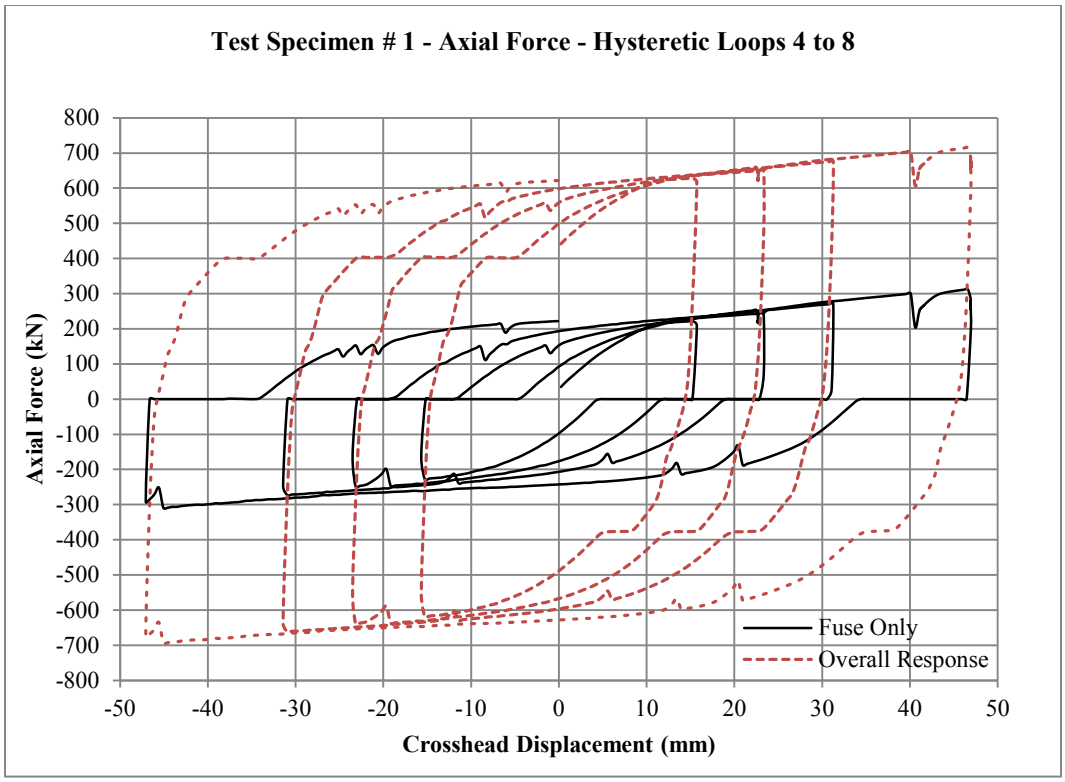

Figure 5-9: Axial Force versus Displacement - Test Specimen # 1 - Hysteretic Loops 4 to 8

Resistance degradation out-of-plane behaviour was observed during stage two which start to become apparent in cycles 9 and 10, as shown in Figure 5-10. Fuse plate resistance degradation due to buckling during cycles nine and ten was relatively small in a range of 16 %, as shown in Figure 5-11.

Figure 5-10: Test Specimen # 1 – Buckling of Steel Fuse Plate – Cycles 9 and 10

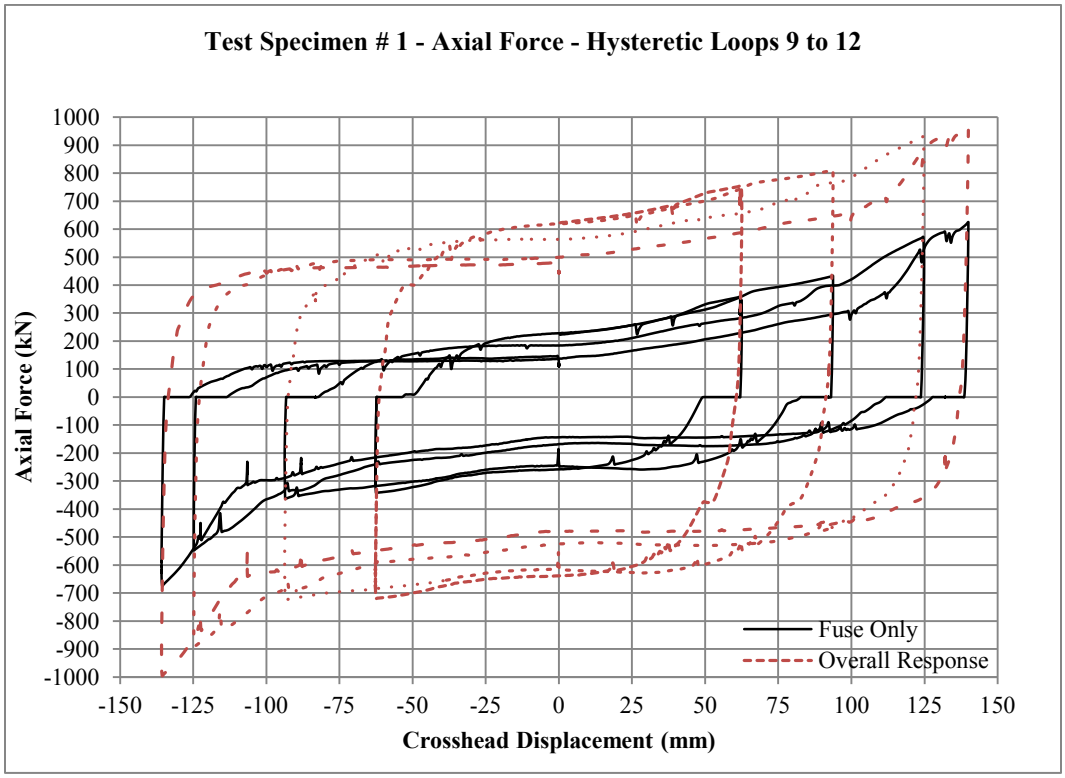

Figure 5-11: Axial Force versus Displacement - Test Specimen # 1 - Hysteretic Loops 9 to 12

Stage four is characterized by significantly larger out-of-plane deformations and introduction of tension within the shear link due to it reaching the end of the attachment plate slot, as shown in Figure 5-12.

Figure 5-12: Test Specimen # 1 – Buckling of Steel Fuse Plate – Cycles 11 and 12

At zero crosshead displacement, overall degradation of the steel fuse plate at the end of cycle 12 was recorded to be ~37%. Given extent of the buckling during last two cycles of the test a "pinching" effect has been observed, i.e. the slope of force – displacement curve at zero crosshead displacement was slightly negative. Nevertheless at extreme deformation significant stiffening of the system was observed due to change of the boundary condition within the link. If detailed properly, such boundary condition can serve as an effective limit to the lateral story drift of the building.

Overall deformation capacity achieved by the test was +/- 140 mm. However, at such deformation buckling of the plate became a response defining factor and caused significant degradation in load carrying capacity. In future study buckling of the shear link can be reduced by varying its cross-section and /or carefully designing boundary conditions at the top of the link in such a way that does not introduce compressive axial demands and initial out -of -plane moment due to bending of the shear links caused by the assembly.

5.2.6 Test Specimen # 2 - Load versus Displacement

Test Specimen # 2 was carried out on the same specimen configuration as Test Specimen # 1 (Figure 5-13), except fuse plates C1 were used. Loading history has been applied in full as per section 4.5.3, unlike Test Specimen # 1, which was subjected to reduced loading history.

Figure 5-13: Test Specimen # 2 - Prior to Test

Friction pretest has been performed prior to full test. Hysteretic loops of the friction pretest were very stable and friction resistance in tension at zero displacement was equal to 346 kN. Friction resistance of the prototype brace was also measured after the completion of full loading history of Test Specimen # 2 and was recorded to be 298 kN at zero displacement.

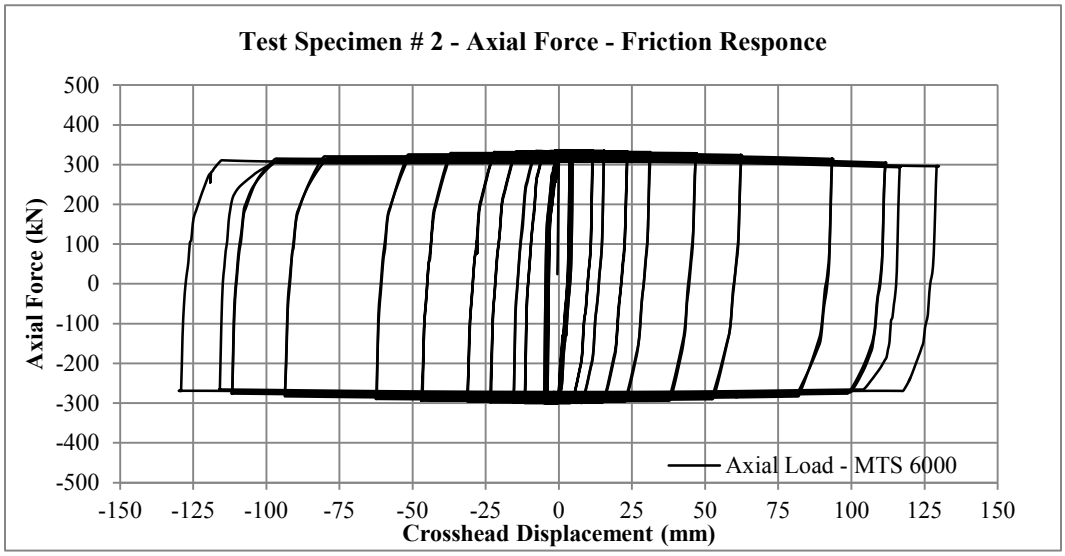

Figure 5-14: Axial Force versus Displacement - Test Specimen # 2 - Friction Response

Similar to Test Specimen # 1, relaxation of the friction force is attributed to wear and setting of friction material that occurred due to significant compressive force applied to the friction interface by a "bottomed out" shear links.

Combined response of the prototype brace exhibited positive slope, as shown in Figure 5-15. Up to deformation cycle of 60 mm the effect of lateral-torsional buckling on overall response was minimal. Deformation cycles with amplitude of 90 mm and larger, the capacity of fuse plates was visibly affected by out-of-plane behaviour of the shear link. Change in boundary condition at the tip of the link at large deformations resulted in significant stiffening at the last cycles of the test, which offsets loss of capacity due to buckling of the link.

Maximum deformation achieved by the prototype brace was recorded at +/- 130 mm. Steady state pre-fuse-buckling load carrying capacity was recorded to be 560 kN tension after 47 mm cycle at 0 mm displacement.

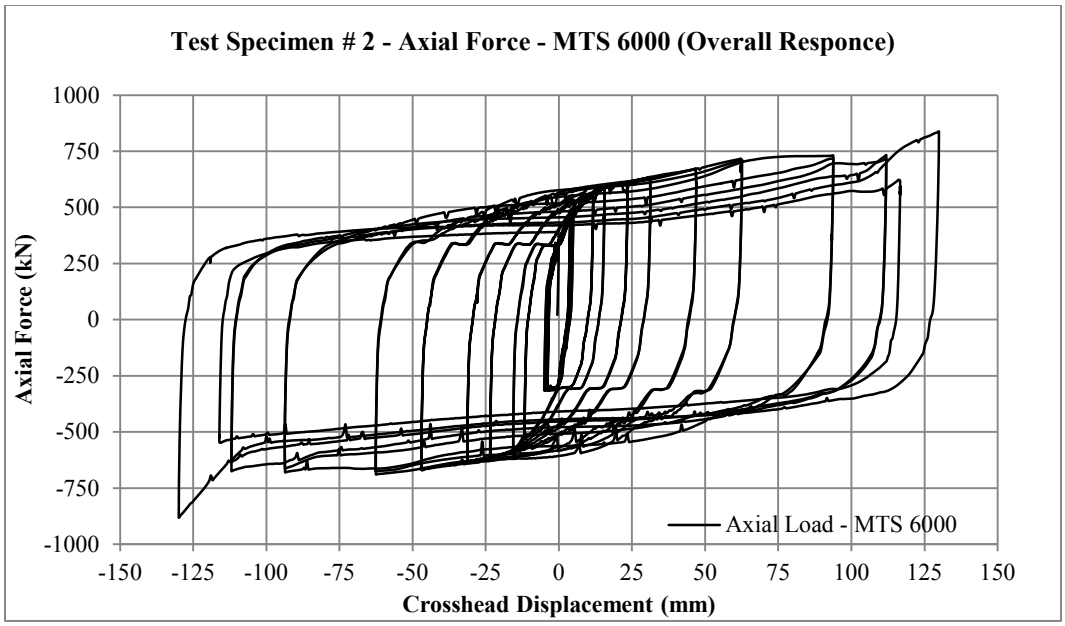

Figure 5-15: Axial Force versus Displacement - Test Specimen # 2 - Combined Response

As evident from load versus displacement curve, load drops attributed to deterioration of the slot attaching tip of the shear link is present and similar to the Test Specimen # 1. At the end of the test the "widening" of the slot due to bearing deformation became more pronounced, as shown in Figure 5-16, when compared to Test Specimen # 1. Concerns are expressed regarding the possibility of using same fuse attachment points for all five brace prototype tests.

Figure 5-16: Deterioration of Slots within Fuse Attachment Plate

Similar to Test Specimen # 1, overall response can be separated into four regions: in-plane elastic, in-plane plastic, out-of-plane plastic, out-of-plane plastic with stiffening due to boundary condition change. Those stages are correspondingly presented in Figure 5-17 to Figure 5-20. Inelastic steel fuse plate response is presented alongside combined brace response where by doing so the clarity of the figure is unaffected. When compared to Test Specimen # 1, Test Specimen # 2 exhibited significantly larger capacity degradation due to twice the number of cycles of the loading history. At zero displacement at the end of cycle 22, overall resistance degradation of the prototype brace was ~30%, and overall degradation of the steel fuse plate resistance due to buckling was recorded to be ~63%. It is important to note that significant capacity degradation due to lateral-torsional buckling of steel shear link occurred at amplitude higher than 95 mm; at the end of the cycle 18 (amplitude = 94 mm) capacity degradation of the steel fuse plate was 30%. Brace capacity degradation was partially offset by the eventual stiffening due to boundary condition change at the tip of the shear link.

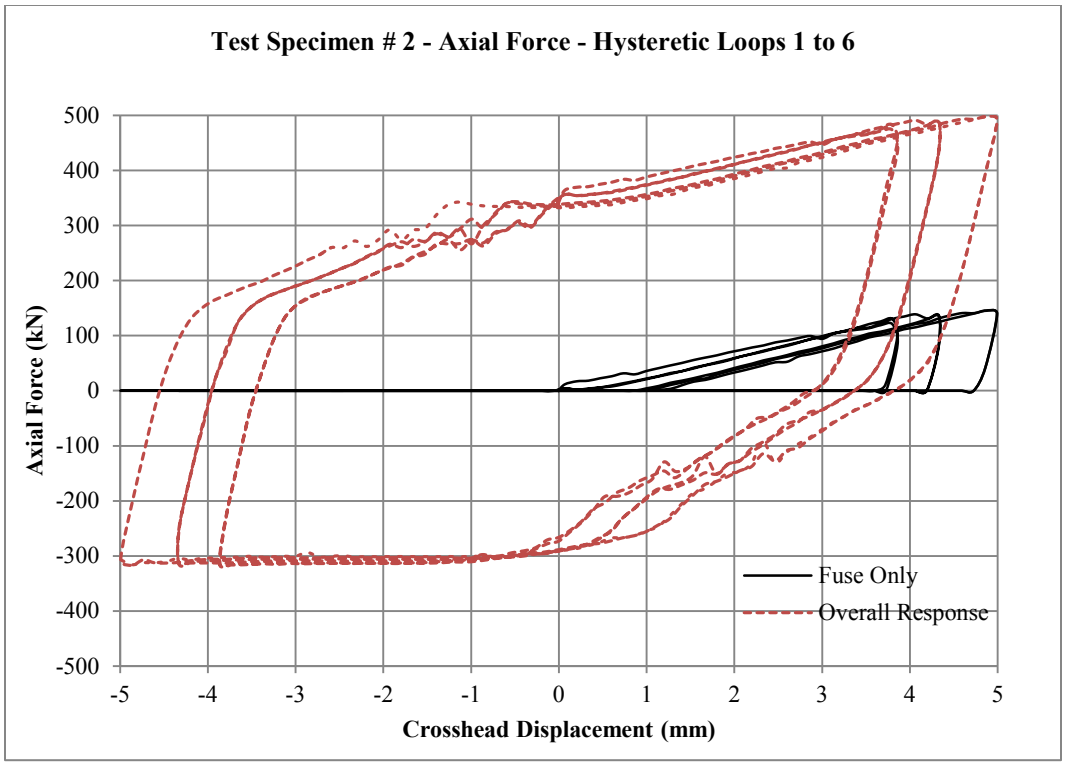

Figure 5-17: Axial Force versus Displacement - Test Specimen # 2 - Hysteretic Loops 1 to 6

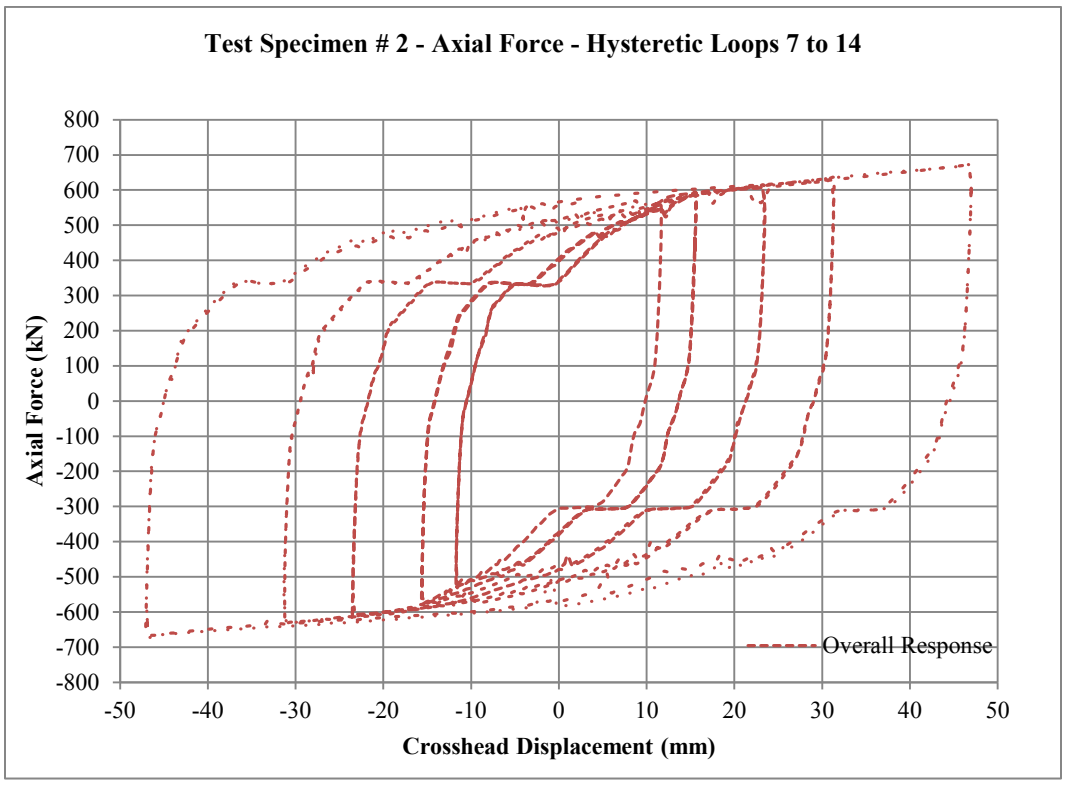

Figure 5-18: Axial Force versus Displacement - Test Specimen # 2 - Hysteretic Loops 7 to 14

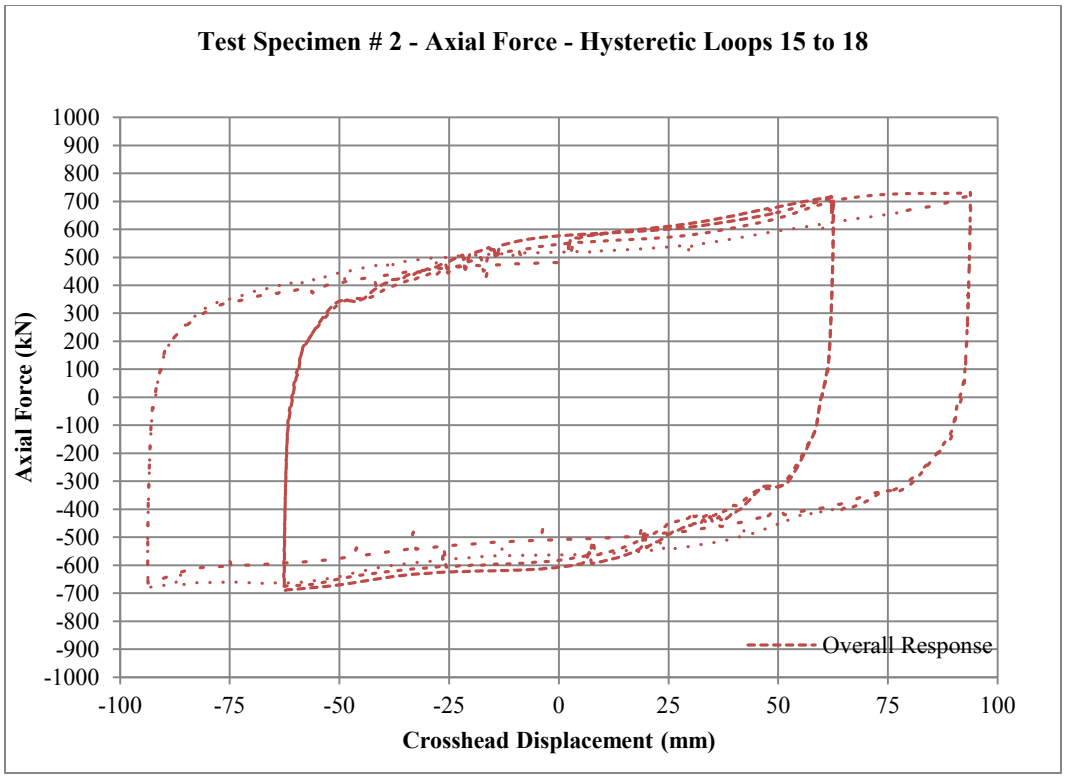

Figure 5-19: Axial Force versus Displacement - Test Specimen # 2 - Hysteretic Loops 15 to 18

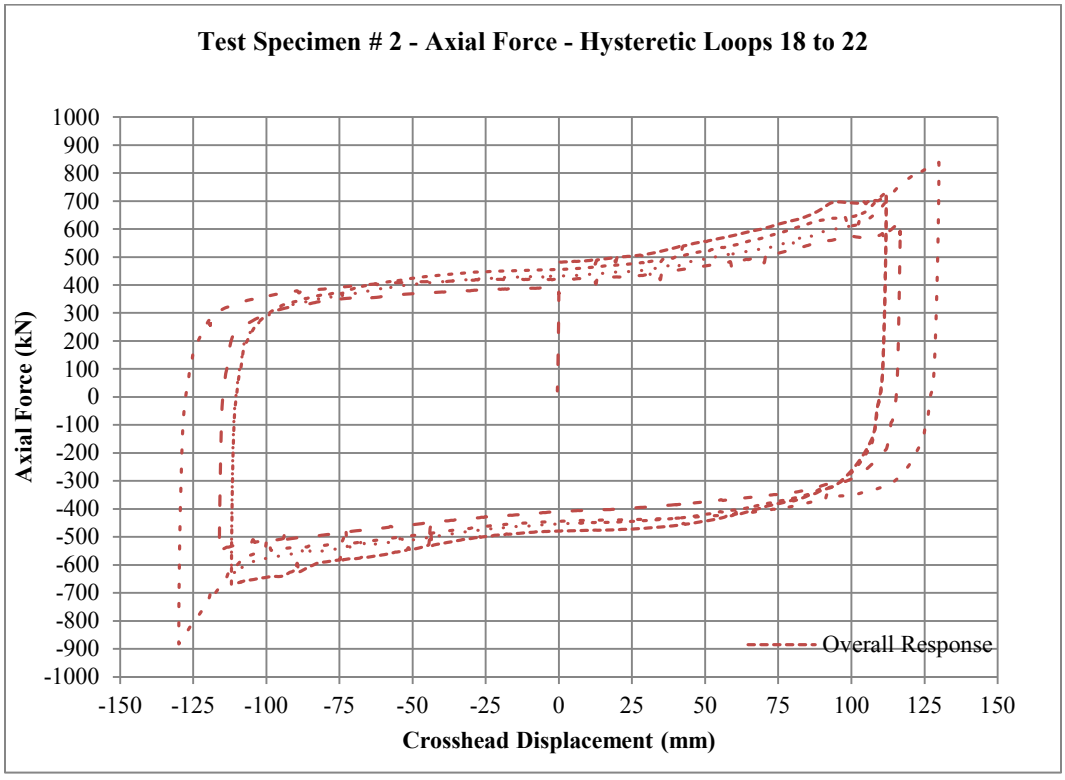

Figure 5-20: Axial Force versus Displacement - Test Specimen # 2 - Hysteretic Loops 18 to 22

5.2.7 Test Specimens # 3, # 4 and # 5 – Load versus Displacement

Loading history for Test Specimens 3, 4 and 5 was identical to loading history of Test Specimen # 2, and is described in section .The only exception was the amplitude of the two last loading cycles, which is dependent on the occurrence of stiffening, and is such to avoid rapture of the shear links within steel fuse plate. Condensed test results for Test Specimens 3, 4 and 5 will be provided in sections 5.2.8 to 5.2.10 inclusive. Load versus displacement response of prototype brace specimens # 3, # 4 and # 5 were similar to response of Test Specimen # 2 with exception to several specific details steel fuse plate.

5.2.8 Test Specimen # 3 - Load versus Displacement

Prototype brace specimen with a fuse type C3 was evaluated in Test Specimen # 3, as shown in Figure 5-21.

Figure 5-21: Test Specimen # 3 - Prior to Test

Prior to test, friction of the brace prototype was measured to be 413 kN tension at zero crosshead displacement and after the test it was recorded to be 349 kN.

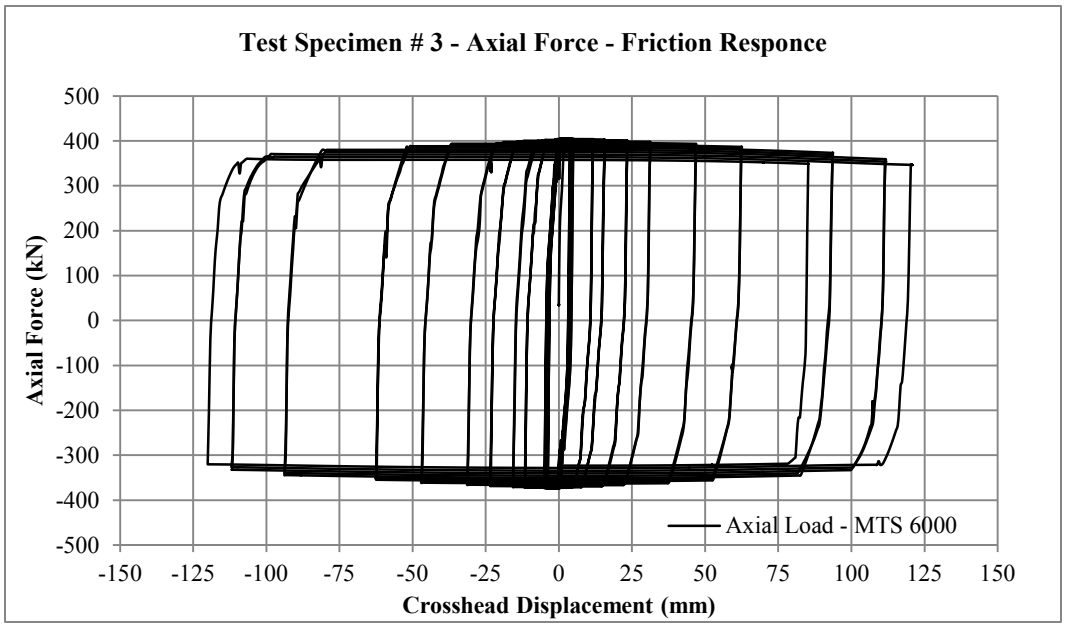

Figure 5-22: Axial Force versus Displacement - Test Specimen # 3 - Friction Response

Test Specimen 3 was terminated early during the cycle number 22 at the deformation of 65 mm due to the fracture of one of the shear links, as shown in Figure 5-23. Fracture occurred at the location of the fabrication imperfection – a notch unintentionally cut by the manufacturer at the neck of the steel shear link initiated the fracture. This is unlikely to have happened otherwise. Capacity loss due to fracture of a single shear link at that stage of loading caused capacity loss of approximately 40 kN. If each shear link were to carry equal load, at that stage of the test the combined load capacity of shear links would be 160 kN. Based on the estimated friction resistance and combined response of the prototype brace, steel fuse plateload carrying capacity of steel fuse plates prior to fracture was 153 kN, which corellates well with the capacity lost due to fracture.

Figure 5-23: Test Specimen 3 - Shear Link Fracture

Maximum longitudinal deformation achieved by brace prototype was +/- 120 mm and was limited by the boundary condition at the tip of the shear link, as shown in Figure 5-24. Steady state pre-

fuse-buckling load carrying capacity was recorded to be 594 kN tension after 47 mm cycle at 0 mm displacement.

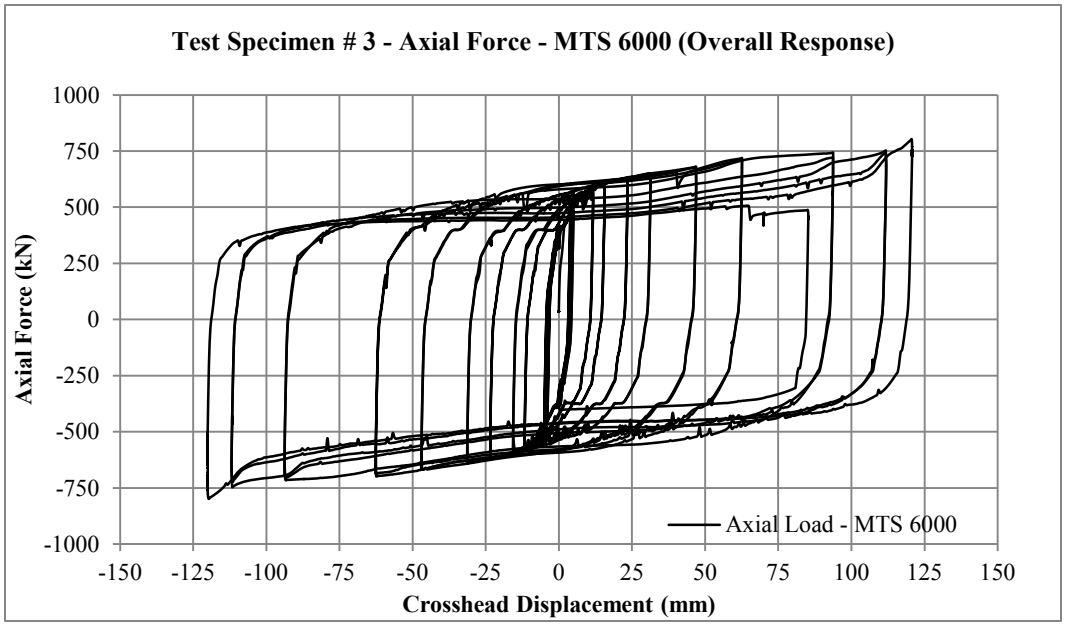

Figure 5-24: Axial Force versus Displacement - Test Specimen # 3 - Combined Response

Similar to previous tests, hysteretic loops 1 to 6 exhibited elastic behaviour of the steel fuse plate, loops 7 to 14 exhibited in-plane elasto-plastic behaviour, loops 15 to 18 showed initiation of out-of-plane buckling. At the end of the cycle 18, capacity degradation of steel fuse plate at zero displacement was recorded to be 39 % when compared to pre-buckling value. Cycles 19 to 22 showed further capacity loss due to lateral torsional buckling of the shear link followed by stiffening due to change in boundary conditions. Those stages are correspondingly presented in Figure 5-25 to Figure 5-28; inelastic steel fuse plate response is presented alongside combined response where by doing so the clarity of the figure is unaffected. Pre-stiffening capacity loss of steel fuse plate at the end of cycle 21 was 58 % when compared to pre-buckling value, while overall brace capacity loss was calculated to be 26 %. Capacity loss after cycle 22 could not be estimated due to fracture of the steel shear link.

Overall hysteretic response of the brace prototype was characterized by increased “jitter” due to incremental slippage at the slots that are attaching tips of steel fuse plate shear links.

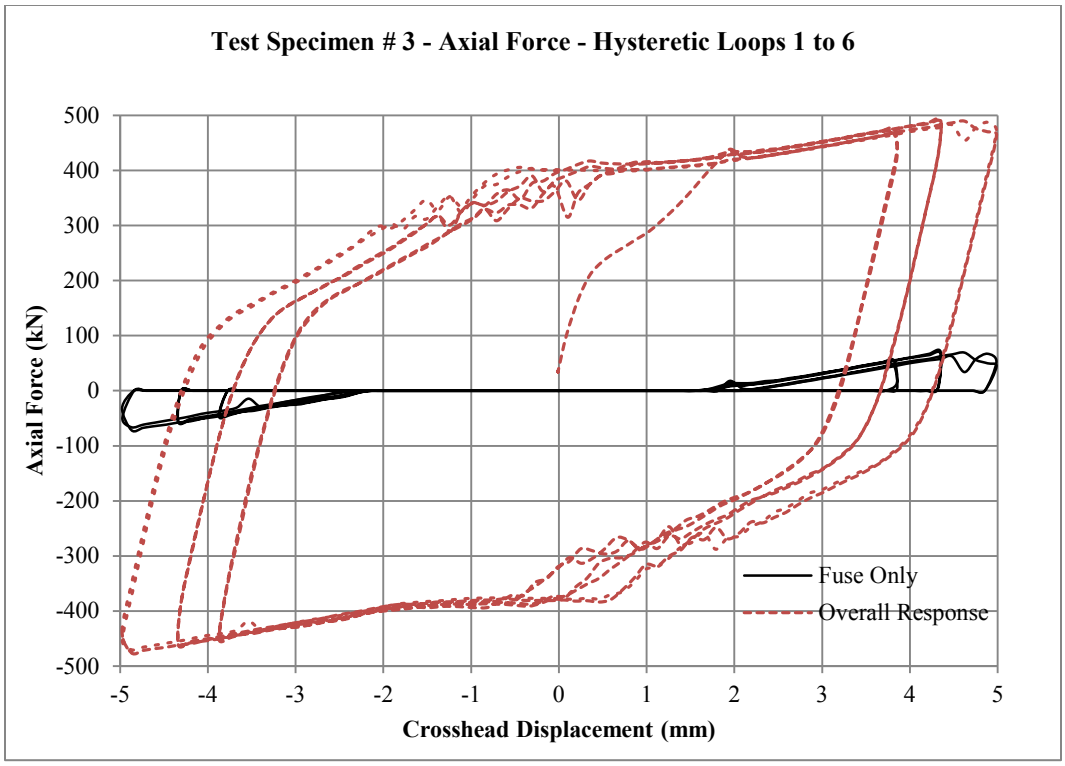

Figure 5-25: Axial Force versus Displacement - Test Specimen # 3 - Hysteretic Loops 1 to 6

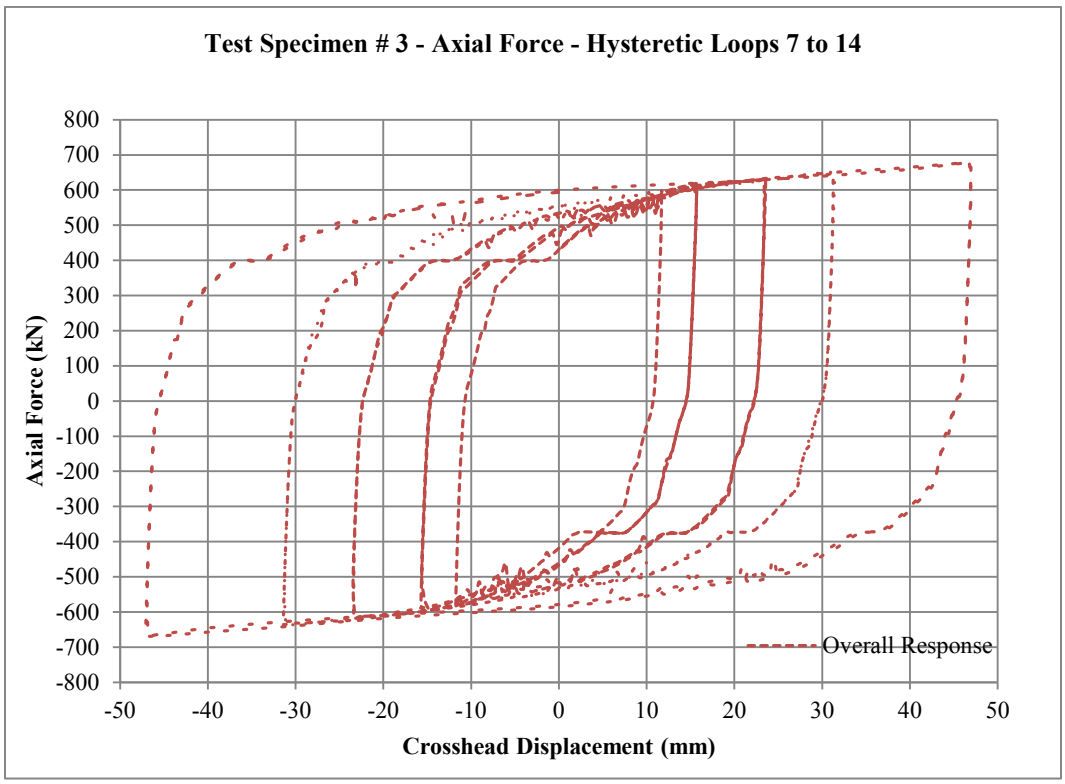

Figure 5-26: Axial Force versus Displacement - Test Specimen # 3 - Hysteretic Loops 7 to 14

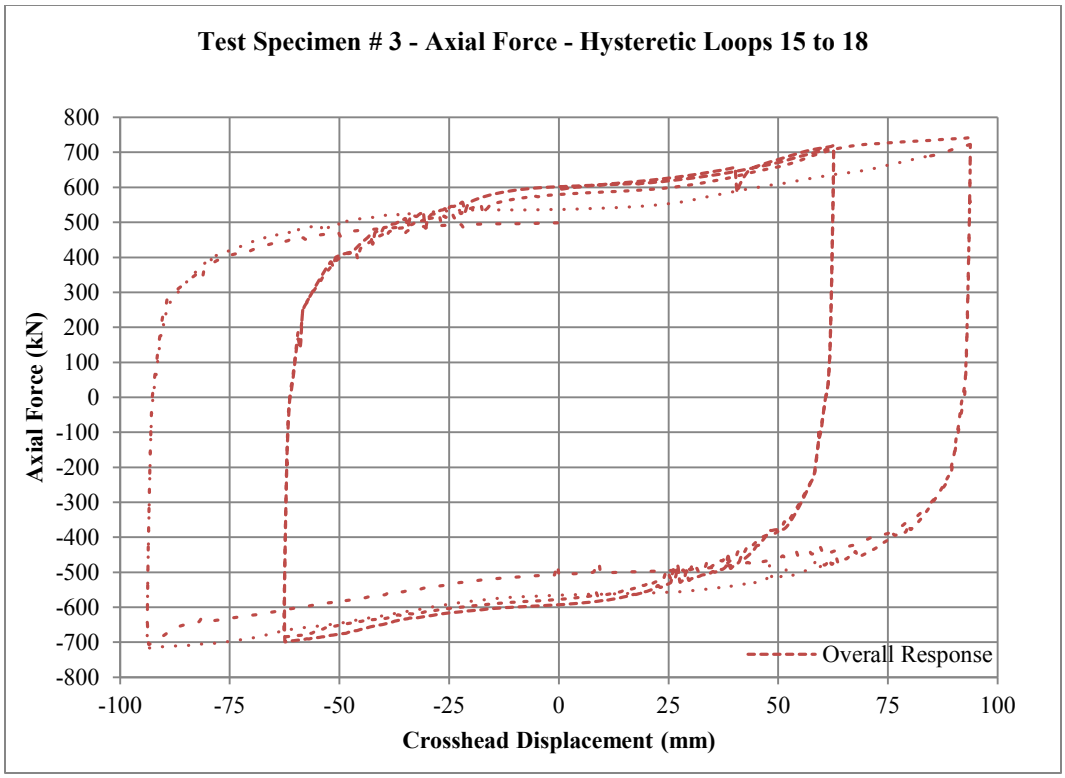

Figure 5-27: Axial Force versus Displacement - Test Specimen # 3 - Hysteretic Loops 15 to 18

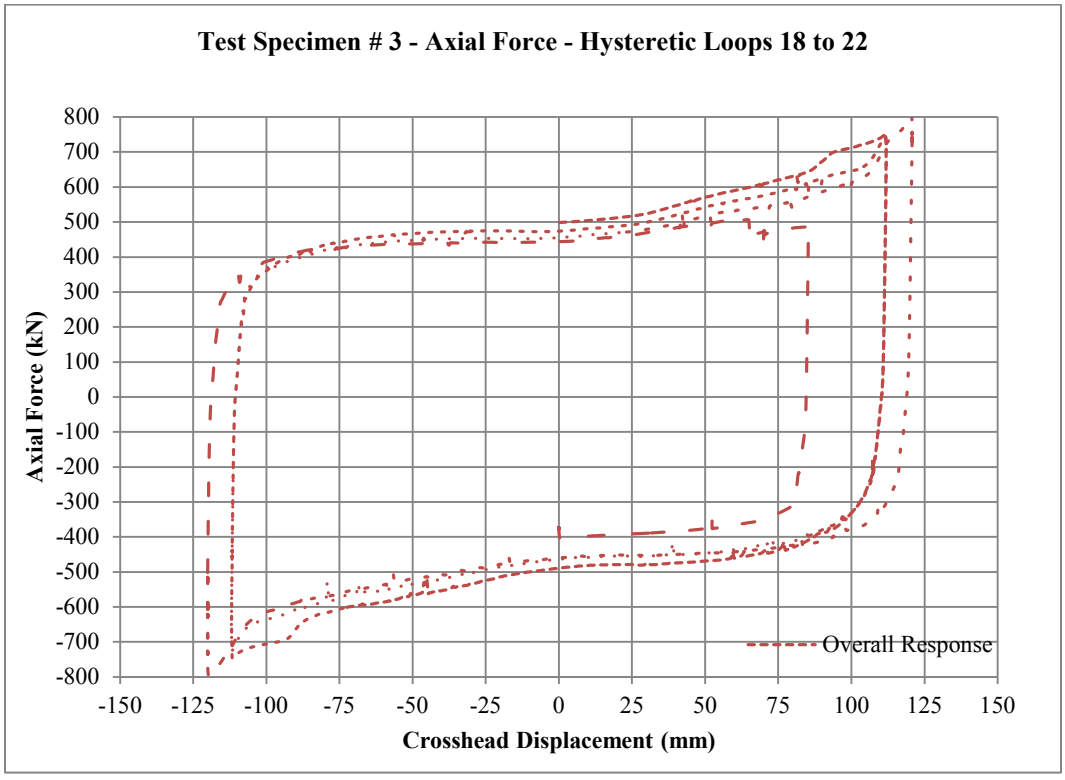

Figure 5-28: Axial Force versus Displacement - Test Specimen # 3 - Hysteretic Loops 18 to 22

5.2.9 Test Specimen # 4 - Load versus Displacement

Prototype brace specimen with two pairs of fuse type C4 attached was subjected to full load history outlined in section 4.5.3, as shown in Figure 5-29.

Figure 5-29: Test Specimen # 4 - Prior to Test

Unlike previous tests, this tests specimen has two pairs of steel fuse plates attached at top and bottom of the prototype brace. In previous tests friction component of the combined resistance was dominant over inelastic component; in the case of test specimen # 4 it was decided to reduce friction component to see what effect it would have on overall response. At each slotted connection (as per Figure 4-10) eight A325 7/8″ diameter bolts were pre-tensioned to 100 ft-lb each. Prior to test, friction of the brace prototype was measured to be 247 kN tension at zero crosshead displacement and after the test it was recorded at 220 kN.

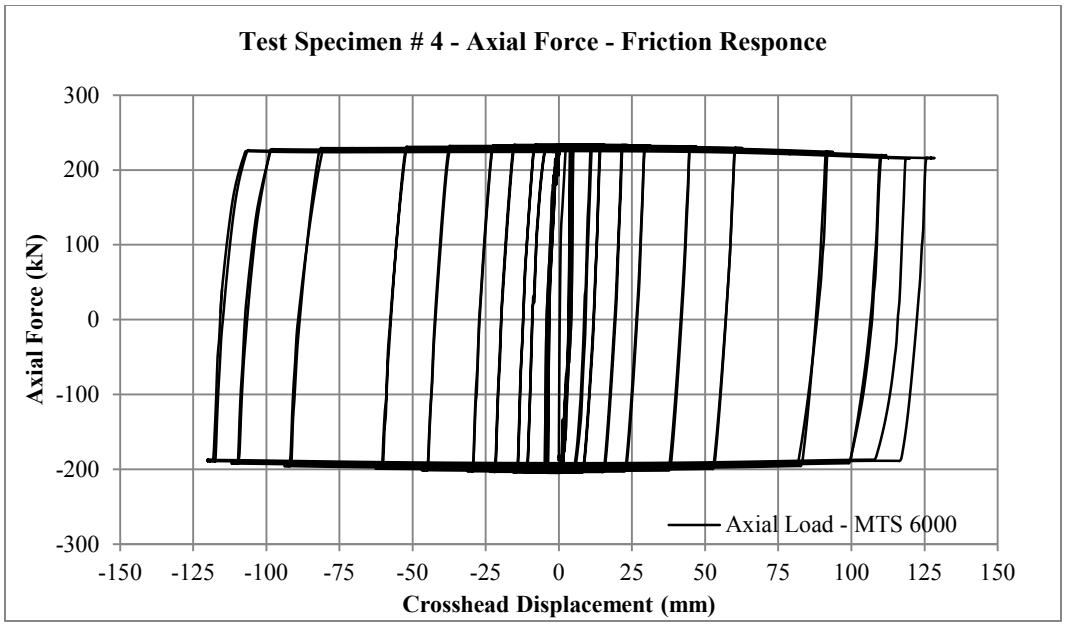

Figure 5-30: Axial Force versus Displacement - Test Specimen # 4 - Friction Response

Maximum longitudinal deformation achieved by brace prototype was +128 /-120 mm and was limited by the boundary condition at the tip of the shear link. Steady state pre-fuse-buckling load carrying capacity was recorded to be 694 kN tension after 47 mm cycle at 10 mm displacement, as shown in Figure 5-31. Overall hysteretic response of the brace prototype was characterized by increased "jitter" due to incremental slippage at the slots that are attaching tips of steel fuse plate shear links.

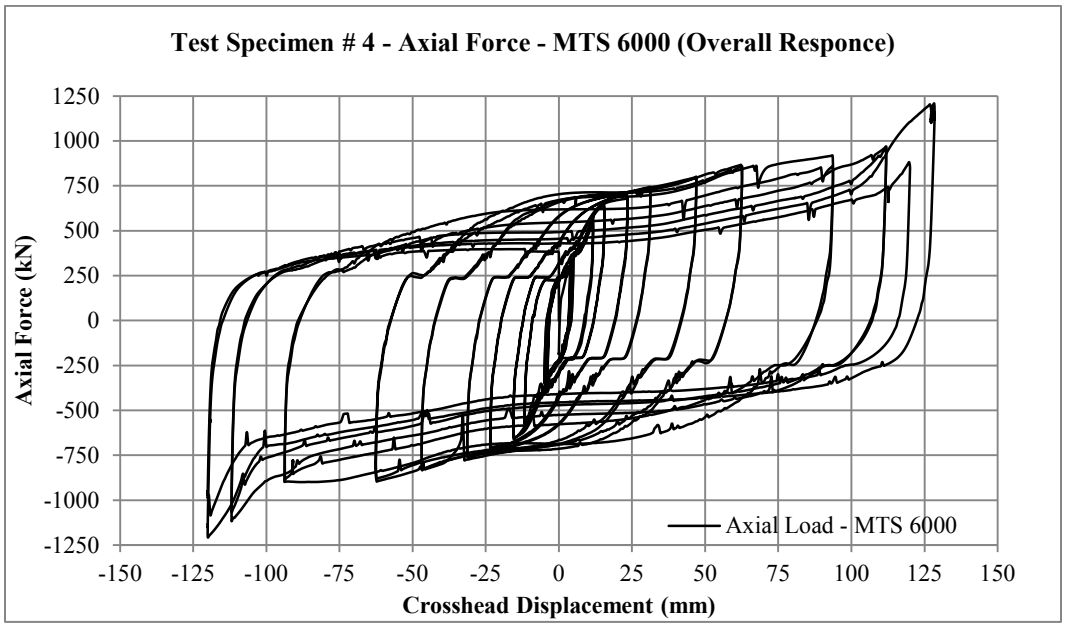

Figure 5-31: Axial Force versus Displacement - Test Specimen # 4 - Combined Response

Similar to previous tests, hysteretic response of test specimen # 4 can be separated in distinct four stages. Those stages are correspondingly presented in Figure 5-32 to Figure 5-35; inelastic steel fuse plate response is presented alongside combined response where by doing so clarity of a chart is unaffected. Hysteretic loops 1 to 6 exhibited elastic behaviour of the steel fuse plate, loops 7 to 14 in-plane elasto-plastic behaviour, and loops 15 to 18 showed initiation of out -of -plane buckling. At the end of the cycle 18, capacity degradation in tension of steel fuse plate at zero displacement was recorded to be 31 % when compared to pre-buckling value. Cycles 19 to 22 showed further capacity loss due to lateral -torsional buckling of the shear link followed by stiffening due to change in boundary conditions. Pre-stiffening tension capacity loss of steel fuse plate at the end of cycle 22 at zero displacement was 64 % when compared to pre-buckling value, while overall brace capacity loss was calculated to be 45 %. At the extreme deformations of the same cycle 22, however, capacity degradation was offset by the eventual stiffening due to boundary condition change at the tip of the shear link.

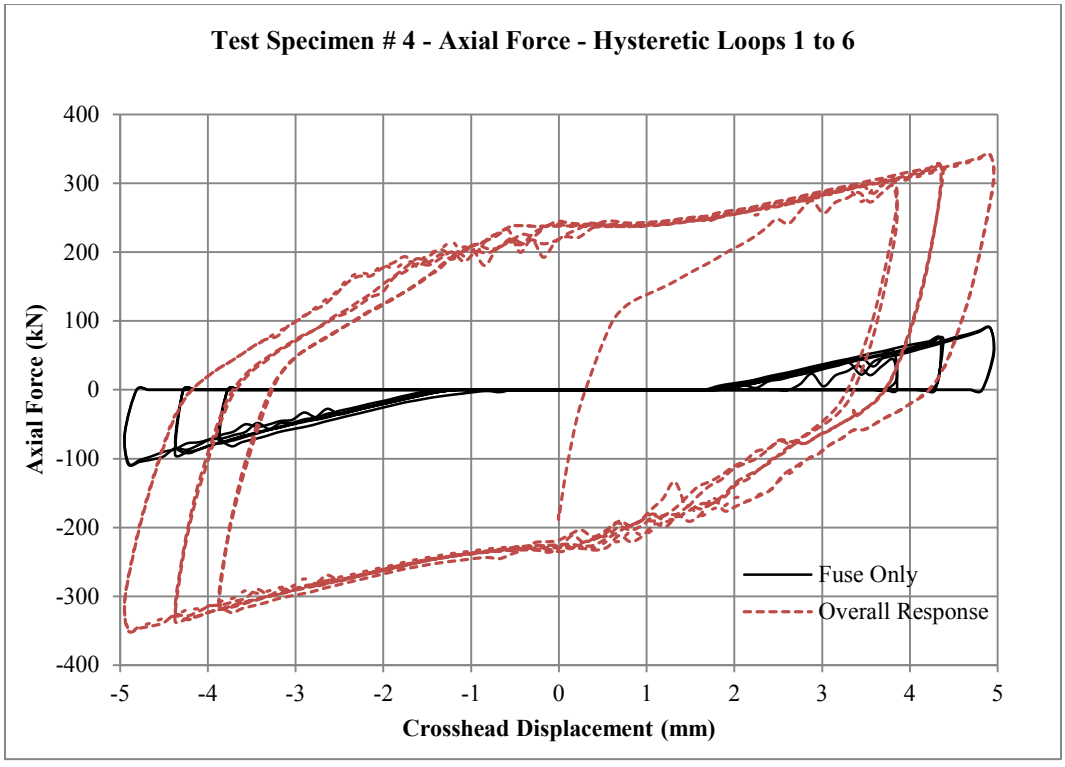

Figure 5-32: Axial Force versus Displacement - Test Specimen # 4 - Hysteretic Loops 1 to 6

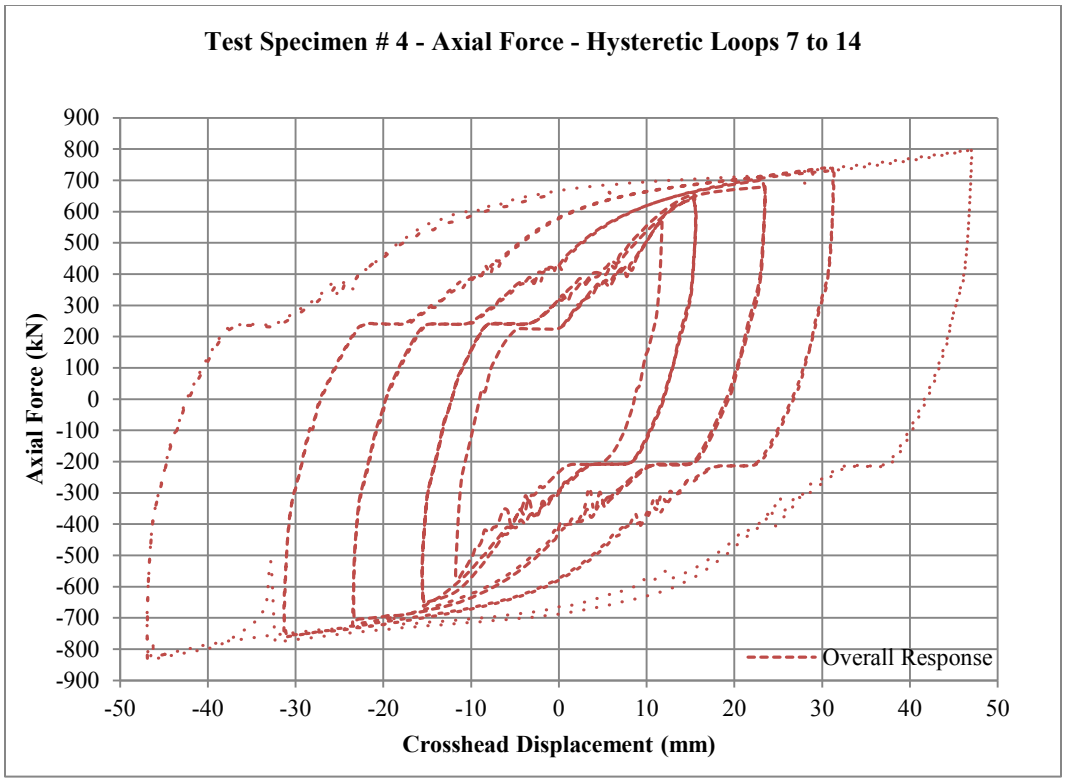

Figure 5-33: Axial Force versus Displacement - Test Specimen # 4 - Hysteretic Loops 7 to 14

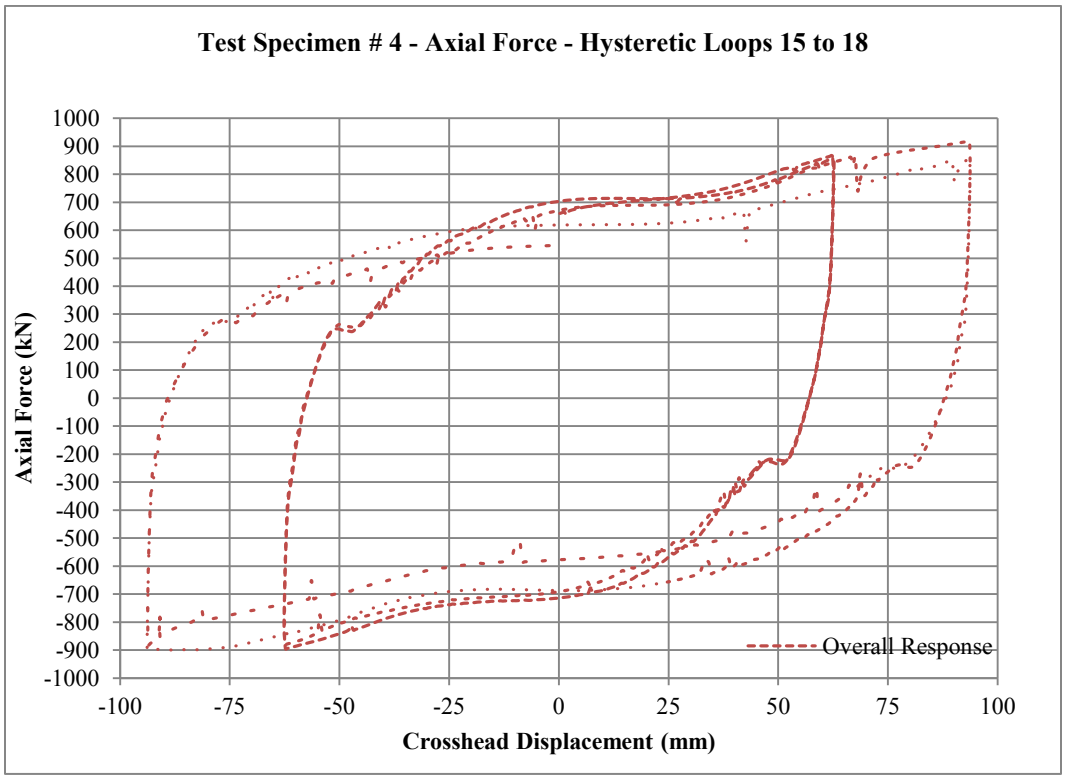

Figure 5-34: Axial Force versus Displacement - Test Specimen # 4 - Hysteretic Loops 15 to 18

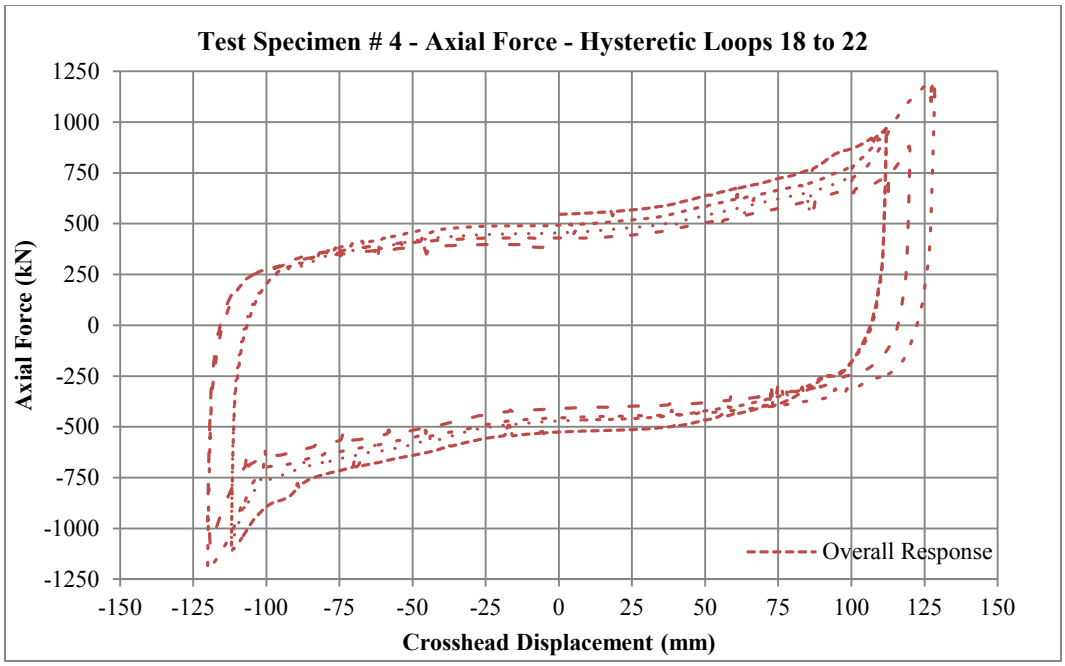

Figure 5-35: Axial Force versus Displacement - Test Specimen # 4 - Hysteretic Loops 18 to 22

5.2.10 Test Specimen # 5 - Load versus Displacement

Prototype brace specimen with one pair of steel fuse plates type C2 attached was subjected to full load history outlined in section 4.5.3. Fuse plate was attached at the location L2 as per Figure 4-5 (top of the brace member as tested). Friction inducing pretension at slotted connection was left unchanged from previous test on Test Specimen # 4. Prior to test, friction of the brace prototype was measured to be 210 kN tension at zero crosshead displacement and after the test it was recorded at 193 kN.

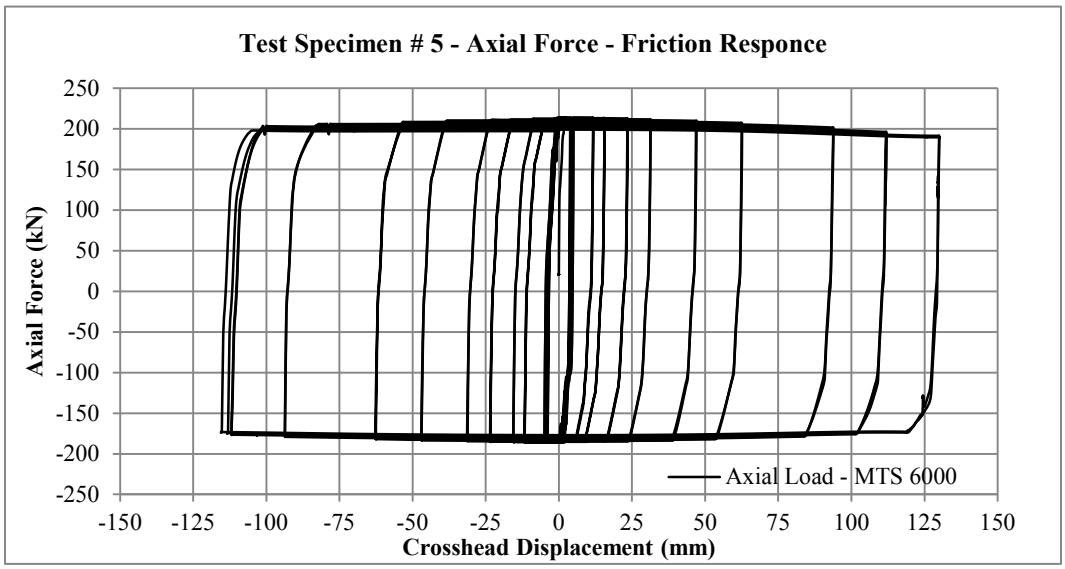

Figure 5-36: Axial Force versus Displacement - Test Specimen # 5 - Friction Response

Maximum longitudinal deformation achieved by brace prototype was +130 /-115 mm limited by the boundary condition at the tip of the shear link. Steady state pre-fuse-buckling load carrying capacity was recorded to be 320 kN tension after 47 mm cycle at 0 mm displacement, as shown in Figure 5-37.

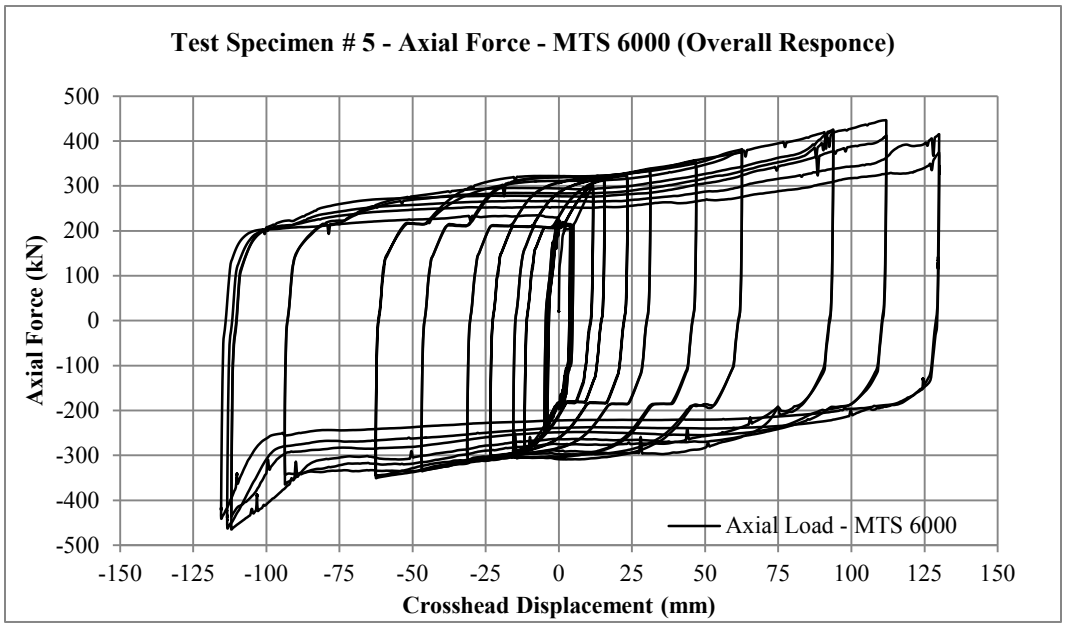

Figure 5-37: Axial Force versus Displacement - Test Specimen # 5 - Combined Response

Hysteretic response of test specimen # 5 can be separated into elastic, in-plane plastic, out-of-plane plastic and out-of-plane plastic with stiffening stages. Those stages are correspondingly presented in Figure 5-38 to Figure 5-41. Separate response of steel fuse plate is presented alongside combined prototype brace response in figures where such side-by-side presentation does not affect clarity of the chart. Hysteretic cycles 1 to 6 display elastic behaviour of the steel fuse plate, cycles 7 to 14 show in-plane elasto-plastic behaviour, cycles 15 to 18 exhibit initiation of out -of -plane buckling.

It is important to note that during first cycle of 93.9 mm amplitude, capacity degradation due to the buckling of the specimen was not observed at the tensile extreme of the cycle. Lateral-torsional buckling of the shear link initiated at the compression part of the cycle and afterwards capacity degradation due to buckling was similar to tests specimen # 4.

At the end of the cycle 18, capacity degradation in tension of steel fuse plate at zero displacement was recorded to be 31 % when compared to pre-buckling value. Cycles 19 to 22 showed further capacity loss due to lateral -torsional buckling of the shear link followed by stiffening due to change in boundary conditions. Pre-stiffening tension capacity loss of steel fuse plate at the end of cycle 22 at zero displacement was 63 % when compared to pre-buckling value, while overall brace

capacity loss was measured to be 33 %. At the end of the test shear link showed signs of near rupture due to low cycle fatigue, as shown in Figure 5-42.

At the extreme deformations of the same cycle 22, capacity degradation was offset by the eventual stiffening due to boundary condition change at the tip of the shear link.

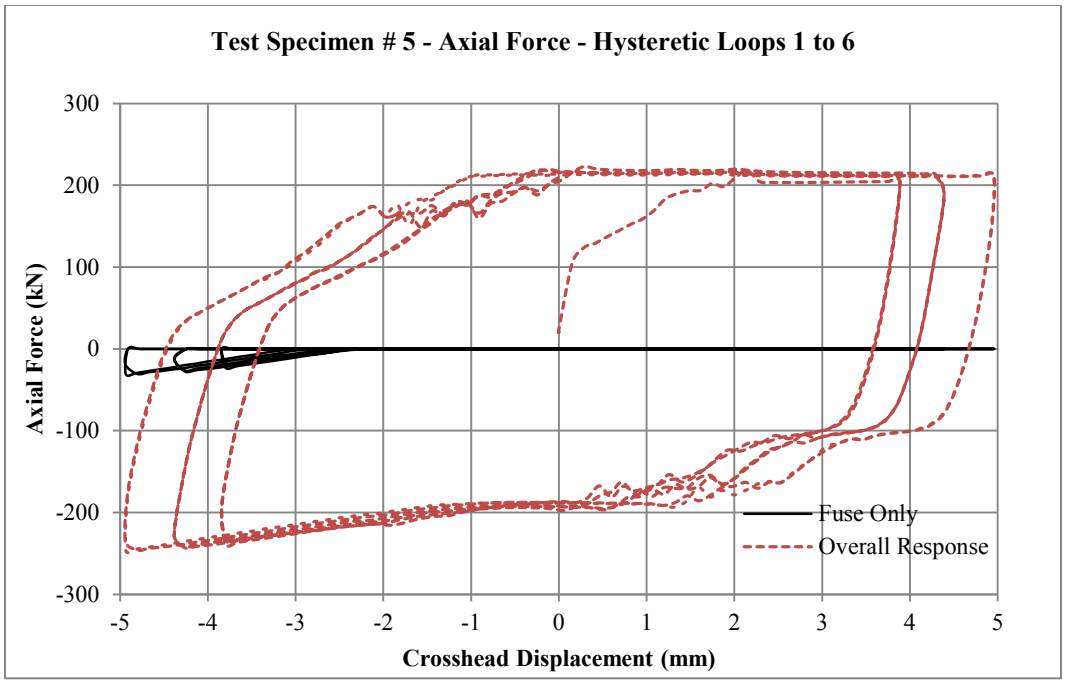

Figure 5-38: Axial Force versus Displacement - Test Specimen # 5 - Hysteretic Loops 1 to 6

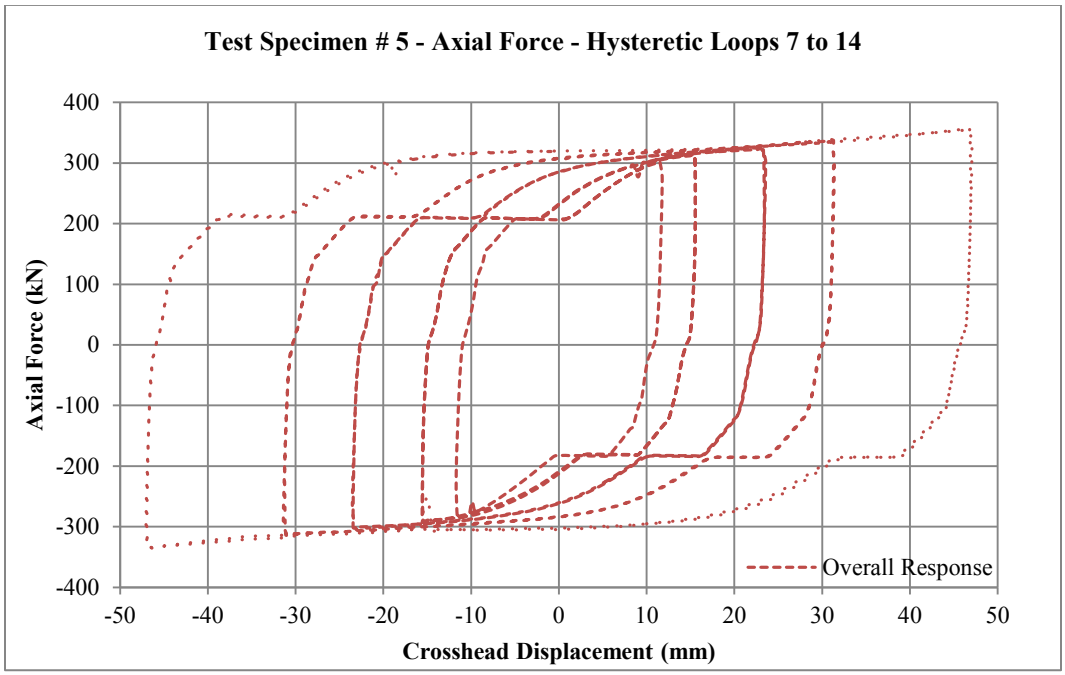

Figure 5-39: Axial Force versus Displacement - Test Specimen # 5 - Hysteretic Loops 7 to 14

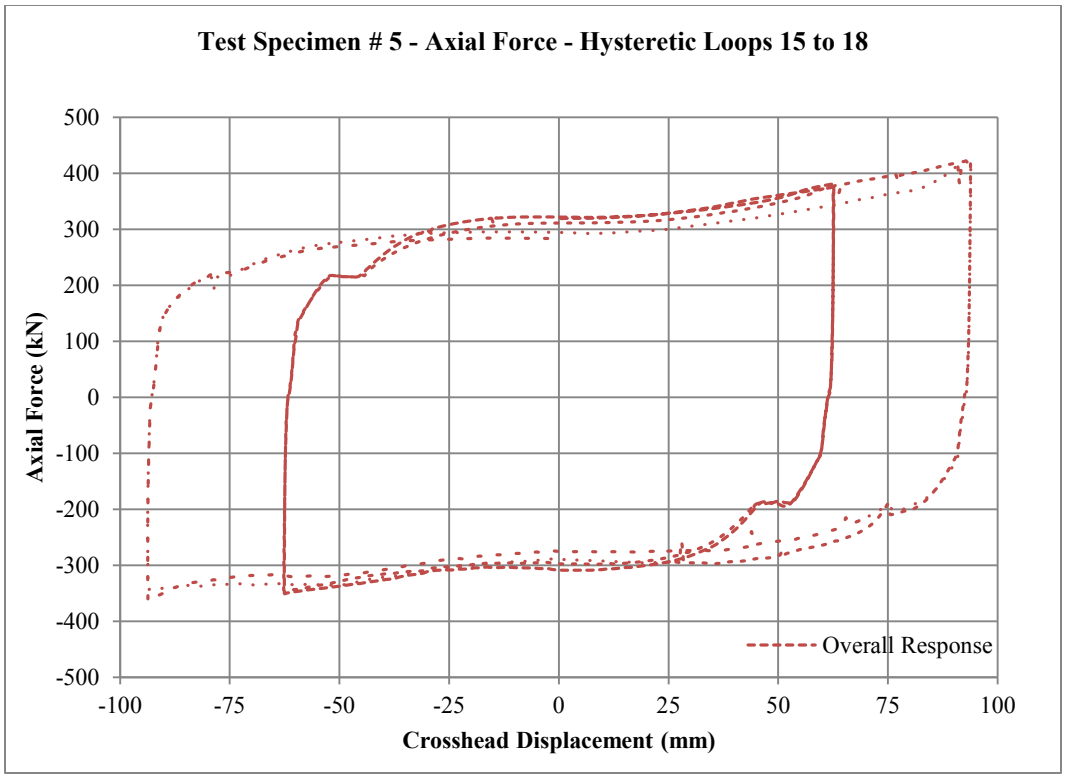

Figure 5-40: Axial Force versus Displacement - Test Specimen # 5 - Hysteretic Loops 15 to 18

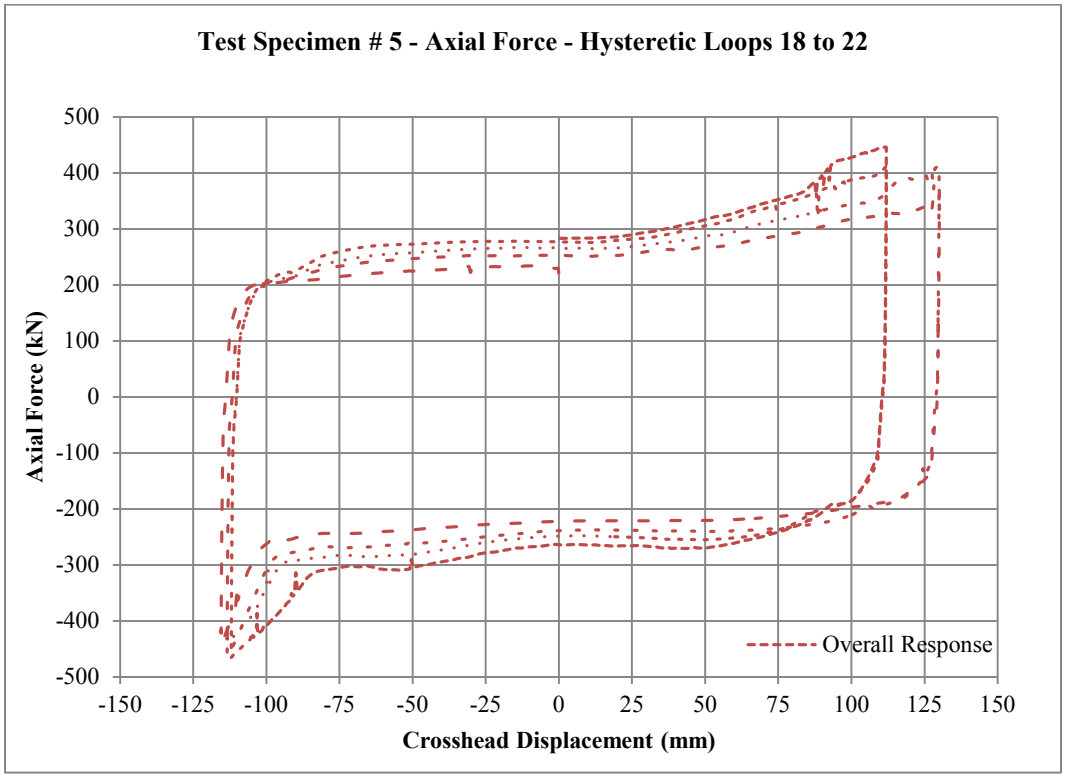

Figure 5-41: Axial Force versus Displacement - Test Specimen # 5 - Hysteretic Loops 18 to 22

Figure 5-42: Test Specimen #5 - Shear Link Damage

6 Prototype Energy Dissipater – Discussion and Evaluation

6.1 Prototype Energy Dissipater in a Scope of Canadian Design Code

Three primary factors come into play when evaluating the effectiveness of seismic energy dissipaters according to National Building Code of Canada (2010) and CAN/CSA S16-09 (2009): requirements imposed on physical component testing, seismic demand reduction factor due to ductility of SFRS (R_d) and inter-story drift of the structure.

CAN/CSA S16-09 provides several requirements for experimental tests of BRB, the most important of which were summarized in section 3.1.1.2.

Experimental program of every Test Specimen successfully completed loading history developed in section 4.5.3 up to deformation amplitude that was at least +/-110 mm for any given test and was limited by boundary conditions of the steel fuse plate; i.e. deformation capacity can be larger if designed accordingly. Hysteretic loops were stable with positive force versus displacement slope and did not cause failure of the prototype brace. As per section 4.5.2, in order to satisfy loading history requirements of Appendix T of ANSI/AISC 341-05, in addition to subjecting the brace member to loading cycles of certain amplitude, cumulative plastic deformation of the ductile element shall be more than 200 times of at-yield deformation.

At yield deformation of the prototype member can be approximated assuming yield is reached at 0.2% strain. In case of the prototype energy dissipater developed, the yield elongation is a combination of at yield deformation of the fuse plate in the direction of the brace axis and elastic brace elongation due to introduced axial force. It is reasonable to assume that demand within primary load carrying members of the prototype brace (W200 x 59 section shown in Figure 4-6) will not reach higher than 90% of the yield capacity. Given that assumed braced frame dimension used in the design stage of the research project was 3700 mm x 6000 mm, the length of the assumed prototype brace is 7050 mm, and the length of the member as tested was 2450 mm. 90% of the yield brace elongation that would correspond to a difference in length between the actual and assumed member is equivalent to 4.4 mm. Based on experimental data at yield deformation of the tested prototype, the brace member is 9.0 mm for test specimens that incorporate fuse plates C2 and C4, 8.0 mm for fuse plate type C1 and 9.5 mm for fuse type C3. Note that the yield elongation is equal to the brace deformation at the time instance when the correlated camera solution registered a strain of 0.2%; this value includes brace elongation due to slip. Average at-yield deformation of the prototype brace is ~13.5 mm. Loading history applied to the prototype brace satisfies requirements of Appendix T of ANSI/AISC 341-05 for testing of BRB specimens, which are referenced in S16-09 and shown in Table 6.1.

Table 6.1: Loading History - As-Tested Cumulative Inelastic Deformation

Load Step #	peak deformation, θ	number of cycles, n	brace elongation, ΔL	rate	Cumulative Inelastic Deformation
	rad		mm	mm/min	x Δ_{by}
1	N/A	2	3.875	4	0
2	N/A	2	4.438	4	0
3	N/A	2	5.000	4	0
4	0.00375	2	11.80	10	2.791
5	0.005	2	15.73	15	7.844
6	0.0075	2	23.58	15	17.41
7	0.01	2	31.42	15	31.49
8	0.015	2	47.08	15	54.59
9	0.02	2	62.71	15	86.68
10	0.03	2	93.86	15	136.7
11	N/A	2	111.9	15	197.1
12	N/A	2	130.0	15	267.9

SFRS ductility factor (μ) is one of the major parameters that influences seismic demand reduction factor due to SFRS ductility R_d (Mahmoudi and Zaree, 2010; Miranda, 1997). Factor μ is used to effectively quantify ratio of a peak deformation of a SFRS (in our case a prototype brace member) to its at yield deformation; μ can be calculated as follows:

(6.1) $$\mu = \frac{u_m}{u_y}$$

where u_m is the absolute peak deformation capacity of the prototype energy dissipater and u_y is the yield deformation capacity (Chopra, 1995). Value of μ calculated by equation (6.1), was obtained for each test specimen evaluated in the experimental program and is presented in Table 6.2.

Table 6.2: Experimental Results - SFRS ductility factor (μ)

Specimen ID	u_y [assumed 7 m brace]	u_m [min out of +/-]	μ
	mm	Mm	
Test Specimen # 1	13.4	135	10.1
Test Specimen # 2	12.4	130	10.5
Test Specimen # 3	13.9	120	8.6
Test Specimen # 4	13.4	120	9.0
Test Specimen # 5	13.4	115	8.6

In comparison, National Building Code of Canada suggests using $R_d = 4.0$ for a braced frame that utilizes BRB; ductility factor of a typical buckling restrained brace is ≥ 10 which is comparable to ductility factor of a proposed energy dissipater.

In addition to ductility requirements, NBCC imposes certain inter-story drift limits that are caused by design seismic event based on the intended occupancy and purpose of the structure.

According to the literature study carried out in chapter 2, no alternative energy dissipater with the exception of friction damper for CBF has a capability of imposing limitations on allowed inter-story drift; at the same time drift limit inherently built into slotted connection of the friction damper is abrupt and its dynamic implications are not well understood. Energy dissipater

evaluated within the scope of this research project has a capability of limiting overall deformation of the prototype brace member by providing significant stiffening over a short deformation range at predetermined deformation amplitude. Such behaviour can physically impose story drift limits defined in National Building Code of Canada (2010) in a manner that will not abruptly change response of the brace member from ductile to practically elastic and will not introduce associated dynamic force on brace member components and connections.

The prototype brace is capable of satisfying requirements imposed by both CSA S16-09 and NBCC (2010) on BRB members.

6.2 Energy Absorption Characteristics

Energy dissipated by each of five test specimens has been computed as a function of total cumulative brace axial deformation. Energy absorbed by deformation of brace prototype as a whole, and deformation of ductile steel fuse plates in particular is presented in Figure 6-1 and Figure 6-2 correspondingly. The level of energy dissipated achieved by prototype brace response demonstrates its capability but it does not possess significant analytical value since it strongly depends on the slip load of the friction interface.

Energy dissipated by steel fuse plates relates the type and quantity of the steel fuse plates used, as well as their capacity degradation properties to the overall amount of energy that was dissipated by the system.

The global slope of the fuse plate only energy dissipation curve largely depends on the magnitude of resistance provided by the fuse plates – it is steepest in test configuration that incorporates eight shear links and least steep in configuration with two shear links. In case of Test Specimen # 3, at a cumulative deformation of approximately 3600 mm a decrease in the slope angle is observed due to the fracture of one of the shear links.

The slope angle of the fuse plate only energy dissipation curve decreases due to steel fuse plate capacity degradation. However, its reduction is not as significant as one might expect. One possible explanation is that soon after the capacity degradation due to buckling takes place, eventual stiffening of the response offsets its effect.

This finding shows that even though buckling of the shear links has significant impact on the response of the brace prototype, its influence on the energy dissipating capability of the entire structure is not crucial, as long as stiffening of the response is present and is sufficient offset the effect of capacity degradation due to shear link buckling.

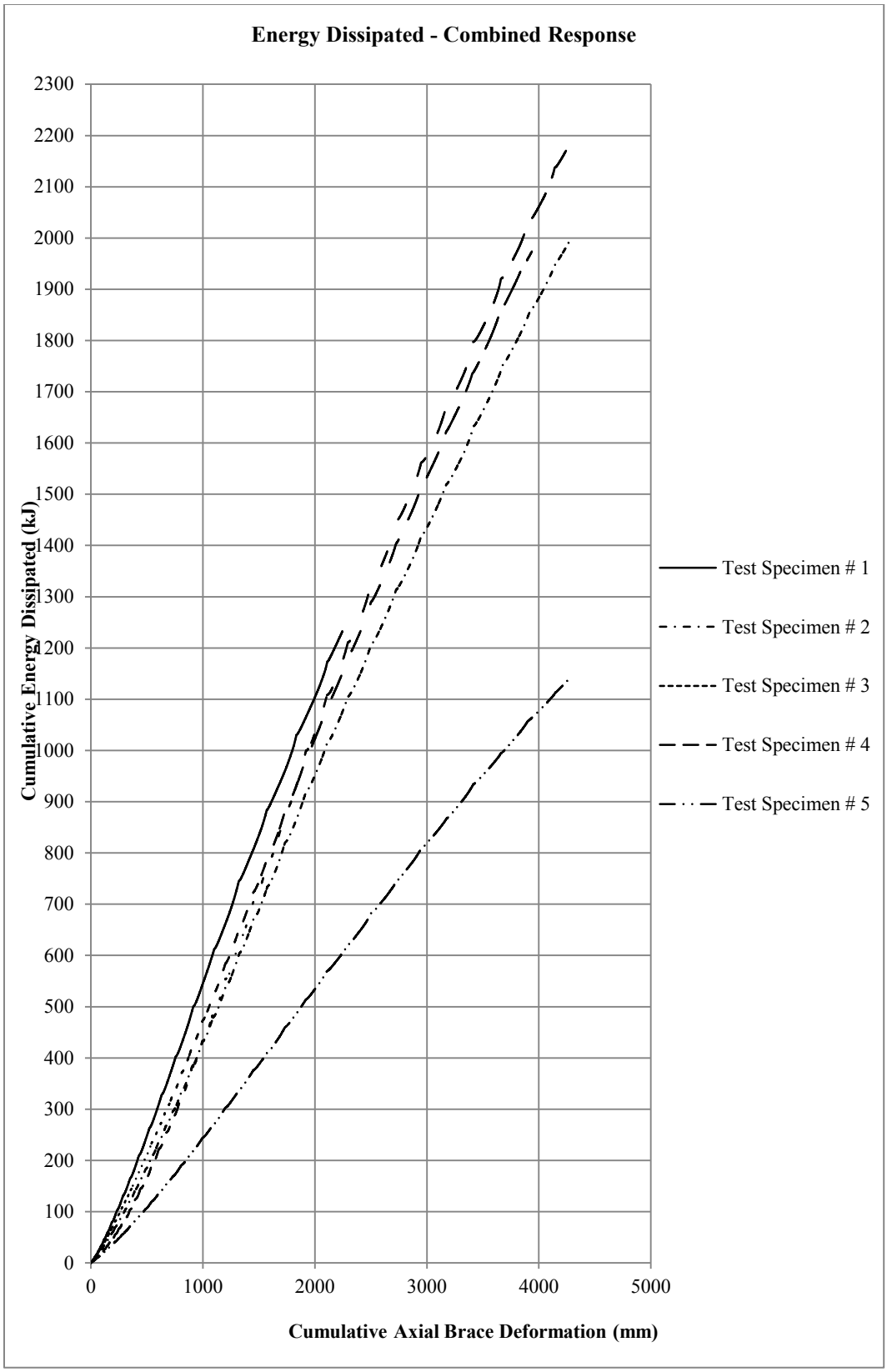

Figure 6-1: Energy Dissipated - Combined Response

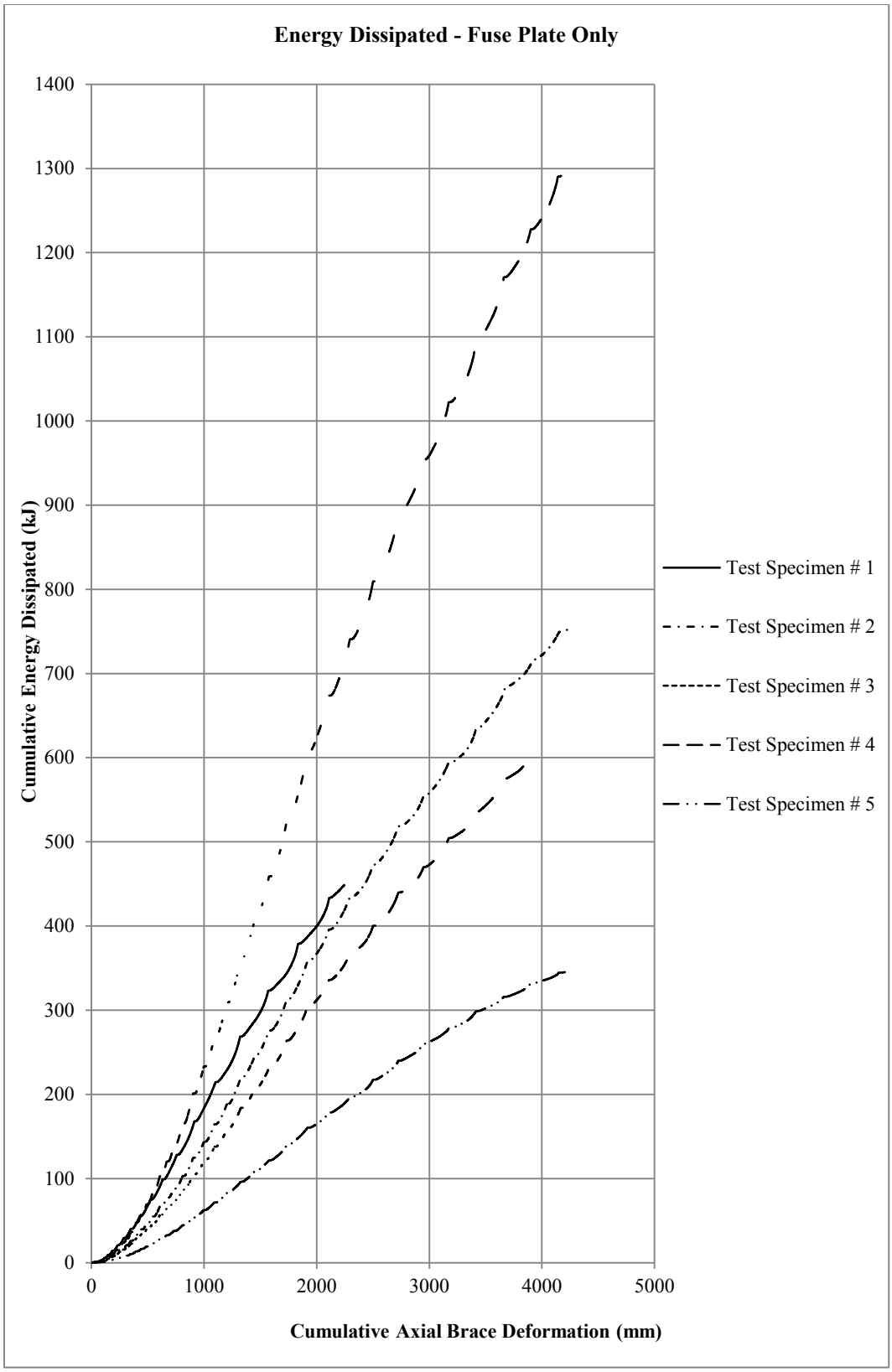

Figure 6-2: Energy Dissipated - Steel Fuse Plate Only

6.3 Friction Interface – Evaluation of Experimental Observations

Hysteretic response of the prototype brace that uses friction interface as the only source of resistance to axial demands proved to be very stable with minimum variation between load cycles. After initial setting of the material, a combined coefficient of friction, which includes friction forces from the PTFE and glass fiber reinforced friction sheet material, is equal to 0.51. Given that friction coefficient of the PTFE material is estimated to be ~0.05, the friction coefficient value for glass fiber reinforced friction sheet material is ~0.46 which is somewhat different from value of 0.52 quoted by the manufacturer of the material.

In addition to stable and predictable friction properties, friction sheet material used has exhibited excellent resistance to wear after cumulative slip of approximately 20 000 mm, as shown in Figure 6-3.

Figure 6-3: Post-Experiment Surface Condition of Non-asbestos Glass Fiber Reinforced Friction Sheet Material

Nevertheless friction sheet material used within the slotted connection has a serious drawback. Due to its compressibility, it is challenging to predict the resistance of the friction interface after certain time since initial pre-tensioning of the bolts. The magnitude of the pretension loss due to

material compressibility can potentially vary between different batches of the material if they happen to have somewhat different density. This drawback is successfully mitigated in a laboratory environment by performing a friction only pre-test and post-test before and after every test of prototype brace specimen.

6.4 Ductile Steel Fuse Plate – Evaluation of Experimental Observations

6.4.1 Evaluating the Effect of the Ductile Steel Fuse Plate Shape

As discussed in section 3.3.5.2, several shapes of steel fuse plate were proposed to achieve an optimal strain distribution within the shear link that can potentially prolong shear link resistance to low cycle plastic fatigue.

Steel fuse plate "C1" was developed to allow for uniform yielding along its shear link accounting for both moment and shear demand within the link. The shape of steel fuse plate "C3" was derived to develop uniform yielding along the edge of the shear link by accounting for moment demand only. Steel fuse plate "C4" is very similar to "C1". However, the curved outline of the shear link within "C1" was replaced by a straight line connecting the top and bottom points of shear link edge within steel fuse plate "C1". This served a dual purpose of simplifying fabrication of the shear link as well as placing a minor strain concentration at the midpoint of the shear link away from locations of geometric stress concentration – fillets at top and bottom of the shear link.

The experimental program demonstrated that shape of the shear link had significant implications on initial yielding pattern as well as strain distribution.

White wash was applied to an otherwise un-treated steel fuse plate surface (which was covered in mill scale). As the steel fuse plate was going through inelastic deformation, mill scale was flaking off its surface, removing the white wash layer. The change in white wash layer coverage was recorded by cameras and will be presented herein as indication of the yield pattern within all three types of steel fuse plates.

As initially suggested by finite element analysis, fuse plate type "C1" demonstrated initial yielding closer to the bottom of the shear link, from which it progressively developed through the entire height of the shear link, as shown in Figure 6-4. Nevertheless, at axial brace deformation of 62.7 mm it is apparent that plastic strain is largest at the bottom of the link, given that region of plastic strain propagation is significantly wider at the base of the shear link within fuse plate "C1".

Fuse plate "C3" exhibited uniform yielding along the entire height of the shear link. Yielding initiated uniformly along approximately three quarters of the entire shear link at axial brace deformation of 15.7 mm and progressively increased towards the ends of the shear link afterwards. At a brace axial elongation of 62.7 mm, yielded width is distributed uniformly along the height of

the shear link; some minor plastic strain concentration was still present at the base of the shear link, as shown in Figure 6-5.

Fuse plate "C4", as expected, initially yielded approximately at the mid-height of the shear link. As brace axial deformation continued to increase, the zone of initial yield started to strain harden, imposing larger stress on the steel material on either end of initially yielded zone. Such larger stress eventually caused the surrounding steel material to reach its at-yield strain, propagating yielded zone away from the center towards either end of the shear link, as shown in Figure 6-6. At a brace axial elongation of 47.0 mm, the yielded zone distributed through approximately 90% of the shear link height. At 62.7 mm, the yielded zone distributed through entire height of the shear link with no stress concentration present at either the top or the bottom of the shear link. However, given that yielding initiated at the mid height of the link, a certain degree of rotational hinge was introduced at the link's midpoint, allowing for instability initiation. Flaking of the white wash through the entire thickness of the type "C4" fuse plate's shear link strongly suggests initiation of inelastic buckling at that location due to presence of axial compressive force within the link. Note that by placing stress concentration at the mid height of the shear link, stress concentration at either the top or bottom of the shear link became non-existent. Concentrated plastic strain at the midpoint, not encountering any geometric discontinuity, redistributed to a larger portion of the shear link height as indicated by progressive white wash flaking as well as finite element analysis carried out in section 3.3.5.2 resulting in a practically uniform plastic strain distribution.

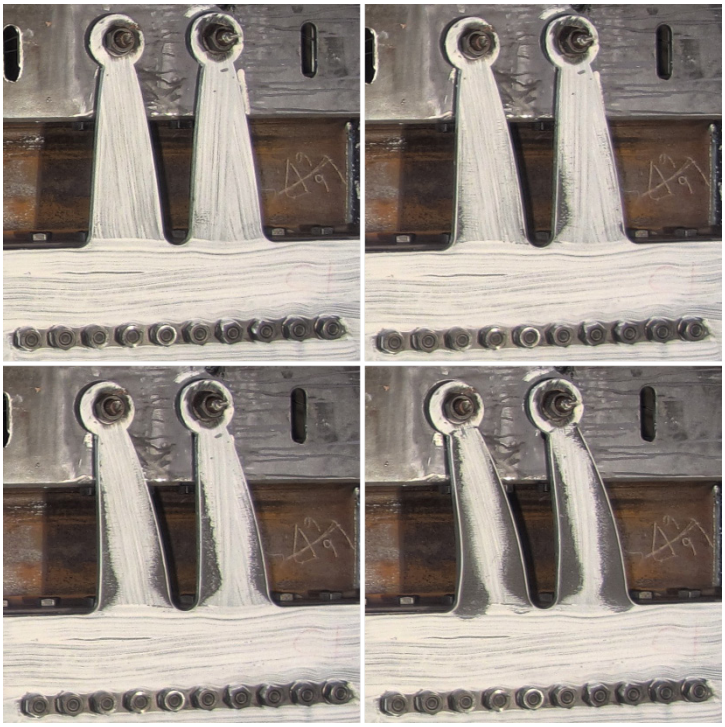

Figure 6-4: Fuse Plate C1 - Yield Pattern at 15.7 mm, 31.4 mm, 47.0 mm and 62.7 mm Brace Axial Deformation

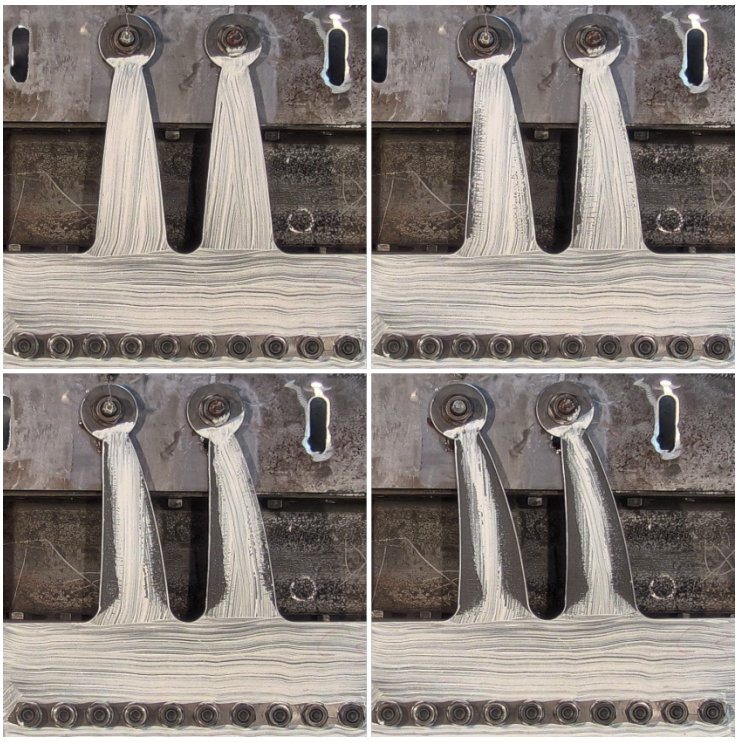

Figure 6-5: Fuse Plate C3 - Yield Pattern at 15.7 mm, 31.4 mm, 47.0 mm and 62.7 mm Brace Axial Deformation

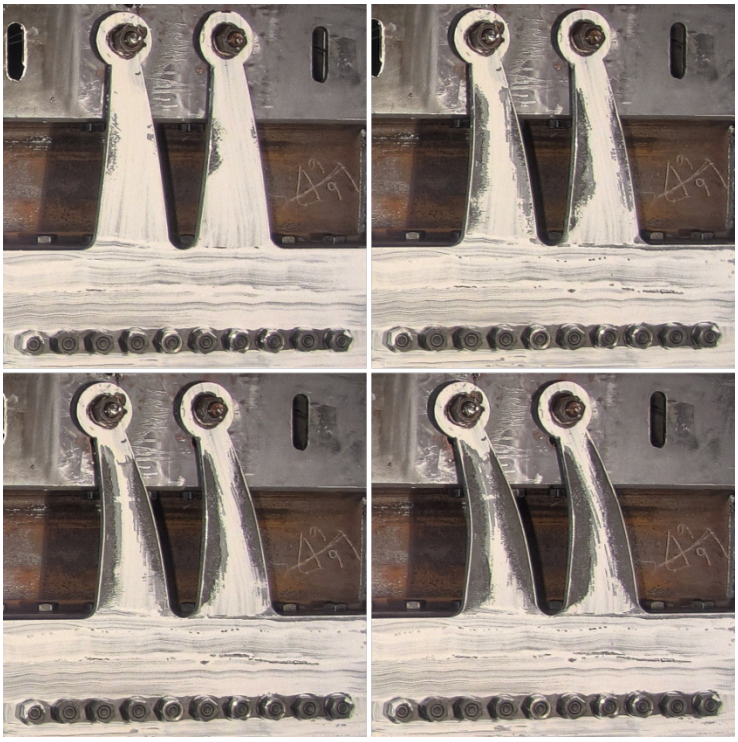

Figure 6-6: Fuse Plate C4 - Yield Pattern at 15.7 mm, 31.4 mm, 47.0 mm and 62.7 mm Brace Axial Deformation

To accurately visualize strain distribution within a steel fuse plate, output from a correlated cameras solution was used. In Figure 6-7, a comparison between strain distribution patterns at axial brace deformation is shown. It is apparent that while fuse plates C3, C4 (and correspondingly C2, the shear link shape of which is identical to C4) show a strain gradient that is relatively uniform along the edge of the shear link, steel fuse plate type C1 has an apparent strain concentration at the base of the shear link.

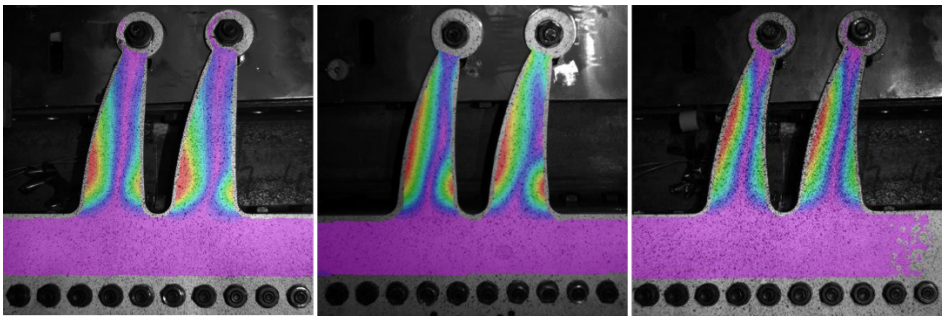

Figure 6-7: Strain Pattern at 62.7 mm of Axial Brace Deformation for Fuse Plates C1, C3 and C4 Correspondingly

Given the above, it is rather challenging to decide on the optimal shape of the shear link. It seems that from stand point of low cycle plastic fatigue, steel fuse plate types C3 and C4 possess defined uniformity of strain distribution at large axial brace deformations. In addition the shape of the shear link of the steel fuse plate type C4 eliminates strain concentration at the base of the link and thus is preferable over steel fuse plate type C3. Plastic strain within steel fuse plate "C1" is least uniformly distributed along the shear link height when compared to both steel fuse plate "C3" and "C4", however its concentrated rotational hinge at the bottom of the link induces less instability for out-of-plane buckling at the link.

Depending what will prove to be more critical in the further study – fracture of the material or instability within shear link, decision can be made with regard to what strain distribution pattern will be more beneficial. If low cycle fatigue of the shear link proves to govern design, steel fuse plate type C4 demonstrates uniform strain pattern that does not exhibit distinct strain concentration. In case eliminating out-of-plane behaviour due to axial compressive force within the shear link takes priority over low cycle fatigue susceptibility, steel fuse plate type C1 will become a preferred option.

6.4.2 Qualitative Implications of the Slot Boundary Condition at the Top of the Shear Link

As a general rule, the ultimate deformation capacity of the prototype brace member was limited by the length of the slot within the fuse attachment plate. As the prototype brace was deforming axially, shear links within the steel fuse plate were bending with the top of the link gradually

moving within the slot. At the instance of time when shear link "bottoms out" (i.e. reaching the end of the slot) tension is effectively introduced within the shear link due to boundary condition change, as shown in Figure 6-8.

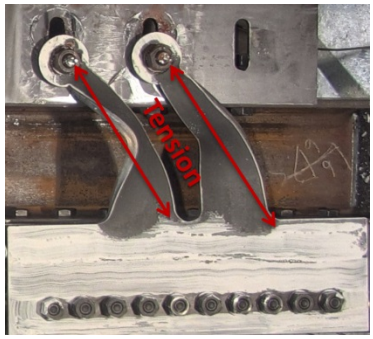

Figure 6-8: Shear Link - Tension Inducing Boundary Condition

Change in the boundary condition at the top of the shear link introduced significant stiffening of the brace prototype hysteretic response. Deformation mode of the shear link changed from bending to tensile elongation that could eventually result in shear link fracture. To address this phenomenon, the shear link could be detailed such that at its top, an extended "neck area" was introduced to deform in tension once the bottom of the slot was reached, as shown in Figure 6-9.

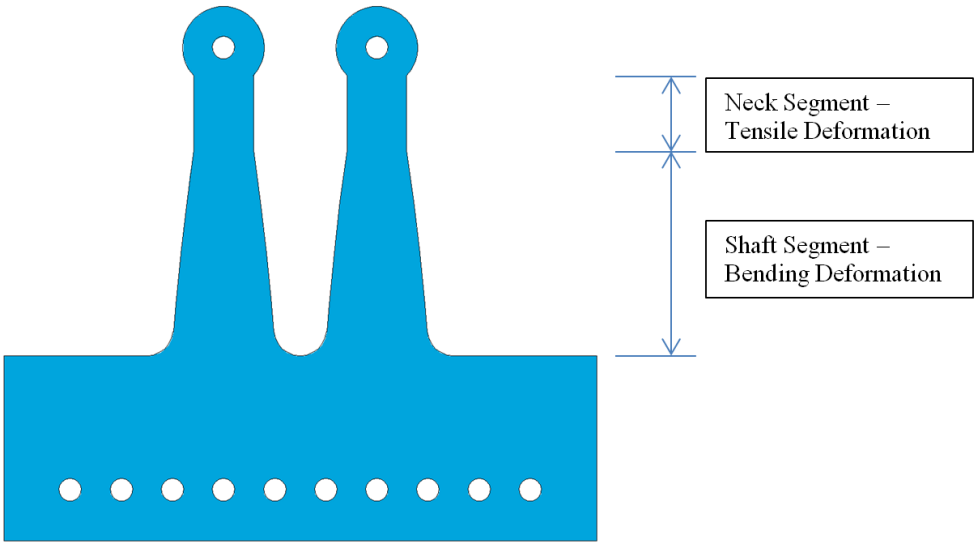

Figure 6-9: Alternative Detail of Shear Link to Address the Tension Stiffening Effect

If coupled with a bolt of appropriate strength, the proposed shear link can introduced significant stiffening over relatively large deformations that will not result in fracture of the link. If used as a part of the currently studied brace prototype, such a steel fuse plate can effectively limit lateral story drift of an implied braced bay in a gradual, non – abrupt manner. Such imposed limit, coupled with significant stiffening of hysteretic response curve can be very effective at preventing

a “soft story” mechanism within a structure that utilizes concentrically braced bays as well ensuring more uniform distribution of post-earthquake residual story drift.

6.4.3 Qualitative Implications of the Number of Shear Links within Ductile Steel Fuse Plate

The number of shear links used in a brace prototype was one of the variables of the experimental program. The shape of the shear links was identical in Test Specimens # 1, # 4 and # 5. Test Specimen # 1 had one pair of steel fuse plates with two shear links each, Specimen # 4 had two pairs of steel fuse plates with two shear links each and Specimen # 5 had one pair of steel fuse plates with one shear link each.

Increase of the ratio of resistance provided by the ductile inelastic component over resistance provided by the friction component of the prototype energy dissipater resulted in slightly reduced initial stiffness, increased post-buckling capacity loss and more pronounced stiffening stage due to introduction of the boundary condition at the top of the shear link as discussed in section 6.4.2. At the same time pre-buckling load carrying capacity per single shear link of Test Specimen # 4 (eight shear links) and # 5 (two shear links of same type) is very similar. For example, at 31.4 mm of assumed brace elongation, an average resistance provided by a single shear link in case of Test Specimen # 4 was 62.3 kN, while in case of Test Specimen # 5 it was 63.1 kN.

Number of shear links per steel fuse plate was an unintentional variable introduced into experimental program. Steel fuse plate type C2 incorporated a single shear link per plate, while fuse plate type C4 incorporated two shear links per plate (shear link shape is identical for fuse plates C2 and C4). Reduction of the number of shear links from two per fuse plate (Specimen # 4) to one (Specimen # 5) resulted in a significant change within the hysteretic response curve. As evident from section 5.2, Test Specimen # 5 was the only instance in the experimental program when an amplitude extreme of 93.9 mm was reached with practically no degradation of capacity due to buckling of the shear link (i.e. when compared to Specimen # 4 which incorporated the steel fuse plate with two shear links of identical shape and was subjected to identical loading history).

Fuse plate deformation data output from the correlated camera setup is used to interpret the hysteretic response of Specimen # 5 when compared to Specimen # 4 at the deformation amplitude of 93.9 mm, as shown in Figure 6-10. At the onset of 93.9 mm cycle both specimens exhibit significant compression buckling of the shear links (due to compressive axial force from the previous cycle).

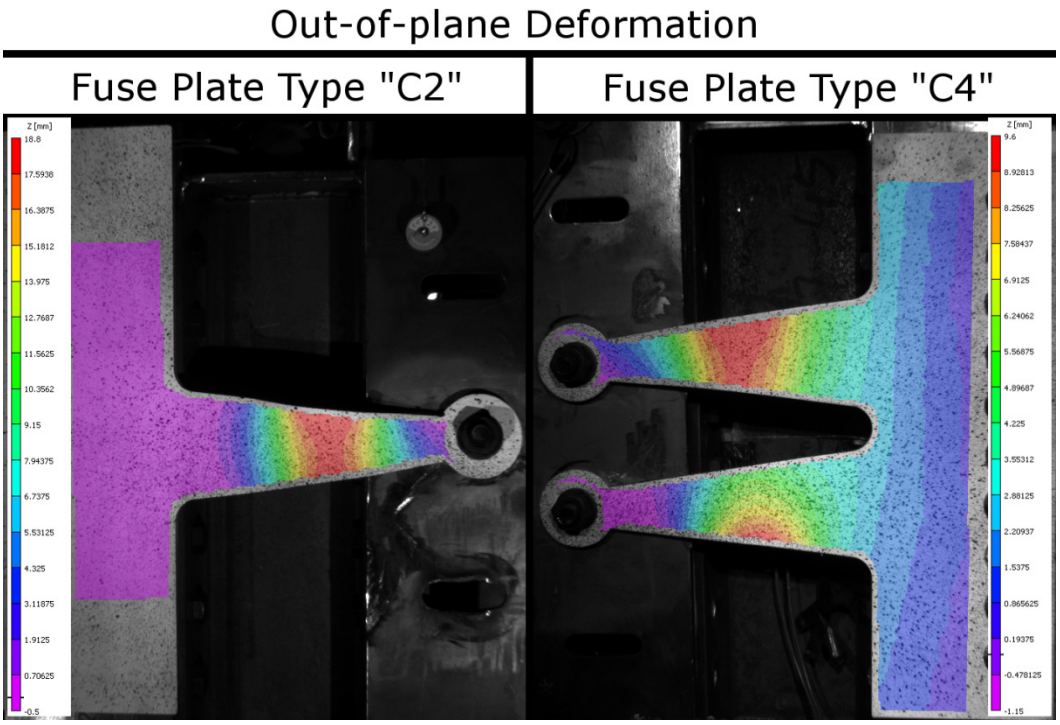

Figure 6-10: Steel Fuse Plate: One vs. Two Shear Links - Onset of 93.9 mm Cycle

At the beginning of 93.9 mm, cycle compression buckling is apparent in both steel fuse plates types “C2” and “C4”. Out-of-plane displacement due to compression buckling within the shear link in steel fuse plate “C2” is 19.0 mm and 8.5 mm in steel fuse plate type “C4”.

At the maximum deformation of 93.9 mm, cycle shear links in both types of fuse plates experience substantial lateral-torsional buckling. In fact, the shear link within fuse plate C2 experiences maximum torsional out-of-plane deformation equal to 20.0 mm (deformation between opposite edges of the shear link) while shear link within fuse plate C4 is subjected only to 17.0 mm of maximum torsional out-of-plane deformation.

Close to the top of the shear link, distribution of the out-of-plane deformation gradient is very similar for both fuse plates at a maximum deformation of 93.9 mm. At the base of the shear link, rotational fixity seems to be different for a fuse plate with one shear link when compared to a fuse plate with two shear links per plate. As shown in Figure 6-11, a fuse plate with one shear link provides full fixity to out-of-plane deformation up to 50.0 mm away from the base of the link. Fuse plate with two shear links shows that out-of-plane deformation of the steel plate occurred at the very base of the shear link (1.5 mm magnitude). Torsional out-of-plane deformation was also initiated 25 mm away from the base of the shear link (deformation of 1.4 mm between opposite edges of the shear link).

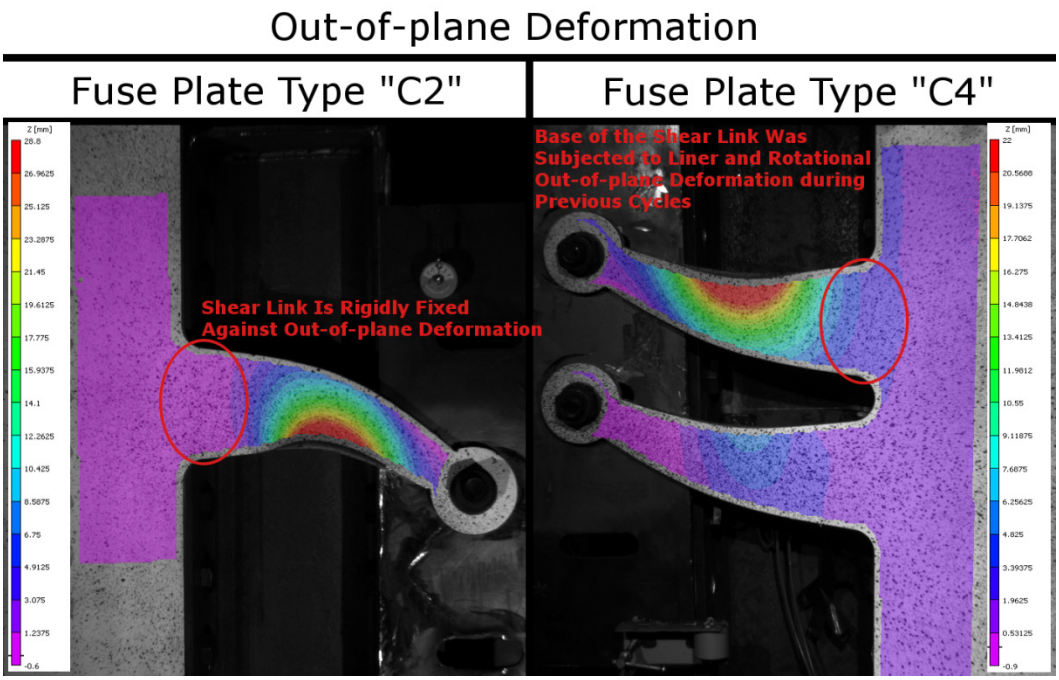

Figure 6-11: Steel Fuse Plate: One vs. Two Shear Links – Maximum Deformation of 93.9 mm Cycle

A steel fuse plate with single shear link provides more rigid boundary condition at the base of the shear link effectively reducing the unsupported length of the link that is subjected to lateral-torsional buckling (and ultimately increasing torsional capacity of the shear link). A possible explanation of this condition is that two shear links double the demand applied to the supporting steel plate causing its permanent plastic deformation and altering the boundary condition at the base of the link.

More experimental data is necessary to prove this hypothesis. However, one can draw a preliminary conclusion that in order to improve bending capacity of the shear link (to minimize torsional buckling) it can be beneficial to use either single shear link per fuse plate or increase the spacing between shear links, in order to make sure that torsional demands from neighboring shear links do not superimpose to deform the boundary condition at the base of the link.

6.5 Finite Element Analysis – Refined Fuse Plate Model Based on as Tested Material Properties

Based on the specimen measurements and material properties obtained from the experimental program a refined FEA model has been derived. It is important to note that FEA model of the steel fuse plate developed herein is based on monotonic loading and does not account for a Bauschinger effect and steel plate deterioration inherent in cyclic loading response.

A S4R Shell Element has been used to model ductile deformations in the steel fuse plate. Detailed properties of the element are as follows (provided within ABAQUS): a 4-node doubly curved thin or thick shell, reduced integration, hourglass control, and finite membrane strains.

Material properties of the mild steel that was used to fabricate the steel fuse plate energy dissipating elements were obtained from tension coupon tests as described in section 4.2.1. In particular, corresponding values of elastic modulus, true plastic strain and stress have been incorporated into ABAQUS FEA model. Poisson's ratio value was assumed to be 0.3.

Load applied was specified in a Static Riks analysis step which is an arc-length analysis method that is incrementally changing applied load with increments small enough to find a determinate solution (Memon and Su, 2004). Load was applied at the top of the shear link along the axis of a brace prototype. Initial load value was 1.0 kN (arc length of 1.0) with an arc length increment that varied 1E-5 to 1E+36 in subsequent steps.

6.5.1 Refined FEA Model - Buckling Initiation and Propagation

The finite element analysis model of the steel fuse plates that have been used in the development stage of the research project did not indicate susceptibility of the fuse plate to torsional buckling of the shear links.

During the experimental program, initial buckling was observed at approximately 60 mm and at brace axial deformation of approximately 90 mm. Shear link buckling visibly impacted the load carrying capacity of the prototype brace. Overall buckling of the steel fuse plate resulted in lack of consistency of hysteretic loops for cycles with deformation amplitude larger than 63 mm.

In order to improve on buckling behaviour of the shear links, it is essential to develop an FEA model that correctly models this phenomenon. As discussed in section 4.3.4, it became clear that boundary conditions at the top of the shear link within the steel fuse plate used in the initial FEA model did not correspond to actual boundary conditions observed in an as-tested brace prototype. The boundary condition at the base of the fuse plate was set to mimic fixity applied by a line of bolts. The boundary condition at the top of the shear link were set to be pinned (rotation about "X", "Y" and "Z" axes) and fixed against displacement along the "Z" axis to properly account for distorted cross-section shapes of the prototype beam assembly (see section 4.3.4 for more details), as shown in Figure 6-12.

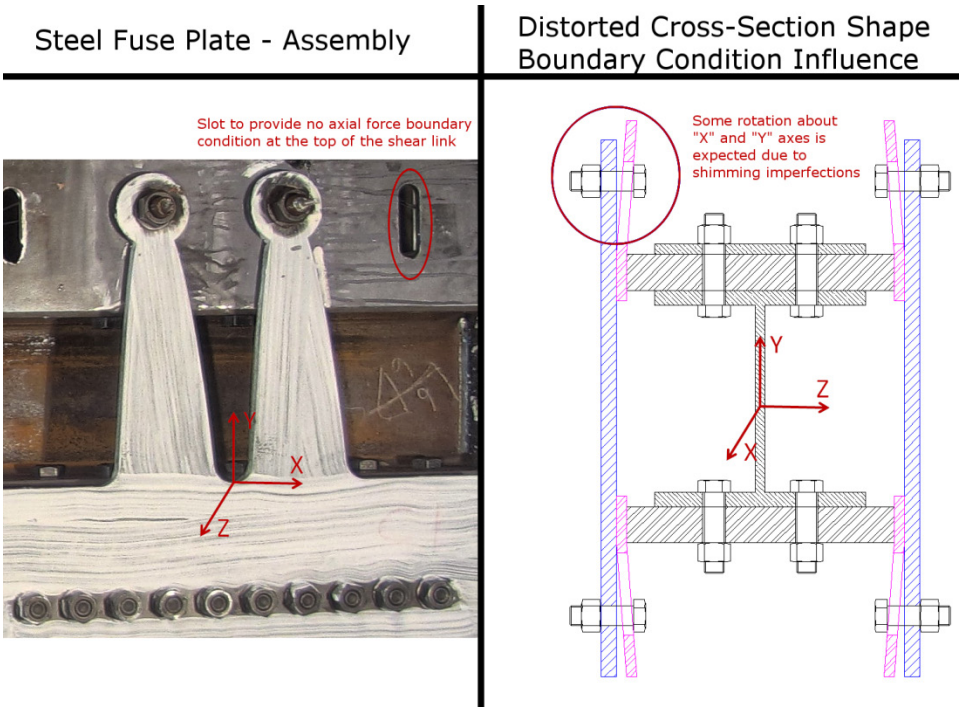

Figure 6-12: Refined FEA Model; As-Built Boundary Condition at the Top of the Shear Link

In addition, 2.0 mm displacement along the "Z" axis was introduced at the top of the shear link to model initial deflection imperfection due to tightening of the connecting bolt. Force was applied to the fuse plate at centroid of the bolt hole at the top of the shear link. "X" axis displacement of two shear links within single fuse plate was matched using "link" constraint in ABAQUS.

The above changes to the FEA model of steel fuse plate introduced lateral-torsional buckling within the shear link, the magnitude of which increased with deformation, as shown in Figure 6-13.

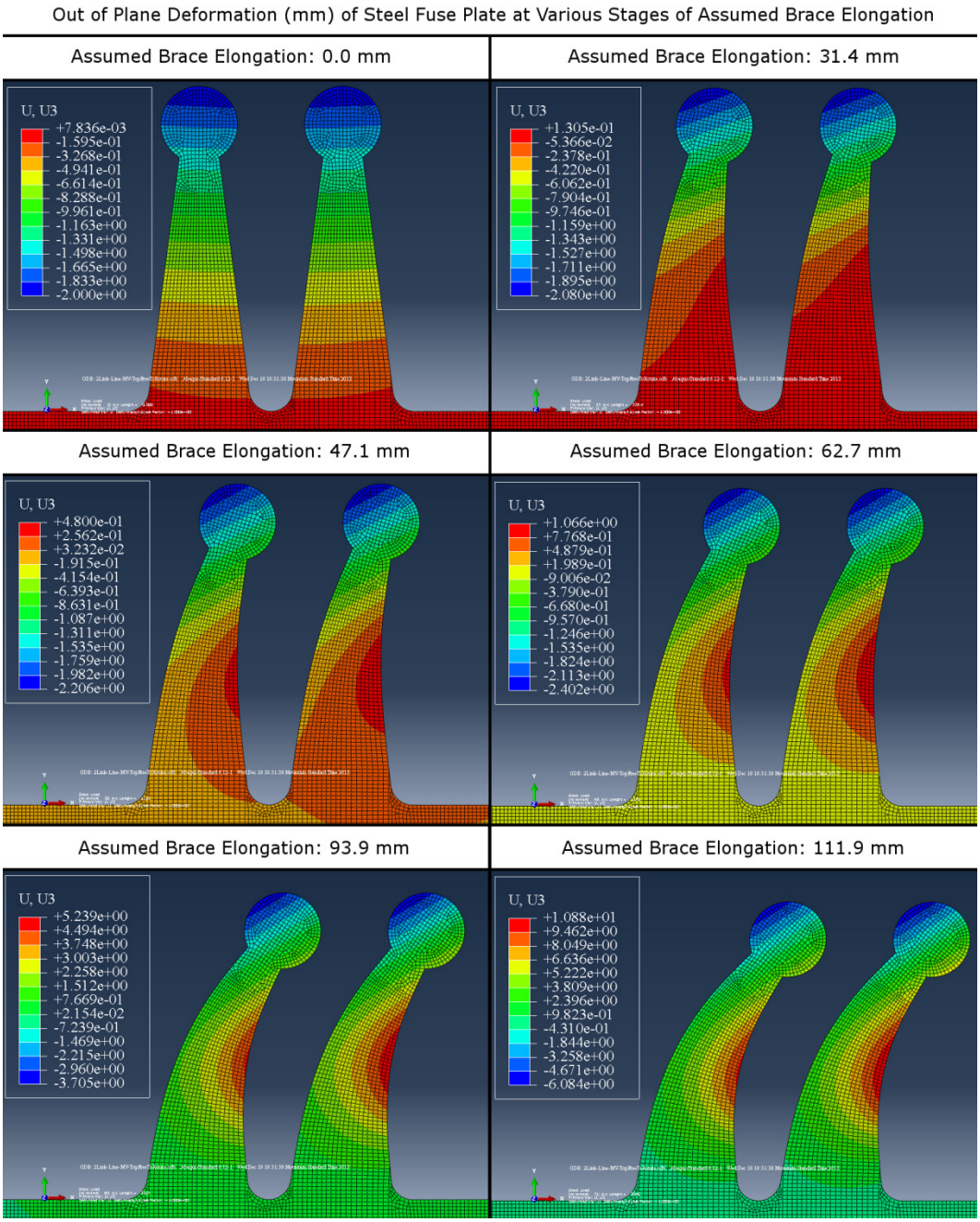

Figure 6-13: Refined FEA Model - Propagation of Torsional Buckling within Shear Link

The buckling pattern as well as magnitude of out-of-plane deformation of the shear link as a function of axial brace elongation is very similar for steel fuse plate types C1-C4. Buckling propagation within shear link of steel fuse plate type C4 is summarized below as an example.

Steel shear link went through elasto-plastic deformation without exhibiting any significant out-of-plane behaviour up to the point when the assumed value of brace elongation reached 47.1 mm. At this stage, out-of-plane deformation of the steel shear link (measured from initial shear link

profile) was recorded to be 1.3 mm. At 62.7 mm of assumed brace elongation value of out-of-plane deformation of shear link was 2.0 mm; at 93.9 mm of assumed brace elongation it was 6.2 mm; and at 111.9 mm of assumed brace elongation it was 12 mm. Out-of-plane deformation of the shear link kept increasing past 111.9 mm of assumed brace elongation. However, its magnitude value ceased to be reliable since rotational allowance due to shimming at the top of the shear link was exhausted. Overall stages of buckling initiation and propagation correlated well with experimental results that suggest measurable onset of buckling at approximately 60 mm of brace elongation after which out-of-plane deformation of the shear link starts to rapidly increase.

Load carrying capacity as a function of assumed brace elongation of a steel fuse plate with shear link free to buckle is compared to the capacity of a steel fuse plate which shear link is restrained from out-of-plane deformation in Figure 6-14. Steel fuse plate type C4 is used in the figure as an example.

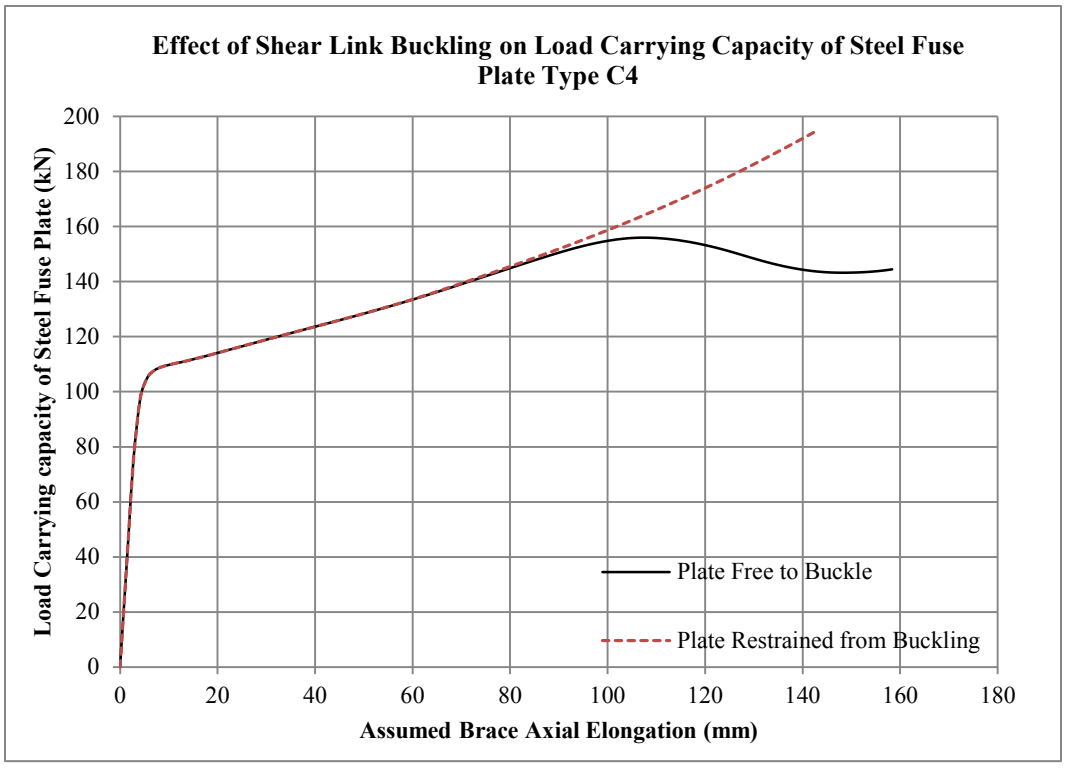

Figure 6-14: Effect of Shear Link Buckling on Load Carrying Capacity of Steel Fuse Plate

The FEA model of the steel fuse plate type C4 suggests that buckling of the steel fuse plate starts to visibly affect its load carrying capacity at an assumed axial brace elongation of approximately 85 mm and higher, which is consistent with experimental results obtained in section 5.2.

6.5.2 Comparing Load Carrying Capacity of Steel Fuse Plate Obtained from Experimental Results and FEA Model

Load carrying capacity of the steel fuse plates was evaluated assuming realistic boundary conditions at the top of the shear link that allows for some rotation about "X", "Y" and "Z" axes. Load carrying capacity of a single steel fuse plate obtained by the FEA model was recorded at axial brace deformation of 15.7 mm, 31.4 mm, 62.7 mm, 93.8 mm and 111.9 mm as per loading history that prototype brace member was subjected to. Corresponding deformations in the "X" direction at the location of the bolt centroid at the top of the shear link is approximately equal to 14.0 mm, 29.0 mm, 60.0 mm, 92.0 mm and 109.0 mm assuming 2.0 mm slip within the bolted joint at the top of the shear link on average. The comparison of experimental and FEA results of the load carrying capacities of steel fuse plates C1 to C4 are shown below.

Table 6.3: Steel Fuse Plate Resistance as a Function of Deformation – Experimental Results vs. FEA

Steel Fuse Plate Type "C1"

	Fuse Plate Capacity @ "X" Axis Displacement of:				
	14.0 mm	29.0 mm	60.0 mm	92.0 mm	109.0 mm
	kN	kN	kN	kN	kN
Experimental Data	128	147	196	208	206
FEA Model Output	134	140	157	164	153
% Discrepancy	5%	-5%	-20%	-21%	-26%

Steel Fuse Plate Type "C2"

	Fuse Plate Capacity @ "X" Axis Displacement of:				
	14.0 mm	29.0 mm	60.0 mm	92.0 mm	109.0 mm
	kN	kN	kN	kN	kN
Experimental Data	53	65	85	113	105
FEA Model Output	56	59	66	74	77
% Discrepancy	5%	-9%	-23%	-35%	-27%

Steel Fuse Plate Type "C3"

	Fuse Plate Capacity @ "X" Axis Displacement of:				
	14.0 mm	29.0 mm	60.0 mm	92.0 mm	109.0 mm
	kN	kN	kN	kN	kN
Experimental Data	107	127	165	185	196
FEA Model Output	111	115	127	144	150
% Discrepancy	4%	-9%	-23%	-22%	-24%

Steel Fuse Plate Type "C4"

	Fuse Plate Capacity @ "X" Axis Displacement of:				
	14.0 mm	29.0 mm	60.0 mm	92.0 mm	109.0 mm
	kN	kN	kN	kN	kN
Experimental Data	106	128	159	173	187
FEA Model Output	111	118	132	149	155
% Discrepancy	5%	-8%	-17%	-14%	-17%

One can observe that at smaller deformations, the load carrying capacity due to steel fuse plates within the prototype brace are predicted well by FEA model. At the same time, at larger axial deformations of the assumed prototype brace, the discrepancy between load carrying capacity of steel fuse plate predicted by FEA and obtained from experimental results increases significantly. The experimental results were consistently higher than the ones predicted by FEA model.

This discrepancy is not a result of an error within FEA model of steel fuse plate but, in fact, is introduced due to the limitations of the FEA model. The slot within fuse attachment plate (see Figure 6-12 for example) was initially assumed to provide roller boundary condition to the high strength bolt at the top of the shear link due to the smoothness of the slot and properties of lubricant used. During the experiment it was, however, noted that significant plastic deformations of the slot as the bolt travels along the slot length changed the boundary condition at the top of the shear link. The plastic deformation changes the geometry of the slot, allowing it to provide resistance to the bolt at the top of the steel shear link (see Figure 6-12) along both "X" and "Y" axes. Slot reaction force along the "Y" axis introduces additional normal force within the friction interface of the prototype brace increasing its overall resistance to deformation.

Fraction of brace axial load carrying capacity due to introduction of steel fuse plate consists of two components: load carrying capacity due to ductile deformation of the steel fuse plate and load carrying capacity due to additional normal force applied at the friction interface. Load carrying capacity of the steel fuse plate obtained from the FEA model is derived exclusively from ductile deformation of the fuse. At small axial deformations of the prototype, the brace normal force increase within the friction interface is minimal and load carrying capacity attributed to introduction of steel fuse plate is very close to capacity estimated by the FEA model. As brace elongation increases, magnitude of the resistance provided by the slot along "Y" axis increases as well, introducing larger normal force within the friction interface and increasing the discrepancy between resistances due to steel fuse plate obtained from experimental data and FEA model.

6.5.3 Shear Link Buckling – Parametric Study

Buckling of the shear link within the steel fuse plate introduces inconsistency into hysteresis of the prototype brace behaviour, eventual capacity degradation and is deemed to be undesirable. An attempt will be made herein to vary certain parameters of the shear link design to postpone or eliminate buckling of the shear link at large brace deformations. Steel fuse plate type C2 will be evaluated as an example. Two parameters are to be varied in the study: boundary condition at the top of the shear link and its width to thickness ratio.

The effect of boundary condition at the top of the shear link on its out-of-plane behaviour is quantified by varying it from fixed against rotation about "X" and "Y" axes and displacement

along “Z” axis to pinned about “X” and “Y” and fixed against displacement along “Z” axis (see Figure 4-14 for more detail).

Given that the width of the shear link within steel fuse plate type C2 varies linearly as a function of distance from the base of the shear link, width to thickness ratio at midpoint of the shear link is deemed to be an acceptable parameter of the study. Width to thickness ratio of the steel shear link was varied by keeping width the same and changing thickness of the steel fuse plate.

Maximum out-of-plane deformation of the steel shear link is used as criteria for evaluating the magnitude of buckling, which is checked at several values for assumed axial brace elongation: 31.4 mm, 47.1 mm, 62.7 mm, 93.9 mm, 111.9 mm and 130.0 mm. The out-of-plane deformations corresponding to the chosen axial brace elongations with respect to varied width to thickness ratios at midpoint are summarized in Table 6.4 and Table 6.5 for torsionally pinned and torsionally fixed boundary conditions at the top of the shear link, respectively.

Table 6.4: Shear Link Out-of-Plane Deformation vs. b/t Ratio – Top of Shear Link Torsionally Pinned

Plate Thickness	Plate b/t Ratio	Maximum Out-of-plane Deformation of the Shear Link With Torsionally Pinned Boundary Condition at Several Values of Assumed Axial Brace Elongation					
		@ 31.42 mm	@ 47.08 mm	@ 62.71 mm	@ 93.86 mm	@ 111.9 mm	@ 130.0 mm
mm	mm/mm	mm	mm	mm	mm	mm	mm
16	4.45	0.4	0.9	1.6	5.5	11.6	22.0
18	3.95	0.4	0.6	0.9	2.0	3.4	6.5
20	3.56	0.3	0.4	0.6	1.1	1.7	2.6
22	3.23	0.3	0.4	0.5	0.8	1.0	1.4
24	2.96	0.3	0.3	0.4	0.6	0.7	1.0
26	2.74	0.3	0.3	0.4	0.5	0.6	0.7
28	2.54	0.3	0.3	0.4	0.4	0.5	0.6
30	2.37	0.3	0.3	0.3	0.4	0.4	0.5
32	2.22	0.3	0.3	0.3	0.4	0.4	0.5

Table 6.5: Shear Link out-of-Plane Deformation vs. b/t Ratio – Top of Shear Link Torsionally Fixed

Plate Thickness	Plate b/t Ratio	Maximum Out-of-plane Deformation of the Shear Link With Torsionally Pinned Boundary Condition at Several Values of Assumed Axial Brace Elongation					
		@ 31.42 mm	@ 47.08 mm	@ 62.71 mm	@ 93.86 mm	@ 111.9 mm	@ 130.0 mm
mm	mm/mm	mm	mm	mm	mm	mm	mm
12	5.93	0.7	1.4	2.4	18.9	31.6	42.7
13	5.47	0.6	1.0	1.5	4.4	13.7	27.9
14	5.08	0.5	0.8	1.2	2.1	3.8	13.0
15	4.74	0.5	0.7	0.9	1.6	2.1	4.3
16	4.45	0.5	0.6	0.7	1.2	1.5	2.4
17	4.18	0.5	0.6	0.7	0.9	1.2	1.6
18	3.95	0.5	0.6	0.7	0.9	1.0	1.3
19	3.74	0.5	0.6	0.7	0.8	0.9	1.1
20	3.56	0.5	0.6	0.7	0.8	0.9	1.0
21	3.39	0.5	0.6	0.7	0.8	0.8	0.9
22	3.23	0.5	0.6	0.7	0.8	0.8	0.9

To better visualize effects of both boundary condition at the top of the shear link and its mid-height b/t ratio, relationship between b/t ratio and out-of-plane deformation of the shear link at 130.0 mm of assumed brace elongation is plotted in Figure 6-15 for shear links with both torsionally fixed and pinned boundary conditions at the top.

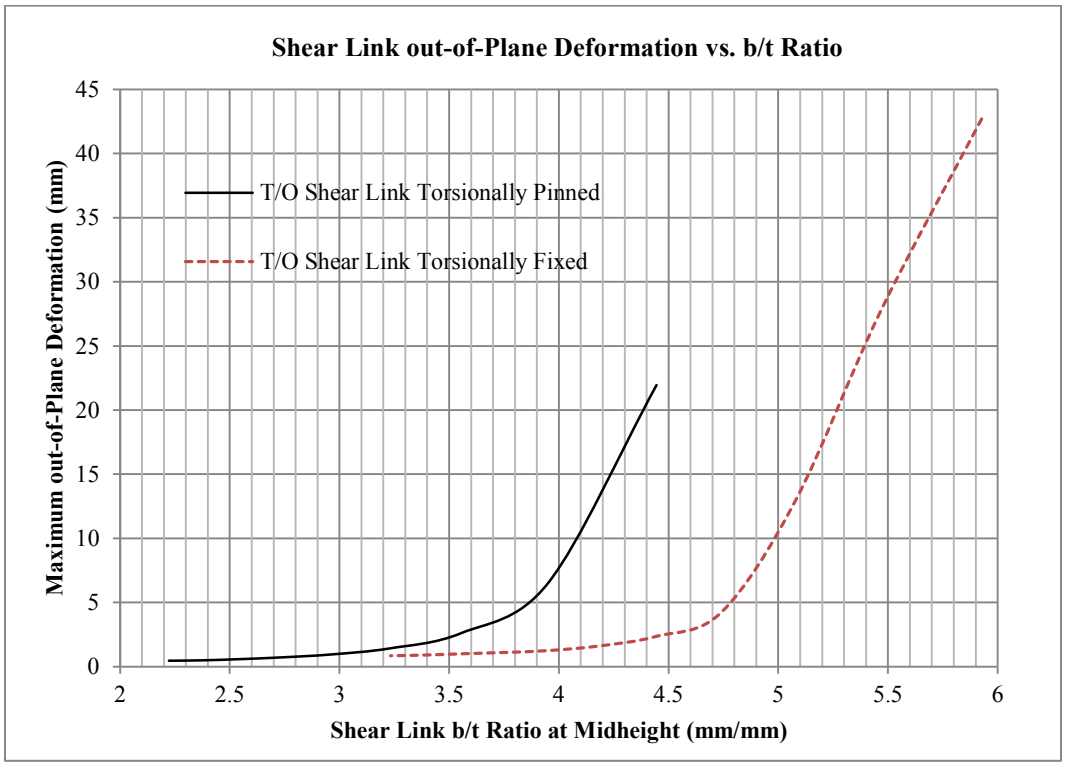

Figure 6-15: Shear Link out-of-Plane Deformation vs. b/t Ratio at 130.0 mm of Assumed Brace Elongation

Boundary condition at the top of the shear link has a major effect on its out-of-plane behaviour. In fact, a 17 mm thick shear link that is torsionally fixed at its top will exhibit similar out-of-plane deformation as a 22 mm thick shear link that has torsionally pinned boundary condition at its top. Nevertheless, unless a practical solution can be derived to achieve torsional fixity at the top of the shear link it might be more viable to vary the thickness of steel fuse plate instead.

From the chart above it is apparent that the relationship between b/t ratio of shear link and its susceptibility to buckling is highly nonlinear, and at a certain point, further reduction of b/t ratio will not provide significant benefit. In case of shear link within a fuse plate type C2, if an out-of-plane deformation value of 1.5 mm is chosen as a limit, decreasing b/t ratio past 3.2 and 4.0 for shear link with torsionally pinned and torsionally fixed boundary condition at its top, respectively, will not provide significant benefit. Corresponding thickness of the shear link in these cases will be 22.0 mm and 17.0 mm.

6.6 Stability of Prototype Brace due to Force Path Eccentricity

Two slotted plates (see Figure 4-6 and Figure 4-7) at each side of the brace create load path redundancy due to the fact that load carried by each plate can be different depending on test specimen configuration (if fuse plates are attached at both locations L1 and L2 or just at L1 or L2 as per Figure 4-5) or if fracture of steel plate shear link occurs. Even with no steel fuse plates attached, force in slotted plates can be different due to incrementally different pretension value that results in different friction at either interface. This axial force eccentricity within prototype brace introduces certain amount of local concentrated moment about strong axis of W200 x 59 beam. The concentrated in-plane moment, if unrestrained, can cause formation of rotational plastic hinge within a brace member with subsequent in-plane buckling.

In order to eliminate possibility of instability within the test setup and to focus on behaviour of the prototype energy dissipater, boundary condition of the brace member were set to fixed at either end within testing apparatus. Strong axis moment demand due to internal axial load eccentricity was recorded at either end of the brace member.

If prototype brace boundary conditions were set to pinned to better represent boundary conditions of actual brace member, moment demand due to axial load eccentricity would be resisted by two slotted plates. This moment demand can be calculated as a sum of recorded moments about strong axis of w-section at the ends of the prototype brace.

Maximum moment demand imposed on slotted plates assuming pin-pin boundary condition along with corresponding axial force and crosshead displacement was recorded by EDAQ and is presented in Table 6.6 for each test specimen configuration.

Table 6.6: Calculated Moment Demands at Slotted Plate Assembly

Test ID	Crosshead Displacement	Axial Load (MTS 6000)	Calculated Moment Demand Applied to Slotted Plates
	mm	kN	kN.m
Friction Test #4	139.3	-401.4	12.9
Test Specimen #1	139.6	666.6	66.4
Test Specimen #2	129.6	574.2	62.1
Test Specimen #3	120.3	469.6	46.5
Test Specimen #4	-9.4	-510.0	23.6
Test Specimen #5	90.0	382.9	24.4

Results from Friction Test # 1 are not presented in the table given different friction interface was used when compared to every other test performed.

In case of Friction Test # 4 no steel fuse plates were attached and the moment demand imposed by differential slippage at two friction planes was minimal out of all six tests considered. Test Specimen # 4 incorporated four steel fuse plates symmetrically attached to it at locations L1 and L2 (Figure 4-5); unbalanced loading within slotted plates due to fuse plates is minimal and thus moment demand imposed by axial load eccentricity within two slotted plates is 2nd lowest out of the group.

Test specimens #1 and #2 had steel fuse plates attached at location L1 (bottom), while plates within test specimens #3 and #5 where attached at location L2 (top). Steel fuse plate within test specimen #5 had only one shear link instead of two for every other plate. Test specimens #1, #2, #3 and #5 represent worst possible condition (with regards to moment demand in a slotted plate) which would correspond to situation when two out of an assumed four steel fuse plates are fractured. In this case the worst moment demand seems to occur when the direction of axial force applied changes (i.e. at ultimate deformation of any given amplitude cycle).

Based on the cross-section properties of a single slotted plate assembly, the yield initiation nominal moment resistance is calculated to be 71.6 kN.m. Two slotted plate assemblies will provide combined nominal moment resistance of 143.2 kN.m, which is well above moment demand imposed.

Based on the above, this particular brace prototype was properly designed and was not susceptible to implied instability of pin-pin boundary conditions.

6.7 Comparing Proposed Energy Dissipater to Alternative Systems

Buckling restrained brace, friction damper and cast steel yielding brace system are energy dissipaters for CBFs that are more commonly used in North America (in the order specified).

The prototype energy dissipater developed in this research can be thought of as a combination of the behaviour of friction damper and cast steel YBS which dissipates seismic energy through bending of cast steel yielding fingers that are similar in function to shear links. In addition, the proposed prototype brace possesses qualities that make it a potentially better option than the three seismic force dissipaters mentioned above.

6.7.1 Ease of Fabrication

Except for the friction damper, two other alternative energy dissipaters for CBFs require manufacturing equipment or techniques that are not common among typical steel fabricators and/or concrete suppliers. In particular, cast steel YBS requires specialized equipment to manufacture an engineered three dimensional cast steel shape; BRB relies on carefully designed concrete to steel core interaction within a surrounding hollow section to provide stable hysteretic behaviour.

Every single component of the prototype brace specimen developed in this research can be fabricated using a CNC plasma cutter that is typically available at a typical steel fabricator shop. Even though it is not the case with test specimens in this experimental program, the prototype brace specimen can be designed in such a way that it can be easily assembled in-shop or on-site using structural bolts with no field welding required.

6.7.2 Customizable Stiffening Behaviour

Out of the three alternative energy dissipaters, the friction damper provides the highest stiffness at service loads (up to slip point) and lowest (zero slope) stiffness at loads that exceed yield or slip capacity. Zero slope post slip hysteretic behaviour can allow for post-earthquake residual story drift concentrating in the bottom stories of the structure. BRB and cast steel YBS do exhibit defined positive slope after yielding took place. The proposed brace prototype on the other hand not only exhibits both high stiffness at service load and defined positive slope at ultimate limit states but can also be designed to introduce significant stiffening at certain deformation effectively limiting inter-story drift of the structure.

6.7.3 Complete Failure of the Brace Member

Due to redundancy in load carrying mechanism, prototype brace developed does not lose its entire capacity even after fracture of its shear links. Fracture of the buckling restrained brace will result in zero capacity braced bay failure. Even though experiments indicate that it can sustain as much as 17 cycles at 2% strain amplitude, there is always a chance that failure can occur sooner due to prior loading history or fabrication deficiencies. The proposed energy dissipater is not susceptible to prior loading history given that any overload at service will be carried by friction connection resistance.

6.7.4 Ease of Post-Earthquake Replacement

Unlike BRB, the proposed prototype brace can be fully rehabilitated after a major seismic event. In order to bring the brace member back to service, steel fuse plates shall be replaced and bolts at slotted hole connection shall be re-tightened to a pre-determined value if needed.

6.7.5 Improvement Needed for Proposed Prototype Energy Dissipaters

Even though the prototype brace does not have clearly defined drawback on conceptual level when compared to existing solutions, its current implementation does require several improvements. Shape of the steel fuse plate shall be re-designed to postpone shear link buckling and associated capacity deterioration, such as an extended "neck area" at the top of shear link proposed in 6.4.2. Boundary condition at the top of the shear link shall be improved to minimize damage of non-replaceable brace components. From manufacturing perspective, in order to reduce costs, a built-up welded slotted plate assembly shall be replaced with a rolled or plate steel section.

6.8 Design Guidelines

During design, fabrication as well as experimental stage of the research project, several practical considerations were noted and are summarized in this section.

6.8.1 Primary Load Carrying Components

Non energy dissipating components of the brace prototype shall be designed to carry demands imposed by energy dissipating components multiplied by appropriate safety factors. Demand imposed by inelastic deformations shall be calculated using FEA model of steel fuse plate with simplified boundary conditions. If FEA software is not available, demand force can be calculated as a minimum value (taken along the shear link length) of shear link section plastic moment resistance divided by distance from location of calculation to the bolt connecting top of the shear link. Probable yield strength of steel subjected to inelastic deformations is to be taken to be larger of 385 MPa or $R_y \cdot F_y$ where $R_y = 1.1$ (CAN/CSA S16-09, 2009 Section 27.1.7). Demand imposed by friction on primary load carrying members shall account for potential statistical variation of material friction properties.

6.8.2 Bolted Connections

Bolted connections at the location of friction interface shall use tension controlled bolts; this is to be done for consistency of pretension force at friction interface. Bolts at the connection imposing boundary condition at the top of the shear link shall have enough capacity to accommodate tensile yielding of the shear link once maximum brace elongation is reached and stiffening takes place; high strength bolts are recommended.

6.8.3 Shape of Ductile Steel Fuse Plate

Ensure fuse plate proportions are such to postpone initiation of lateral torsional-buckling within the shear link (refer to section 6.5.3 for initial considerations). Implement a “neck” region as discussed in section 6.4.2 to better control stiffening behaviour of the brace prototype at deformation extremes.

6.8.4 Boundary Condition at the Top and Bottom of Shear Link

Revise the implementation boundary condition at the top of the shear link to further minimize axial load within the link and to provide effective torsional restraint. Either use a single stronger shear link per fuse plate or provide sufficient spacing between the shear links in order to improve torsional boundary condition at the base of the shear link (as discussed in section 6.4.3).

6.8.5 Friction interface

Friction sheet material is recommended over direct steel-to-steel contact as a friction interface. It is suggested to use only one plane with friction sheet material in order to minimize bending demands imposed on friction inducing bolts. Care should be taken to confirm pre-tension force within the friction interface after the initial setting of the material. Teflon shall be used to minimize friction at the other friction plane; a layer of sand paper glued to the “washer” plate as outlined in section 4.3.2 is recommended to prevent PTFE sheet from slipping out of the connection interface after few cycles of hysteretic loading.

7 Summary, Conclusions and Recommendations

7.1 Summary

Seismic performance of the CBF can be significantly enhanced by using brace members acting as energy dissipaters. Energy dissipaters that currently exist on the market do exhibit stable hysteretic behaviour under the earthquake load. At the same time they require specialized manufacturing process and /or equipment that are typically not available to a steel fabricator. This limits the number of companies who can actually produce the product and correspondingly increases its end cost. A comprehensive research program has been carried out to develop and evaluate a seismic energy dissipater for a CBF whose performance characteristics match or exceed those of existing alternatives and that can be easily manufactured using common steel grades by a typical steel fabricator.

A prototype energy dissipater that incorporates friction and metallic damper has been chosen as a system that provides redundancy of the load carrying mechanism, is not susceptible to a zero capacity failure, introduces positive slope within the force versus displacement response and can be designed to impose a gradual limit on overall axial brace deformation.

Non-asbestos non-metallic glass fiber reinforced friction sheet material has been chosen for use within the friction interface of the dissipater. The choice was based on exceptionally stable friction properties that have minimal variation from cycle to cycle. The sacrificial metallic steel fuse plate element has been designed to accommodate axial deformation of the brace prototype through shear and bending deformation of a number of shear links. The design priority was to minimize the magnitude of maximum plastic strain within steel fuse plate in order to prevent rupture of the shear links due to the low cycle fatigue. The finite element analysis model was used to narrow down to four different configurations of steel fuse plates that incorporated a varying number and / or different shape of the shear links. Those four different types of steel fuse plates served as a basis for five configurations of the prototype brace tested in the experimental portion of the research program.

The experimental program consisted of nine physical tests: four friction only tests and five tests of a complete brace prototype that incorporates both friction and metallic damper. The first friction only test was based on a steel-to-steel friction interface, which proved to be unstable and susceptible to rapid surface deterioration; it was decided to abandon the steel-to-steel interface in favor of non-asbestos non-metallic glass reinforced friction sheet material.

Findings of the experimental program has been confirmed and enhanced by FEA model aimed at replicating behaviour of ductile steel fuse plate.

7.2 Conclusions

Primary findings of the experimental program and subsequent analytical and numerical analysis are summarized below:

- Proposed energy dissipater satisfies requirements imposed on buckling restrained brace by National Building Code of Canada (2010) and CAN/CSA S16-09 (2009).
- Maximum axial deformation achieved by the prototype brace member was 140 mm.
- Force versus displacement response of all five brace configurations showed capacity degradation ranging between 20% to 45 % at 0 mm crosshead displacement during the last cycle of loading history due to torsional buckling of the shear links.
- The shape of the shear link did influence its initial yield pattern and confirmed strain distribution within the link to be similar to preliminary FEA model. It has been concluded that steel fuse plates type C2 and C4 have the most uniform yield and strain distribution patterns which is preferred from a stand point of low cycle fatigue.
- The ultimate response of the brace prototype was governed by the torsional buckling of the shear links, thus no conclusion can be made regarding life to rupture of individual links due to low cycle fatigue.
- According to the results of FEA model, for a 300 mm long shear link type C2 (and C4), a width to thickness ratio at midpoint of the shear link of less than 3.2 (shear link top torsionally pinned) and 4.0 (shear link top torsionally fixed) is necessary to eliminate torsional buckling of the shear link.
- Stiffening of the response introduced at pre-determined maximum deformation of the prototype brace (as observed during experimental program) can be used to limit maximum brace elongation and facilitate more uniform residual inter-story drift distribution through entire height of the structure.

All components of the prototype brace can be fabricated using any CNC controlled plasma or water jet cutter from steel grades that are commonly used within the industry. With design optimization of certain prototype brace components, the energy dissipater developed can become a high-performance, cost-effective alternative for seismic retrofit of existing structures and design of new ones.

7.3 Recommendations

The non-linear dynamic numerical analysis of a braced frame that incorporates proposed energy dissipater would be a required continuation of this research program. In particular it is of interest to be able to accurately model hysteretic behaviour of the brace member within the frame, taking into account significant controlled stiffening of the force versus displacement response. The

dynamic non-linear numerical analysis is necessary to validate the hypothesis that the observed response stiffening can be instrumental at controlling inter-story drift of the structure.

Additional research is required to provide experimental evidence of eliminating or minimizing torsional buckling of the shear links by decreasing its width to thickness ratio to the values identified in parametric study. It is anticipated that actual physical boundary conditions at the top of the shear link as well as accumulated plastic strain hardening may influence width over thickness ratio required to constrain out-of-plane shear link deformation. As an alternative to an experimental program one may conduct a cyclic finite element analysis of the entire brace member.

If dynamic numerical analysis validates performance characteristics of the prototype brace member, further refinement of its design shall be made (taking into account the recommendation obtained with regards to width to thickness ratio of the shear link). An experimental program that evaluates performance of scaled model of multilevel braced frame incorporating prototype brace member would be a logical and concluding step of a long-term plan that is necessary to fully evaluate performance of proposed energy dissipater.

8 Bibliography

Abdel Hamid, Z., and Ghayad, I.. (2002). Characteristics of electrodeposition of Ni-polyethylene composite coatings. Mater. Lett. *53*, 238–243.

Aiken, I.D., Kelly, J.M., and Pall, A.S. (1988). Seismic response of a nine-story steel frame with friction damped cross-bracing. Rep No UCBEERC *88*, 17.

ANSI, A. AISC 341–05 (2005) Seismic provisions for structural steel buildings. Am. Inst. Steel Constr. Inc Chic.

Archard, J.F., and Hirst, W. (1956). The wear of metals under unlubricated conditions. Proc. R. Soc. Lond. Ser. Math. Phys. Sci. *236*, 397–410.

Black, C.J., Makris, N., and Aiken, I.D. (2004). Component testing, seismic evaluation and characterization of buckling-restrained braces. J. Struct. Eng. *130*, 880–894.

CAN/CSA S16-09 (2009). CSA-S16-09: Design of steel structures. Mississauga Ont. Can. Can. Stand. Assoc.

Chen, S.J., and Chang, C.C. (2012). Experimental study of low yield point steel gusset plate connections. Thin-Walled Struct. *57*, 62–69.

Chopra, A., K. (1995). Dynamics of Structures (Prentice-Hall, New Jersey).

Clark, P., Frank, K., Krawinkler, H., and Shaw, R. (1997). Protocol for fabrication, inspection, testing, and documentation of beam-column connection tests and other experimental specimens. Report No. SAC/BD-97/ 02, SAC Joint Venture, Sacramento, CA.

DesRoches, R., McCormick, J., and Delemont, M. (2003). Cyclic properties of superelastic shape memory alloy wires and bars. J. Struct. Eng. *130*, 38–46.

Drucker, D., and Providence, R.I. (1956). The effect of shear on the plastic bending of beams. Int J Appl Mech *23*, 509–514.

Gardiner, S., Clifton, G.C., and MacRae, G.A. (2013). Performance, damage assessment and repair of a multistorey eccentrically braced framed building following the Christchurch earthquake series. In Performance, Damage Assessment and Repair of a Multistorey Eccentrically Braced Framed Building Following the Christchurch Earthquake Series, (Christchurch, New Zealand),.

Gray, M.G., Christopoulos, C., and Packer, J.A. (2010). Cast steel yielding fuse for concentrically braced frames. In Proceedings of the 9th US National and 10th Canadian Conference on Earthquake Engineering,.

Gray, M.G., Christopoulos, C., and Packer, J.A. (2011). Full-scale testing of the cast steel Yielding Brace System. In Proceedings of the 7th International Conference STESSA,.

Gray, M.G., Christopoulos, C., Packer, J.A., and Lignos, D.G. (2012). Development, validation and modeling of the new cast steel Yielding Brace System. In 20th Analysis and Computation Specialty Conference, pp. 71–82.

Grondin, G.Y., Jin, M., and Josi, G. (2007). Slip critical bolted connections: a reliability analysis for design at the ultimate limit state. Structural Engineering Report, Department of Civil & Environmental Engineering, University of Alberta (Department of Civil & Environmental Engineering, University of Alberta).

Kelly, J.M. (1986). Aseismic base isolation: review and bibliography. Soil Dyn. Earthq. Eng. *5*, 202–216.

Kimura, K., Takeda, Y., Yoshioka, K., Furuya, N., and Takemoto, Y. (1976). An experimental study on braces encased in steel tube and mortar. In Annual Meeting of the Architectural Institute of Japan (in Japanese),.

Mahmoudi, M., and Zaree, M. (2010). Evaluating response modification factors of concentrically braced steel frames. J. Constr. Steel Res. *66*, 1196–1204.

Memon, B.-A., and Su, X. (2004). Arc-length technique for nonlinear finite element analysis. J.-ZHEJIANG Univ. Sci. *5*, 618–628.

Miranda, E. (1997). Strength reduction factors in performance-based design. In Proceedings of EERC-CUREe Symposium, Berkeley, CA,.

Mullin, D.T. (2005). Gusset Plates as Energy Dissipaters in Seismically Loaded Structures. Ph.D. Thesis. University of Alberta.

National Research Council Canada (2010). National building code of Canada. Natl. Build. Code Can.

Pall, A.S. (1979). Limited slip bolted joints: a device to control the seismic response of large panel structures. Ph.D. Thesis. Concordia University.

Pall, A.S., and Marsh, C. (1982). Response of friction damped braced frames. J Struct Div ASCE *108*, 1313–1323.

Pall, A.S., and Pall, R. (1996). Friction dampers for seismic control of buildings: a Canadian experience. In Proa, 11th World Conf. Earthquake Engrg,.

Perotti, F., and Scarlassara, G.P. (1991). Concentrically braced steel frames under seismic actions: Non-linear behaviour and design coefficients. Earthq. Eng. Struct. Dyn. *20*, 409–427.

Popov, E.P., and Engelhardt, M.D. (1988). Seismic eccentrically braced frames. J. Constr. Steel Res. *10*, 321–354.

Rabinovitch, J.S., and Cheng, J.R. (1993). Cyclic behavior of steel gusset plate connections. Structural Engineering Report, Department of Civil & Environmental Engineering, University of Alberta (Department of Civil Engineering, University of Alberta).

Rai, D.C., Goel, S.C., and Firmansjah, J. (1996). SNAP-2DX: A general purpose computer program for nonlinear structural analysis. Rep. UMCEE 96–21.

Sabelli, R., Mahin, S., and Chang, C. (2003). Seismic demands on steel braced frame buildings with buckling-restrained braces. Eng. Struct. *25*, 655–666.

Stranton, J.F., and Taylor, J.C. (2010). Friction coefficients for stainless steel PTFE (teflon) bearings. Structural Engineering Report, Wisconsin Highway Research Program.

Tamai, H., and Kitagawa, Y. (2002). Pseudoelastic behavior of shape memory alloy wire and its application to seismic resistance member for building. Comput. Mater. Sci. *25*, 218–227.

Tang, X., and Goel, S.C. (1989). A fracture criterion for tubular bracing members and its application to inelastic dynamic analysis of braced steel structures. Proc. Ninth World Con-Ference Earthq. Eng. 9WCEE Organ. Comm. Jpn. Assn Earthq. Disaster Prev. Tokyo *4*, 285–290.

Tremblay, R. (2002). Inelastic seismic response of steel bracing members. J. Constr. Steel Res. *58*, 665–701.

Uang, C.-M., and Kiggins, S. (2003). Reducing residual drift of buckling-restrained braced frames as a dual system. In International Workshop on Steel and Concrete Composite Construction (IWSCCC-2003), Reporte No. NCREE-03, pp. 189–198.

Veletsos, A.S., Newmark, N.M., and Chelapati, C.V. (1965). Deformation spectra for elastic and elastoplastic systems subjected to ground shock and earthquake motions. In Proc. Third World Conf. Earthq. Eng., Wellington, New Zealand, II, pp. 663–682.

Wakabayashi, M., Nakamura, T., and Yoshida, N. (1977). Experimental studies on the elastic-plastic behavior of braced frames under repeated horizontal loading: Part 1 - Experiments of braces with an H-shaped cross section in a frame. Bull. Disaster Prev. Res. Inst. *27*, 121–154.

Watanabe, A., Hitomi, Y., Saeki, E., Wada, A., and Fujimoto, M. (1988). Properties of brace encased in buckling-restraining concrete and steel tube. In Proceedings of Ninth World Conference on Earthquake Engineering, pp. 719–724.

Zhu, S., and Zhang, Y. (2007). Seismic behaviour of self-centring braced frame buildings with reusable hysteretic damping brace. Earthq. Eng. Struct. Dyn. *36*, 1329–1346.

Zhu, S., and Zhang, Y. (2008). Seismic analysis of concentrically braced frame systems with self-centering friction damping braces. J. Struct. Eng. *134*, 121.